Theses and Dissertations

Fall 2010

Modeling the effects of heterogeneous reactions on atmospheric chemistry and aerosol properties

Chao Wei
University of Iowa

Recommended Citation

Wei, Chao. "Modeling the effects of heterogeneous reactions on atmospheric chemistry and aerosol properties." PhD (Doctor of Philosophy) thesis, University of Iowa, 2010.
https://doi.org/10.17077/etd.2xewzpnz

MODELING THE EFFECTS OF HETEROGENEOUS REACTIONS ON

ATMOSPHERIC CHEMISTRY AND AEROSOL PROPERTIES

by

Chao Wei

An Abstract

Of a thesis submitted in partial fulfillment
of the requirements for the Doctor of
Philosophy degree in Chemical and Biochemical Engineering
in the Graduate College of
The University of Iowa

December 2010

Thesis Supervisor: Professor Gregory R. Carmichael

ABSTRACT

In this thesis, a new aerosol module is developed for the STEM model (the Sulfur Transport and dEposition Model) to better understand the chemical aging of dust during long range transport and assess the impact of heterogeneous reactions on tropospheric chemistry. The new aerosol module is verified and first applied in a box model, and then coupled into the 3-Dimentional STEM model. In the new aerosol model, a non-equilibrium (dynamic or kinetic) approach to treat gas-to-particular conversion is employed to replace the equilibrium method in STEM model. Meanwhile, a new numerical method solving the aerosol dynamics equation is introduced into the dynamic aerosol model for its improved computational efficiency and high accuracy. Compared with the equilibrium method, the new dynamic approach is found to provide better results on predicating the different hygroscopicity and chemical aging patterns as a function of size. The current modeling study also takes advantage of new findings from laboratory experiments about heterogeneous reactions on mineral oxides and dust particles, in order to consider the complexity of surface chemistry (such as surface saturation, coating and relative humidity). Modeling results show that the impacts of mineralogy and relative humidity on heterogeneous reactions are significant and should be considered in atmospheric chemistry modeling with first priority. Finally, the upgraded 3-D STEM model is utilized to explore the observations from the Intercontinental Chemical Transport Experiment – Phase B (INTEX-B). The new dynamic approach for gas-to-particular conversion and RH-dependent heterogeneous uptake of HNO_3 improve the model performance in term of aerosol predictions under different conditions. It is shown that these improvements change the modeled nitrate and sulfate concentrations, but also modify their size distributions significantly.

Abstract Approved: _____

                                Thesis Supervisor

                          _____

                                Title and Department

                          _____

                                Date

MODELING THE EFFECTS OF HETEROGENEOUS REACTIONS ON

ATMOSPHERIC CHEMISTRY AND AEROSOL PROPERTIES

by

Chao Wei

A thesis submitted in partial fulfillment
of the requirements for the Doctor of
Philosophy degree in Chemical and Biochemical Engineering
in the Graduate College of
The University of Iowa

December 2010

Thesis Supervisor: Professor Gregory R. Carmichael

Graduate College
The University of Iowa
Iowa City, Iowa

CERTIFICATE OF APPROVAL

_____

PH.D. THESIS

_____

This is to certify that the Ph.D. thesis of

Chao Wei

has been approved by the Examining Committee
for the thesis requirement for the Doctor of Philosophy
degree in Chemical and Biochemical Engineering at the December 2010
graduation.

Thesis Committee: _____
                       Gregory R. Carmichael, Thesis Supervisor

                       _____
                       Vicki H. Grassian

                       _____
                       Charles O. Stanier

                       _____
                       David G. Rethwisch

                       _____
                       Thomas M. Peters

To my parents and xhn

ACKNOWLEDGMENTS

I am happy to take this opportunity to acknowledge and thank all those people who have helped me to reach this stage of my career. I would like to firstly thank my advisor Dr. Gregory R Carmichael for allowing me to pursue this research. With his extreme patience, broad knowledge and understanding, I have learned not only how to use tools, but also how to make and improve tools in my Ph.D. study. I also would like to thank Dr. Xiaohong Liu for leading me to this field of research and helping me to apply for UI.

I would like to extend my sincere thanks to my committee members: Dr. Charles O. Stanier, Dr. Vicki H. Grassian, Dr. David G. Rethwisch, and Dr. Thomas M. Peters for their support and interest in my research.

I would specially thank Dr. Yafang Cheng for her encouragement and help during the darkness before dawn. Without her companion I couldn't catch all deadlines and finish my thesis draft under the double pressure of healthy issue and painful writing.

It has been a pleasure to have worked with Sarika Kulkarni and Bhupesh Adhikary. Our trio group successfully completed so many projects, especially ARCTAS project. I look forward to working together with them on future research projects.

I would like to thank the faculty of the Department of Chemical Engineering for giving me this opportunity to be a part of this program. Linda Wheatley ensured that all the necessary administrative and academic paperwork were taken care of and I am very thankful for her assistance. I am also grateful to Jane Frank and Jeremie Moen for their constant support.

Last but not the least, I would like to express my utmost thank to my parents from the bottom of my heart. In spite of numerous adversities, they have always been on my side. Their unconditional love and support are really immeasurable and fathomless not only during my doctoral study but also throughout my whole life.

ABSTRACT

In this thesis, a new aerosol module is developed for the STEM model (the Sulfur Transport and dEposition Model) to better understand the chemical aging of dust during long range transport and assess the impact of heterogeneous reactions on tropospheric chemistry. The new aerosol module is verified and first applied in a box model, and then coupled into the 3-Dimentional STEM model. In the new aerosol model, a non-equilibrium (dynamic or kinetic) approach to treat gas-to-particular conversion is employed to replace the equilibrium method in STEM model. Meanwhile, a new numerical method solving the aerosol dynamics equation is introduced into the dynamic aerosol model for its improved computational efficiency and high accuracy. Compared with the equilibrium method, the new dynamic approach is found to provide better results on predicating the different hygroscopicity and chemical aging patterns as a function of size. The current modeling study also takes advantage of new findings from laboratory experiments about heterogeneous reactions on mineral oxides and dust particles, in order to consider the complexity of surface chemistry (such as surface saturation, coating and relative humidity). Modeling results show that the impacts of mineralogy and relative humidity on heterogeneous reactions are significant and should be considered in atmospheric chemistry modeling with first priority. Finally, the upgraded 3-D STEM model is utilized to explore the observations from the Intercontinental Chemical Transport Experiment – Phase B (INTEX-B). The new dynamic approach for gas-to-particular conversion and RH-dependent heterogeneous uptake of HNO_3 improve the model performance in term of aerosol predictions under different conditions. It is shown that these improvements change the modeled nitrate and sulfate concentrations, but also modify their size distributions significantly.

TABLE OF CONTENTS

v

LIST OF TABLES

LIST OF FIGURES

ix

CHAPTER 1

INTRODUCTION

1.1 Background and significance

The Earth's atmosphere, made up mostly of gases, has suspended in it liquid and solid particles that play an important role in atmospheric chemistry, climate, and human health. It is well known that particles can influence radiative transfer by absorption and scattering of solar and terrestrial radiation, and by changing the optical properties of clouds through modification of the distribution of cloud condensation nuclei (CCN) [*Charlson et al.*, 1992]. Particulate matter (PM) is included in the National Ambient Air Quality Standards (NAAQS) partly because of its adverse health effects, including premature mortality, exacerbation of asthma and other respiratory-tract diseases, and decreased lung function. Aerosols can also impact atmospheric chemistry in several ways. They can affect the actinic flux and thus alter photolysis rates [*Tang et al.*, 2003]. They can also provide surfaces upon which chemical interactions can occur between gases and aerosols. In addition, through radiative forcing effects, they can change the regional temperature and cloud fields, which in turn may perturb the photochemical processes [*Conant et al.*, 2003; *Tang et al.*, 2003].

Chemical transport models (CTMs) have developed into a major tool in air quality and atmospheric chemistry analysis. Regional CTMs play an indispensable role in assessing, predicting, and interpreting the air-quality-related hazardous events. Regional CTMs with size-resolved and chemically resolved aerosol model are important tools to study the regional distribution of aerosols and understand its impact on atmospheric chemistry. The starting point for an aerosol model is the equation of conservation of particle mass (or number). Within that equation are terms that account for transport and dispersion, gas-to-particle conversion, coagulation, and removal processes. Chemical interactions between gases and aerosols are important mechanisms for gas-to-particle conversion. Understanding the chemical interactions between gases and aerosols is crucial because these processes may result in a change in aerosol composition and size

distribution, and thus alter aerosol optical properties. Furthermore, these processes may perturb the photochemical oxidant and biogeochemical cycles.

1.1.1 Aerosol models in 3-D models

Pilinis and Seinfeld [1988] constructed the first three-dimension size-resolved and chemically resolved atmospheric aerosol model. It included the gas-aerosol partitioning of volatile inorganic compounds and assumed instantaneous gas-aerosol equilibrium for these compounds. Since then most aerosol models used in 3-D models consider the gas-aerosol partitioning of condensable compounds in order to predict secondary aerosol formation more accurately.

There are two primary approaches to treat the gas-aerosol partitioning of condensable compounds. One is the equilibrium approach which assumes the instantaneous chemical equilibrium for volatile compounds between the bulk gas and whole aerosol phase [*Binkowski and Shankar*, 1995]. However it has been shown that for some compounds under certain conditions, equilibrium is slow to be established relative to the timescale over which other changes are occurring [*Wexler and Seinfeld*, 1990; *Meng and Seinfeld*, 1996]. Thus it is desirable that a non-equilibrium approach is used in an aerosol model. The dynamic approach (or kinetic approach) explicitly simulates gas/particle mass transfer for each size section by solving the equation for mass fluxes between the bulk gas-phase and individual particles (or particles in a given size range) [*Meng et al.*, 1998; *Zhang et al.*, 1999]. Chemical concentrations in the bulk gas-phase and in the particles in a given size section may or may not be in equilibrium.

An explicit treatment of kinetic mass transfer is typically at least 100 times slower than solutions that assume equilibrium [*Zhang et al.*, 1999]. By considering computational efficiency, hybrid methods have been used in many 3-D models [*Meng et al.*, 1998; *Zhang et al.*, 2004]. For example, CIT hybrid method [*Meng et al.*, 1998] is based on equilibrium approach and considers diffusion-limited assumptions. The method first calculates at any instant of time the equilibrium for volatile compounds between the gas and bulk aerosol phases and, then distributes the aerosol mass increment over different size sections based on a weighting factor which considers different

mass transfer rate for different size section. In the other method, the CMU hybrid method [*Capaldo et al.*, 2000], the gas phase is first allowed to instantaneously attain equilibrium with the fine aerosol mode and then use a kinetic approach to calculate the mass transfer between the coarse mode and gas phase. A threshold diameter is selected to decide which section is in fine or coarse mode.

Zhang et al. [1999] compared the CIT hybrid method, the full equilibrium method and the full kinetic method in a box model. They found that the full equilibrium method is inaccurate when chloride and carbonate concentrations are significant, whereas the CIT hybrid method and full kinetic method are appropriate. Also, the kinetic method leads to more nitrate present in coarse particles than in the full equilibrium and CIT hybrid methods, and the final particle size distributions differ among the 3 methods. They recommended to use full kinetic approach to the areas where compounds containing chloride or carbonate because mass transfer from the gas phase to coarse particles is the rate limiting process.

1.1.2 Heterogeneous Chemistry

Except for condensation, some gases can also be absorbed onto aerosol by irreversible heterogeneous reactions on the surface of aerosols, which are not limited by chemical equilibrium process. In the atmospheric chemistry literature "aerosol" is commonly defined as the liquid and solid particles suspended in the atmosphere. It is also common practice to refer to "heterogeneous chemistry" as the chemical interactions between gases and aerosols in the atmosphere. Here the term "aerosol" is restricted to non-cloud aerosols, the solid and concentrated liquid particles suspended in the atmosphere, as distinct from the dilute water droplets and ice crystals found in clouds. The discussion on heterogeneous chemistry in the thesis is also focused on non-cloud aerosols. Thus aqueous chemistry and diffusion in the aqueous phase aren't included in the context of the thesis.

It is well proven that heterogeneous chemistry can affect the photochemical oxidant cycle by modeling studies and field observations [*Jacob*, 2000; *Dentener et al.*, 1996; *McNaughton et*

al., 2009]. However, results from laboratory studies show that surface chemistry of aerosols is complex [*Al-Abadleh et al.*, 2005; *Goodman et al.*, 2001; *Grassian*, 2002; *Krueger et al.*, 2004; *Underwood et al.*, 2001; *Usher, et al.* 2003a; *Usher, et al.*, 2003b], which makes it difficult to cope with in atmospheric modeling. Heterogeneous reactions on mineral dust particles are one of the major concerns of the current research. *Usher et al.* [2003a] recommended different mechanisms for heterogeneous chemistry of trace atmospheric gases on dust particles. These mechanisms provide molecular level insight into potentially important tropospheric reactions that can be incorporated into atmospheric chemistry models (More about heterogeneous reactions on dust particles will be discussed in Chapter 3). However, many modeling studies treat heterogeneous reaction in a relatively simplistic manner without considering the complex of surface chemistry [*Dentener and Crutzen*, 1993; *Tang et al.*, 2004]. They assume a heterogeneous reaction is modeled as a pseudo-first order kinetic reaction. The rate constant contains the number density of particles at a given radius, the uptake coefficient, and a gas-particle diffusion correction. But constraints, such as consideration of the status of surface, are not commonly included in these models.

1.1.3 Evolution of aerosol modules in STEM

The Sulfur Transport and Eulerian Model (STEM) is a regional-scale CTM which considers the transport, chemical transformation, emission, and deposition of atmospheric gaseous pollutions and particles. In order to study the chemical interactions between gases and aerosols, a size-resolved and chemically resolved aerosol model has been developed in the version of STEM III [*Carmichael et al.*, 1986; *Carmichael et al.*, 1991; *Song and Carmichael*, 2001]. The aerosol model considers aerosol dynamics, surface chemistry, and gas/particle partitioning. A kinetic approach is used for the mass transfer between gases and inorganic aerosols. SCAPE II (Simulating Composition of Atmospheric Particles at Equilibrium) [*Kim et al.*, 1993a; 1993b; *Kim and Seinfeld*, 1995; *Meng et al.*, 1995], a thermodynamics equilibrium module, is included to calculate gas-particle equilibrium concentrations among inorganic aerosol ions and their gaseous

precursors. Some heterogeneous reactions on dust are also considered. The effect of growth of particles on the size distribution is not considered in the aerosol model because only two size sections are used in the condensation/evaporation part and no mass-exchange between the two sections is assumed.

In STEM version 2K1, the 3-D CTM and the aerosol model have been changed significantly [*Tang et al.*, 2003]. The important changes for the aerosol model in STEM-2K1 are: (1) primary aerosols are emitted and transported in CFORS (Chemical Forecasting System) [*Carmichael et al.*, 2003] which is a multitracer, online system built within the RAMS mesoscale meteorological model [*Pielke et al.*, 1992]; (2) the calculation of photolysis rates on-line, considering the influences of cloud, aerosol and gas-phase absorptions due to O_3, SO_2, and NO_2, using the NCAR Tropospheric Ultraviolet-Visible (TUV) radiation model [*Madronich and Flocke*, 1999]; (3) the extension of the aerosol calculations to include optical information (e.g., extinction) in addition to mass, size, and composition; (4) the heterogeneous reactions of O_3, HNO_3, NO_2, and SO_2 on dust is considered in a simple way [*Tang et al.*, 2004a].

In STEM-2K1 only 4 simple heterogeneous reactions were considered for the chemical interactions between gases and aerosols. This simple treatment limit the performance of the model when it is applied to interpret and compare with field observations which have lots of information about the distribution of size-resolved and chemically resolved aerosols. It is desirable that a new aerosol module with more details on the chemical interactions between gases and aerosols be included in STEM.

The current version is the STEM-2K3 version [*Tang et al.*, 2004b]. Since STEM-2K1, an on-line aerosol thermodynamic module SCAPE II has been added into the STEM model. In STEM aerosol module, the gas-particle equilibrium concentrations among inorganic aerosol ions and their gaseous precursors were obtained by the CIT hybrid method. The CIT hybrid method basically was still an "improved" equilibrium approach, whereas in the real atmosphere, for some compounds under certain conditions, equilibrium is slow to be established instead of instantly. The disadvantage of CIT hybrid method will be further discussed in Chapter 2. This thus leads to main

object of current thesis – to build a new fast performed full-dynamic aerosol module into 3-D STEM model.

1.2 Specific Aims

The specific aims of this research study are listed here:

- Build a new aerosol model with a non-equilibrium (dynamic or kinetic) approach to treat gas-to-particular conversion for STEM model. To cope with the issues regarding the computational efficiency, a new module, AeroSolver, will be introduced to solve the aerosol dynamics equations for the dynamic gas/aerosol partitioning.

- Assess the importance of different complex schemes of heterogeneous reactions on tropospheric chemistry.

- Characterize the outflow of Asian aerosols and precursor gases to the Pacific and subsequently to North America using the STEM model constrained with measurements available from the NASA INTEXB field campaign.

- Analyze the gas-particle partitioning of inorganic species during the long range transport of dust plume. The new dynamic aerosol module will be coupled into STEM and its performance will be assessed by comparing with observations from INTEX-B. This study will also quantify the contribution of heterogeneous chemistry (on dust surfaces) on trace gas concentration farther away from source regions.

1.3 Outline

The main object of this thesis is to build up a new aerosol module for STEM for better understanding the interaction between gas and particles. Chapter 1 of this thesis presented general background about aerosol modeling and heterogeneous reaction for understanding the aging of East Asian aerosols during long range transport. Chapter 2 builds a new aerosol model to deal with gas-to-particular conversion, which is verified in a box model. Chapter 3 presents the results of

sensitivity studies about the effects of the complexity of heterogeneous reactions on atmospheric chemistry. In Chapter 4, the new aerosol module is coupled into STEM-2k9, and the model is used to analysis the chemical aging of dust during the period of INTEX-B field campaign in April 2006. Chapter 4 also quantifies the contribution of aerosols heterogeneous reactions on tropospheric chemistry. Chapter 5 summarizes this research and presents the direction for future work.

CHAPTER 2

UNDERSTANDING THE CHEMICAL INTERACTIONS BETWEEN

GASES AND AEROSOLS – A NEW AEROSOL MODULE FOR

STEM

2.1 Introduction

In the late 1980's, *Pilinis and Seinfeld* [1988] constructed the first three-dimension size-resolved and chemically resolved atmospheric aerosol model. It included the gas-aerosol partitioning of volatile inorganic compounds and assumed instantaneous gas-aerosol equilibrium for these compounds. Since then most aerosol models used in 3-D models consider the gas-aerosol partitioning of condensable compounds.

There are two primary approaches to treat the gas-aerosol partitioning of condensable compounds. One is the equilibrium approach, which assumes the instantaneous chemical equilibrium for volatile compounds between the bulk gas and whole aerosol phase. In full equilibrium methods the transferred material is allocated to the particle size distribution using weighting factors that are derived based on either initial particle mass/surface area or a given distribution. However it has been shown that for some compounds under certain conditions, equilibrium is slow to be established relative to the timescale over which other changes are occurring [*Wexler and Seinfeld*, 1990; *Meng and Seinfeld*, 1996]. In these cases, both transport and thermodynamics are important for the determination of concentrations in aerosol phase. Thus it is desirable that a non-equilibrium approach is used in an aerosol model. The dynamic approach (or kinetic approach) explicitly simulates gas/particle mass transfer for each size section by solving the equation for mass fluxes between the bulk gas-phase and individual particles (or particles in a given size range), e.g., CIT-PFISLM (or referring as dynamic-CIT [*Nguyen and Dabdub*, 2002]). In such an approach, chemical concentrations in the bulk gas-phase and in the particles in a given size section may or may not be in equilibrium.

An explicit treatment of kinetic mass transfer is typically at least 100 times slower than solutions that assume equilibrium [*Zhang et al.*, 1999]. By compromising computational efficiency, two hybrid methods have been used in many 3-D models. One is the CIT hybrid method [*Meng et al.*, 1998] which is based on equilibrium approach but considers diffusion-limited assumptions. The method first calculates at any instant of time the equilibrium for volatile compounds between the gas and bulk aerosol phases and, then distributes the aerosol mass increment over different size sections based on a weighting factor which considers different mass transfer rate for different size section. The other method is the CMU hybrid method [*Capaldo et al.*, 2000] in which the gas phase is first allowed to instantaneously attain equilibrium with the fine aerosol mode and then use a kinetic approach to calculate the mass transfer between the coarse mode and gas phase. A threshold diameter is selected to decide which section is in fine or coarse mode.

Zhang et al. [2004] compared the simple bulk equilibrium method, the CIT hybrid method and the CMU hybrid method in the 3-dimension CMAQ-MADRID model. They concluded that both the CIT and CMU hybrid methods can predict particle size distribution for $PM_{2.5}$ that is reasonably close to the observed size distribution. The accuracy in nitrate predicted by the CMU and CIT methods cannot be determined because of the uncertainties in the nitrate measurements. The CMU hybrid method predicts higher mass concentrations for both fine and coarse nitrate than the CIT method as a result of a larger total mass with a faster growth rate in fine sections and an explicit mass transfer in coarse sections.

Zhang et al. [1999] compared the CIT hybrid method, the full equilibrium method and the full kinetic method in a box model. They found that the full equilibrium method is inaccurate when chloride and carbonate concentrations are significant, whereas the CIT hybrid method and full kinetic method are appropriate. Also, the kinetic method leads to more nitrate present in coarse particles than in the full equilibrium and CIT hybrid methods, while the final particle size distributions differ among the 3 methods.

The STEM model was developed at the University of Iowa in the early 1980s [*Carmichael et al.*, 1986] and has continuously undergone development since then to its current version which is the STEM-2K3 version [*Tang et al.*, 2004b]. Since STEM-2K1 [*Carmichael et al.*, 2003; *Tang et al.*, 2003], an on-line aerosol thermodynamic module SCAPE II [*Kim et al.*, 1993a; 1993b; *Kim and Seinfeld*, 1995; *Meng et al.*, 1995] has been added into the STEM model. In STEM aerosol module, the gas-particle equilibrium concentrations among inorganic aerosol ions and their gaseous precursors were obtained by the CIT hybrid method. As described before, the CIT hybrid method basically was still an improved equilibrium approach, whereas in the real atmosphere, for some compounds under certain conditions, equilibrium is slow to be established [*Wexler and Seinfeld*, 1990; *Meng and Seinfeld*, 1996]. Therefore, the equilibrium-like CIT hybrid approach tends to over-predict the concentrations in aerosol phases. Another disadvantage of the current aerosol module in STEM model is that after equilibrium between gas and aerosol phases, the CIT hybrid method distributes the aerosol mass increment over different size sections based on an empirical weighting factor by considering different mass transfer rate for different size sections. This empirical treatment often tends to under-predict the growth rate of fine particles, while overestimating the growth rate of coarse mode particles. This is because small particles have greater surface area to mass ratios and thus faster equilibrium time scales than larger particles [*Pilinis et al.*, 2000]. The disadvantage of the CIT hybrid method will be further discussed in Section 2.3.2 when it is compared with the dynamic methods in the box model.

Thus, the main purpose of this chapter is to build a new aerosol model with a non-equilibrium (dynamic or kinetic) approach to treat gas-to-particular conversion for STEM model. To cope with the issues regarding the computational efficiency, a new module (AeroSolver, see section 2.2.1) is introduced to solve the aerosol dynamics equations for the dynamic gas/aerosol partitioning.

<div style="text-align:center">2.2 Box model</div>

A box model is built to verify the important parts in the aerosol module before they are added into the 3-D STEM model. Sensitivity studies have been done in the box model to determine the most important schemes, which will be finally embedded and tested in the 3-D STEM model (see Chapter 4). Two methods (the CIT hybrid method and the dynamics method) for the gas/particle partitioning of condensable inorganic compounds between gases and aerosol phases are compared in the sensitivity studies by using the box-model.

<div style="text-align:center">2.2.1 Structure</div>

In the box model there are several plug-n-play parts included. We can integrate different parts into the box model according to the case we choose. The structure of the box model is illustrated in Figure 2.1. Generally, it is integrated with three major components, gas-phase chemistry, aerosol operator, and aerosol tracer processes including emission, removal, transport and dispersion.

Box model simulations were performed using the gas phase mechanism that is in the STEM-II model [*Carmichael et al.*, 1991]. The gas phase chemical mechanism is based on that of *Lurmann et al.* [1986], but has been modified to include low-NOx conditions and an explicit treatment of isoprene. It consists of 83 chemical species and 185 gas phase reactions. Irreversible heterogeneous uptakes of gases are treated as pseudo-first order kinetic reactions and are included in the gas-phase chemistry. The rate constants for the heterogeneous uptake are calculated in the aerosol module considering the surface chemistry. Specifically, for the heterogeneous reactions on dust, the related heterogeneous reaction rates are modified according to laboratory results and different RH conditions (see the discussions in Chapter 3).

The aerosol module is composed of gas/particle partitioning for condensable inorganic compounds and aerosol dynamics, which includes nucleation, coagulation, condensation and evaporation. In the condensation/evaporation part, SCAPE II is utilized to treat the aerosol thermodynamics, and two different gas/aerosol partitioning approaches (equilibrium and

dynamics) are included. Below results from the CIT hybrid (equilibrium approach), CIT-PFISLM (complete dynamic method) and AeroSolver (fast dynamic method) are compared. The calculated composition of aerosols will be used to decide the status of the aerosol surfaces which in turn will change the reaction coefficients (or uptake rates) of the heterogeneous reactions.

2.2.2 Aerosol dynamics

The starting point for the aerosol model is the equation of conservation of particle mass (or number). Within that equation are terms that account for transport and dispersion, gas-to-particle conversion, coagulation, and removal processes. The aerosol module only deals with gas-to-particle conversion and coagulation processes.

2.2.2.1 AeroSolver

AeroSolver is a module to solve the aerosol dynamics equation by using a discretization technique to get the piecewise continuous approximations of the solution. The original version of AeroSolver is the framework for the numerical treatment of aerosol dynamics developed by *Sandu* [2006]. The sectional representation is used to represent the particle size distribution in this method. Compared with other methods to solve aerosol dynamics, this method allows a more accurate, less diffusive representation of particle distributions with sharp peaks when a small number of size bins is employed (see Section 2.1). This feature is important for 3-D air quality models.

A new version of AeroSolver is developed in the present study to correct the volume density issue in the older version by *Sandu* [2006] (see section 2.2.1.1). In this section, the current version of AeroSolver is presented and will be only used to solve the condensation/evaporation term in the aerosol dynamics equations in the 3-D STEM model.

2.2.2.1.1 The General Aerosol Dynamics Equation and Corrected

Form of Particle Growth in AeroSolver

Let $n(v,t)$ be the number concentration of particles with the volume between v and $v + dv$. The equation of conservation governing $n(v,t)$ can be written as [*Gelbard and Seinfeld*, 1978]

$$\frac{\partial n(v,t)}{\partial t} = -\frac{\partial[I(v)n(v,t)]}{\partial v} + \frac{1}{2}\int_0^v \beta_{v-w,w}n(v-w,t)n(w,t)dw - n(v,t)\int_0^\infty \beta_{v,w}n(w,t)dw$$
$$+ S(v,t) - R(v,t)n(v,t)$$

and $n(v,t=0) = n^0(v), n(v=0,t) = 0$ $\qquad$ (2.1)

where $I(v)$ is the particle growth rate due to condensation/evaporation, β is the coagulation kernel function, $S(v,t)$ is any external source of aerosols of volume v (e.g., nucleation), and $R(v,t)n(v,t)$ is the first-order rate of removal of aerosols of volume v (e.g., wet and dry deposition).

In equation (2.1) the modification in the number of aerosols due to growth is

$$\frac{\partial n(v,t)}{\partial t} = -\frac{\partial[I(v)n(v,t)]}{\partial v}$$
$\qquad$ (2.2)

For application to air quality models, one is generally interested in the aerosol mass or volume distribution, rather than the number distribution. We define the volume density as $V(v,t) = vn(v,t)$. Let $v_q(v,t)$, $q = 1,\dots,m$ be the volume of the q-th chemical component in particles of volume $v = \sum_{q=1}^m v_q$, then the multi-component aerosol population is described by the individual volume densities of each constituent $V^q(v,t) = v_q(v,t)n(v,t)$. The total volume density is the sum of the volume densities of its N individual components, $V(v,t) = \sum_{q=1}^m V^q(v,t)$.

The growth rate of species q is $I^q(v,t) = \frac{dv_q}{dt}$, and the total particle growth rate is

$$I(v,t) = \sum_{q=1}^m I^q(v,t).$$

The normalized growth rate of species q in a particle of volume v is $H^q(v,t) = \frac{I^q(v,t)}{v}$, and the total normalized growth rate of a particle of volume v is $H(v,t) = \sum_{q=1}^m H^q(v,t)$.

Using the above definitions, equation (2.2) becomes [*Gelbard and Seinfeld*, 1978; *Pilinis*, 1990]

$$\frac{\partial V^q(v,t)}{\partial t} = H^q(v,t)V(v,t) - \frac{\partial}{\partial v}[vH(v,t)V^q(v,t)]$$

(2.3)

For computational purposes equation (2.3) is transformed to logarithmic coordinates

$$\frac{\partial V^q(x,t)}{\partial t} = H^q(x,t)V(x,t) - \frac{\partial}{\partial x}[H(x,t)V^q(x,t)]$$

(2.4)

where $x = lnv$. Equation (2.4) is the correct form of the wrong equation (6) derived in *Sandu* [2006], which has then been used in the upgraded version of AeroSolver.

2.2.2.1.2 Piecewise Polynomial Discretization

Following the general approach developed by *Sandu and Borden* [2003], the dynamic equation is solved by a semi-discretization in particle size followed by a time integration of the resulting system of ordinary differential equations. The application of this discretization framework for piecewise polynomial basis is outlined in *Sandu* [*2006*].

For simplicity of the presentation in this section we discuss the discretization of the growth Equation (2.4) in the volume density, logarithmic formulation. The finite log volume interval is divided into s bins $I_j = [X^B_j, X^B_{j+1}]$. The point X^B_j is the boundary point between the bins I_{j-1} and I_j, with the endpoints $X^B_1 = X_{min}$ and $X^B_{s+1} = X_{min}$. The center of bin I_j is denoted by X_j. The solution is represented by a k-th order polynomial inside each bin I_j. The polynomials in different bins do not need to satisfy any continuity conditions across bin boundaries, therefore this representation of the solution is only piecewise continuous.

The polynomial representation inside each bin is written in terms of the orthogonal Lagrange basis polynomials. The set of Lagrange polynomials up to order 3 defined on [−1, 1] reads

$$P_0(x) = 1, P_1(x) = x, P_2(x) = -\frac{1}{2} + \frac{3x^2}{2}, P_3(x) = -\frac{3x}{2} + \frac{5x^3}{2}$$

(2.5)

Inside bin I_j the solution is represented as

$$V_h(x,t) = \sum_{l=0}^{k} u_j^l(t)\phi_j^l(x), \phi_j^l(x) = P_l\left(\frac{2(x-X_j)}{X_{j+1}^B - X_j^B}\right)$$

(2.6)

If we use *s* bins and polynomials of order k then the total number of degrees of freedom used to represent the solution is ndof = $s \times (k+1)$. These degrees of freedom are the solution coefficients $u_j^l(t)$ in each bin.

At the initial moment the continuous (in size) distribution $V(x, t^0)$ is available, the discrete solution coefficients are obtained by projecting the solution onto the discrete space,

$$u_j^l(t^0) = \frac{2l+1}{X_{j+1}^B - X_j^B}\int_{I_j} V(x,t^0)\phi_l^j(x)dx$$

(2.7)

In what follows for simplicity we use the single index notation; the vector *u* of discrete coefficients and the family $\{\phi_i\}_i$ of basis functions have ndof components. The bin component u_j^l becomes $u_{(j-1)\times s+l+1}$ in the single index notation, and similarly for the basis functions. For multiple chemical components the volume density distribution of component *q*, and the total volume density distribution are represented in discrete form as

$$V^q(x,t) = \sum_{i=1}^{ndof} u_i^q(t)\phi_i(x)$$

$$V(t) = \sum_{i=1}^{ndof} u_i(t)\phi_i(x) \quad \text{with} \quad u(t) = \sum_{q=1}^{m} u^q(t)$$

(2.8)

After discretization the problem to solve the partial different equations about $V^q(x,t)$ is changed to a problem to solve the ordinary differential equations about $u^q(t)$.

2.3 Case study

2.3.1 Verification of AeroSolver

For the numerical experiments we consider a test case from *Gelbard and Seinfeld* [1978], which admits an analytical solution. Let N_t be the total initial number of particles and V_m the mean initial volume. The initial number distribution is exponential, the coagulation rate is constant, and the growth rate is linear with the volume:

$$n^0(v) = (N_t / V_m)e^{-v/V_m}, \beta(v, w) = \beta_0, I(v) = \sigma_0 v \tag{2.9}$$

The analytical solution (see *Gelbard and Seinfeld* 1978) is

$$n^A(v, t) = \frac{4N_t}{V_m(N_t\beta_0 t + 2)^2} \exp\left(\frac{-2v \exp(\sigma_0)}{V_m(N_t\beta_0 t + 2)} - \sigma_0 t\right) \tag{2.10}$$

The equation was solved on the time interval [$t_{initial}$ =0, t_{final} =48 h] with a time step Δt = 6 min; the time step was chosen such that the time discretization errors are small compared to the size discretization errors. The volume interval is V_{min} =10^{-3} to V_{max} =1 μm^3.

To compare the relative merits of different discretization orders we first show the solutions obtained with ndof=12 degrees of freedom. There are 6 bins for piecewise linear polynomials, and 4 bins for piecewise quadratic. The computed solutions for the growth equations are presented in Figure 2.2. For plotting purposes the values of the piecewise polynomial computed solution is shown at 10 different points inside each bin. In general, all discretizations are able to relatively accurately compute the final solution for the growth-only case. The piecewise character of the solution is clearly visible for the lower order discretization (6bins with basic order of 1). However, when higher order polynomials are used, the solutions are very smooth and nicely follow the exact solution. For example, the third order numerical solutions are hardly distinguishable from the exact solution, even if they only use 4 bins.

A semi-Lagrangian flux scheme (referred as "dyCIT-PFISLM" [*Nguyen and Dabdub*, 2002]) has also been applied to solve the growth equation and the result is compared with AeroSolver in Figure 2.2 as well. It can be seen that even with 20 bins the solutions by the CIT-PFISLM method still differ from the exact solution in the small size section (particle volume less than 5E-3 μm^3 in Figure 2.2) due to numerical diffusion. It is well established that use of small numbers of the aerosol bins can significantly improve the computational efficiency because of consuming less time in the chemical equilibrium model, which is used to calculate the growth rate and needs high time-consumption.

These results help demonstrate AeroSolver is capable to accurately compute solutions of particle growth equations with less particle size bins (e.g., 4 bins with basic order of 3). Comparing with CIT-PFISLM method (considered as a reference for comprehensive dynamic approach), it is more efficient in regards to the computational times.

2.3.2 Equilibrium Versus Dynamics Approaches

In this section we compare two different approaches for the treatment of partitioning between the bulk gas phase and particles. These approaches can be summarized as follows:

1. Kinetic approach, where mass transfer is simulated explicitly; chemical concentrations in the bulk gas phase and in the particles may or may not be in equilibrium. In this approach, the complete dynamic method, dy-CIT-PFISLM and dy-AeroSolver are both applied.

2. CIT hybrid approach (referring as equilibrium approach here), where the bulk gas phase is assumed to be in chemical equilibrium with the whole particulate phase, but the distribution of condensable /volatile species among particles of different sizes is calculated using diffusion-limited assumptions. Although the whole particulate phase is in equilibrium with the gas phase, individual particles (or particles in a given size range) may not be in equilibrium with the gas phase.

To demonstrate the performance of the two gas/particle partitioning methods a scenario of *Pilinis et al.* (2000) was employed. This scenario was chosen because the aerosol compositions evolved in both liquid and solid states representing a realistic evolution for marine air being exposed to urban emissions. The initial aerosol distribution presented in this scenario is designed based on measurements made off the coast of Los Angeles [*Pandis et al.*, 1993]. It has two distinct modes (see Figure 2.3a). The fine mode (section 1-6) mainly consisted of ammonium sulfate and organics; and the coarse mode (section 7-10) is heavily influenced by sea salt.

As described in *Pilinis et al.* [2000], the model simulates gas and aerosol composition over 38 hours for a scenario that loosely represents summertime conditions in Southern California. The initial aerosol distribution is exposed to gas-phase concentrations of 0.3 μg m^{-3} of ammonia and

0.4 μg m^{-3} of nitric acid. Starting at midnight over the ocean, the air parcel is exposed to diurnal temperature and relative humidity changes (see time profile of T and RH in Figure 2.3b) with a constant H$_2$SO$_4$(g) production/emission rate of 0.24 μg m^{-3} h^{-1} for all 38 h of the simulation. At hour 13 (local time 1:00 p.m.) the air parcel reaches land and is exposed to a constant HNO$_3$(g) production of 4.2 μg m^{-3} h^{-1} until nightfall (6:00 p.m.). On the second day (hours 30-38) the same HNO$_3$(g) production rate is applied. These production rates, while reasonable for Southern California, are relatively high for most other locations. Two "spikes" of NH$_3$(g) emission (120 μg m^{-3} h^{-1} for 10 min) are encountered at hours 16 and 32 to stress the models as the local sources (see emission profile in Figure 2.3c).

The box model is used for the comparison of the mass transfer methods for this scenario. As aforementioned, the box model includes production and emission of gas-phase species and interaction between the gas and aerosol phases. However, the air parcel simulated here is a closed system that neglects dispersion and removal processes. The aerosol distribution is represented using 10 fixed sections from 0.05 to 10 μm, as shown in Figure 2.3a. Figure 2.4 and 2.5 presents the results predicted by the two approaches (including three methods, "eq", "dyCIT" and "dyAS" referring the equilibrium, dynamic CIT-PFISLM and dynamic AeroSolver methods, respectively). In addition in *Pilinis et al.* [2000] another comprehensive dynamic aerosol model, MADM (Multi-component Aerosol Dynamics Model), was applied for the same scenario. The results predicted by MADM are also adapted into Figure 2.4 and 2.5 for comparison.

As shown in Figure 2.5 b, d and f, for the first 16 hours of the simulations NH$_3$(g) concentrations are very low by those four methods (MADM, CIT hybrid, dynamic CIT and dynamic AeroSolver). Thus the first hours show only the gradual displacement of chloride by nitrate in the coarse mode (see Figure 2.4a, c and e and Figure 2.5a, c and e). This low ammonia concentration also promotes acidification of the aerosol as H$_2$SO$_4$(g) condenses.

At hour 13 the air parcel reaches land and at hour 16 a large influx of NH$_3$(g) occurs and the aerosol phase is rapidly neutralized by condensation of NH3(g). After NH$_3$(g) becomes available, HNO$_3$(g) and HCl(g) condensation also occurs. The relative humidity is low enough between the

hours of 10 and 19.5 and after hour 31 (7 a.m. on the second day) that at least some portion of the aerosol distribution is solid.

In general, the CIT hybrid method ("eq") predicts higher concentration for fine mode aerosol and lower values for coarse mode aerosol than the dynamics method for nitrate, sulfate, and ammonium after 38 hour because of continued uptake of gases (see Figure 2.4d, and Figure 2.5c and d). This is consistent with *Zhang et al.* [1999] and *Pilinis et al.* [2000] that showed higher concentrations of coarse mode nitrate predicted by the kinetic method than the equilibrium method because of the limitation of mass transfer between gas and aerosol phase. Comparing the dynamic CIT-PFISLM ("dyCIT") and dynamic AeroSolver ("dyAS"), the "dyAS" predicts even lower nitrate, sulfate and ammonium in the fine mode, while predicting higher concentrations in the coarse mode (see Figure 2.4f and Figure 2.5e and f).

Figure 2.4 and 2.5 show some oscillations at certain times for dynamic methods, especially the AeroSolver method. A large minimum time step (600 seconds) was used for dynamic methods in these case studies because this aerosol model is designed for 3-D models and small time step will cause too much computational time spent for large scale simulations. Sometimes the gas-aerosol system reaches equilibrium state faster than the assumed minimum rate, which will cause oscillations with dynamic methods. The AeroSolver method showed more accurate in previous case. So it showed more sensitive under larger time step here.

As shown in Figure 2.3a, the two modes consisted of different chemical compositions in the initial aerosol distribution, which means the hygroscopicity of these two modes are different too. This cannot be specifically treated in the equilibrium approach (CIT hybrid method), since the CIT hybrid method only considers the equilibrium between the bulk aerosol phase and the gas phase; inherently, the two modes only can have the same hygroscopicity. Moreover the absorbed/evaporated water are distributed to the different size sections by the weighting factors in the CIT hybrid method, which causes the smaller size sections to artificially obtain more water. This can be seen in Figure 2.6, where the liquid water untaken by fine and coarse mode particles over 38 hours simulated by equilibrium and dynamic methods (respectively "eq" and "dyCIT") are

presented. The dynamic method can predicate the different hygroscopicity in those two modes. Thus, when comparing Figure 2.6 and Figure 2.3b, the evolution of water uptaken can be clearly seen; lower values of water in the fine mode when relative humidity decreased and higher values when RH increased.

Compared with results from MADM, the prediction by the equilibrium method (CIT hybrid) is closer to the results of MADM than the dynamic methods ("dyCIT" and "dyAS"). However, it is important to notice that the box model comparison cannot distinguish which method is better, even though MADM, "dyCIT" and "dyAS" are all dynamic methods, because their results are not directly compared with the observations. One factor that may cause differences could be that the MADM model used a higher accommodation coefficient ($\alpha=0.1$) than the one we used ($\alpha=0.01$). For example, at hour 16 Figure 2.5 shows a faster mass transfer rate in MADM than our dynamic models for the uptake of HNO_3. The higher accommodation coefficient in MADM will cause the calculated condensation/evaporation rate to be much higher, which causes the system to more quickly moving to equilibrium. In the first hour the air parcel was over the sea with low NH_3 concentrations. The gradual displacement of chloride by nitrate happened only in the coarse mode. The results from the CIT hybrid method and MADE show faster evaporation of chloride from the coarse mode than the dynamics methods (see Figure 2.4). The other possible reason for the differences is that MADM and the new aerosol model use different aerosol thermodynamic equilibrium model, which may lead to different predictions for deliquescence/crystallization behavior.

2.4 Conclusions

In this Chapter, a new non-equilibrium approach, dynamic AeroSolver, to solve the growth equation of aerosol due to condensation/evaporation process in 3-D STEM model is introduced and verified. It is concluded that dynamic AeroSolver is capable to accurately compute solutions of particle growth equations with less particle size bins (e.g., 4 bins with basic order of 3). Higher order polynomials help to deamplify the piecewise character. Comparing with CIT-PFISLM

method (considered as a reference for comprehensive dynamic approach), it is advanced regarding the computational consumption.   This new aerosol module will significantly improve the simulating accuracy and computational efficiency for 3-D STEM model.

Before embedding this new aerosol module into 3-D STEM model, a box model is designed and constructed to evaluate the behaviors of the new dynamic AeroSolver in the scenario studies. With the box model, the new dynamic AeroSolver method has been compared with the equilibrium CIT hybrid method, as well as the comprehensive dynamic CIT-PFISLM and MADM methods, in regarding to the gas/particle partitioning for condensable inorganic compounds between gases and aerosol phases. Compared with the MADE model, the two dynamic methods in the new aerosol model can produce reasonable results. The discrepancies between different approaches and methods are also discussed.

Table 2.1 The initial conditions for the case in Section 2.3.2

	OA (ug/m^3)	NO$_3^-$ (ug/m^3)	NH$_4^+$ (ug/m^3)	Cl$^-$ (ug/m^3)	Na$^+$ (ug/m^3)	SO$_4^{2-}$ (ug/m^3)
Bin1	0.79	0.25	0.17	0	0	0.36
Bin2	0.57	0.25	0.25	0	0	0.5
Bin3	0.5	0.2	0.35	0	0	0.8
Bin4	0.3	0.21	0.49	0	0	1.22
Bin5	0.1	0.09	0.2	0	0	0.6
Bin6	0.06	0.1	0.16	0	0	0.4
Bin7	0	1.58	0.26	0.95	1.22	0.9
Bin8	0	0.5	0	1.08	1	0.3
Bin9	0	0.11	0	0.24	0.21	0.08
Bin10	0	0.07	0	0.15	0.11	0.05
NH$_3$ (ug/m^3)	0.3					
HNO$_3$ (ug/m^3)	4.0					
HCl (ug/m^3)	0.1					

Aerosol operator

Gas chemistry operator

STEMAero Module

Gas Chemistry

C_{gas}, $C_{aerosol}$

Nucleation

Coagulation

k_{heter}= func (size, composition)

Heterogeneous Reactions

Condensation/Evaporation

Equilibrium Option

CIT Hybrid

(SCAPE2 for gas-aerosol thermodynamic equilibrium)

Aerosol tracer

emission, removal, transport/dispersion

$C_{aerosol}$

Dynamics Option

CIT PFISLM

AeroSolver

Figure 2.1 The structure of the box model. The parts with red border are the parts in the new aerosol module.
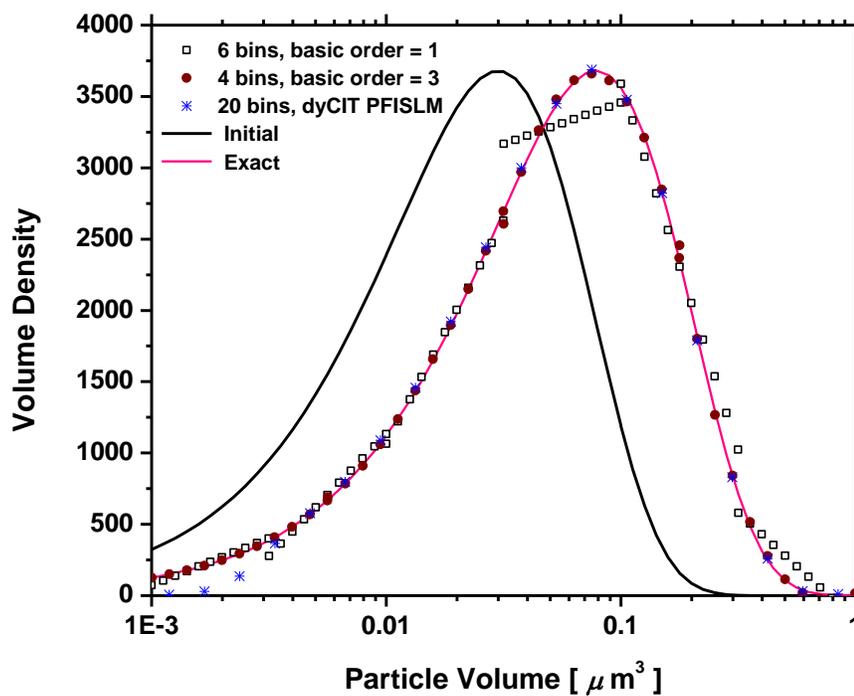
Figure 2.2 The solutions for the growth equation obtained with *ndof*=12 degrees of freedom, different discretization orders. Compared with results from CIT-PFISLM, results with higher order discretization is very accurate despite using a small number of bins.
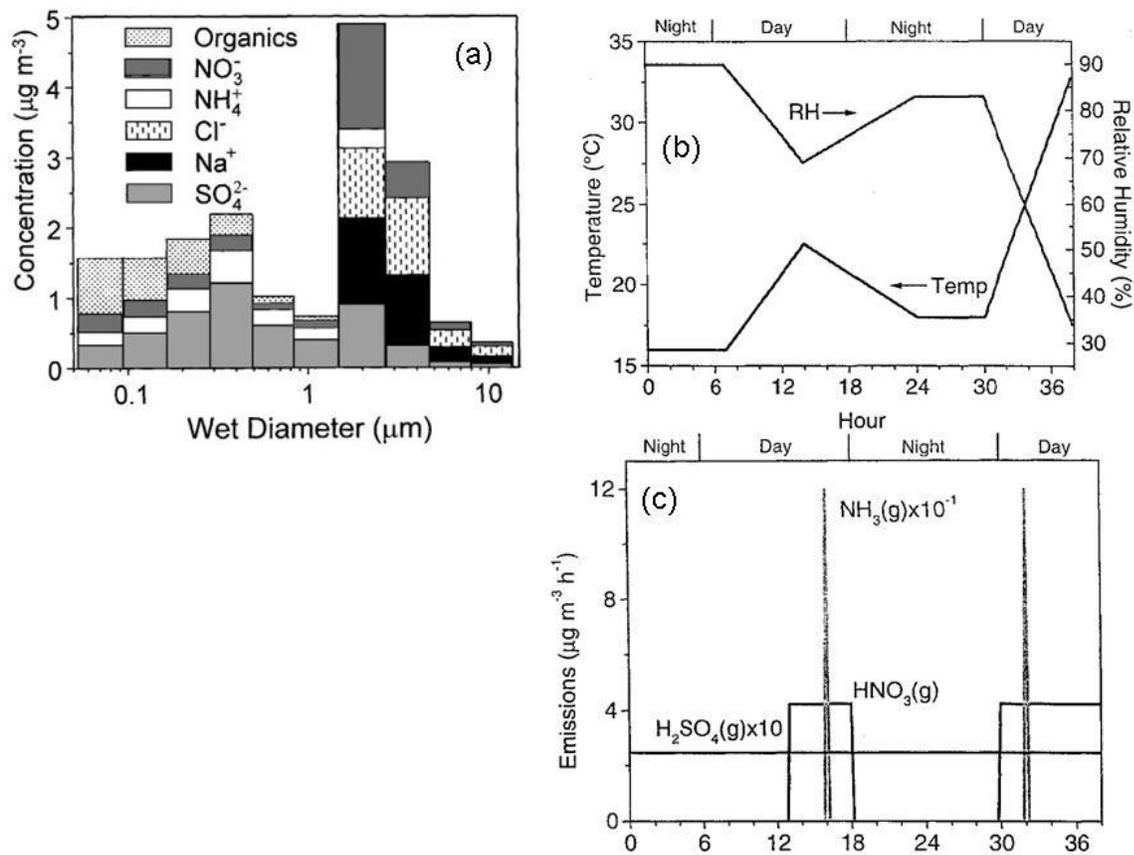
Figure 2.3 Initial aerosol composition and size distribution, temperature and relative humidity profile, and the emission profile for NH_3, HNO_3, H_2SO_4. for the test case in Section 2.2. (adapted from *Pilinis at al.* 2000)
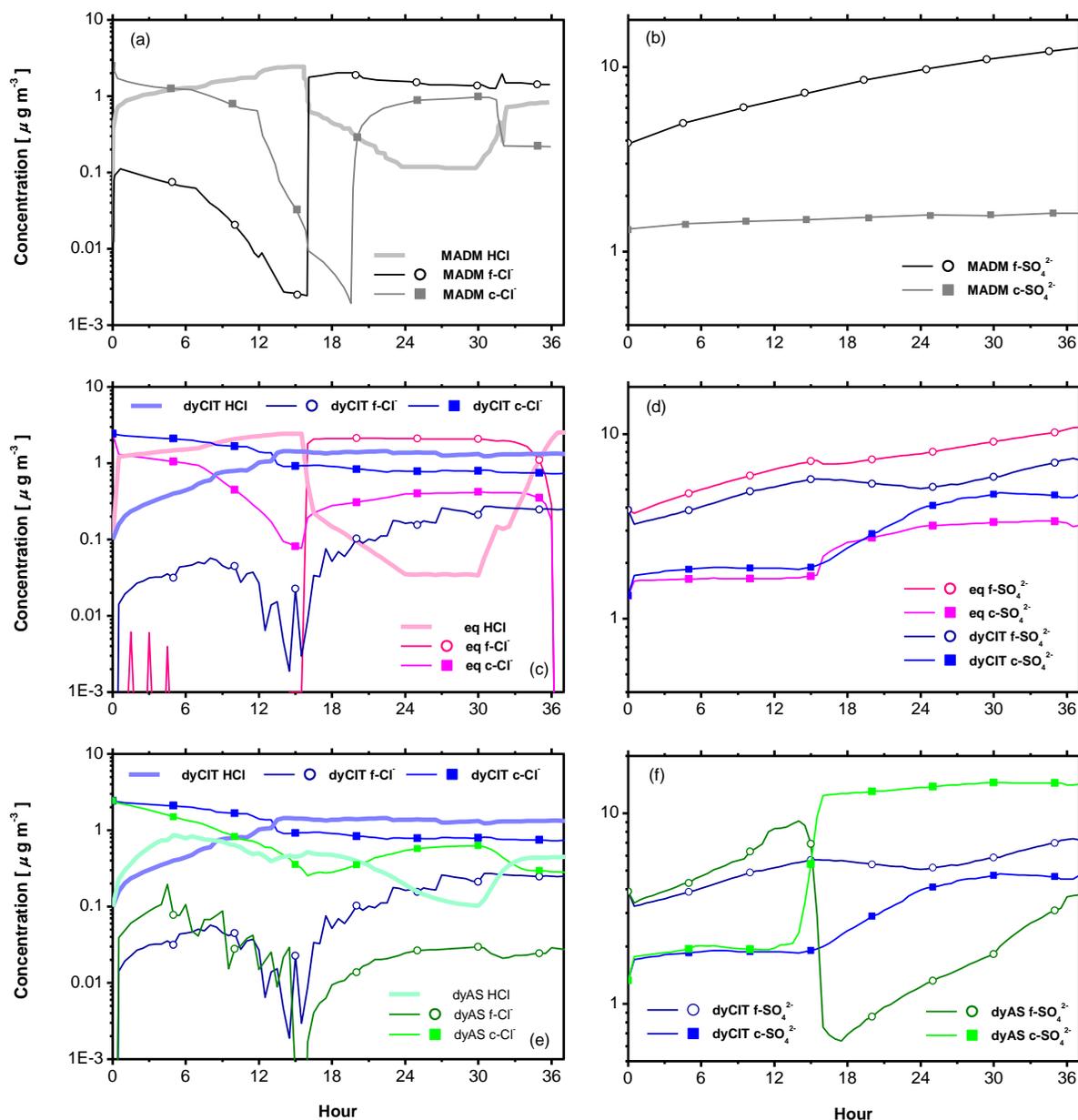
Figure 2.4 Gas and aerosol prediction of the scenario for sulfate and chloride. (a)(b) the results from MADM (adapted from *Pilinis at al.* 2000); (c)(d)(e)(f) the results from the new aerosol module. Results predicted by equilibrium approach are pink color; results from dynamic CIT-PFISLM method are blue; results from dynamic AeroSolver method are green. The fine mode is shown by open symbols; the coarse mode by solid point; the gas phase by line
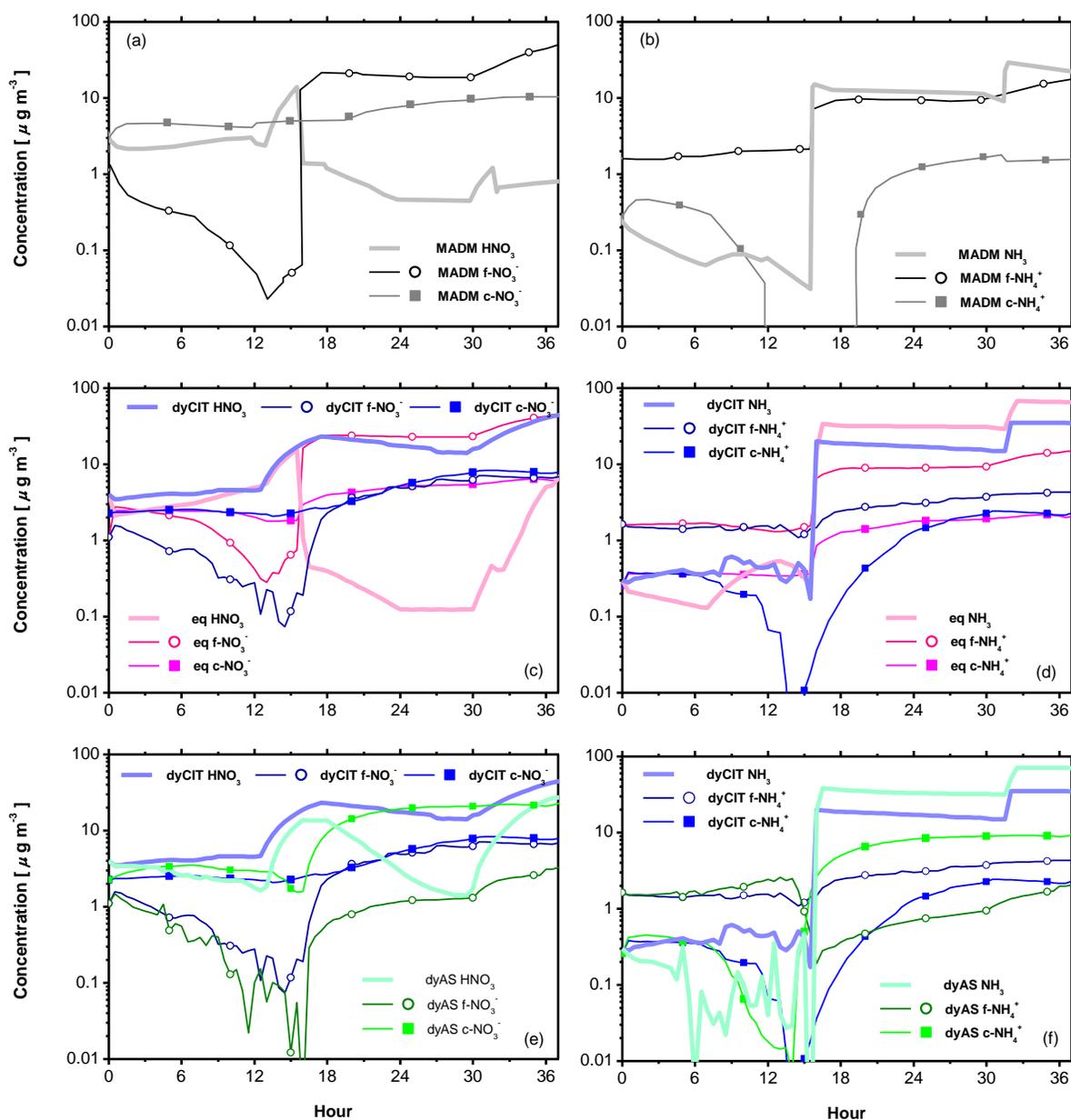
Figure 2.5 Gas and aerosol prediction of the scenario for ammonium and nitrate. (a)(b) the results from MADM (adapted from *Pilinis at al.* 2000);(c)(d) the results from the new aerosol module. Results predicted by equilibrium approach are pink color; results from dynamic CIT-PFISLM method are blue; results from dynamic AeroSolver method are green. The fine mode is shown by open symbols; the coarse mode by the solid point.
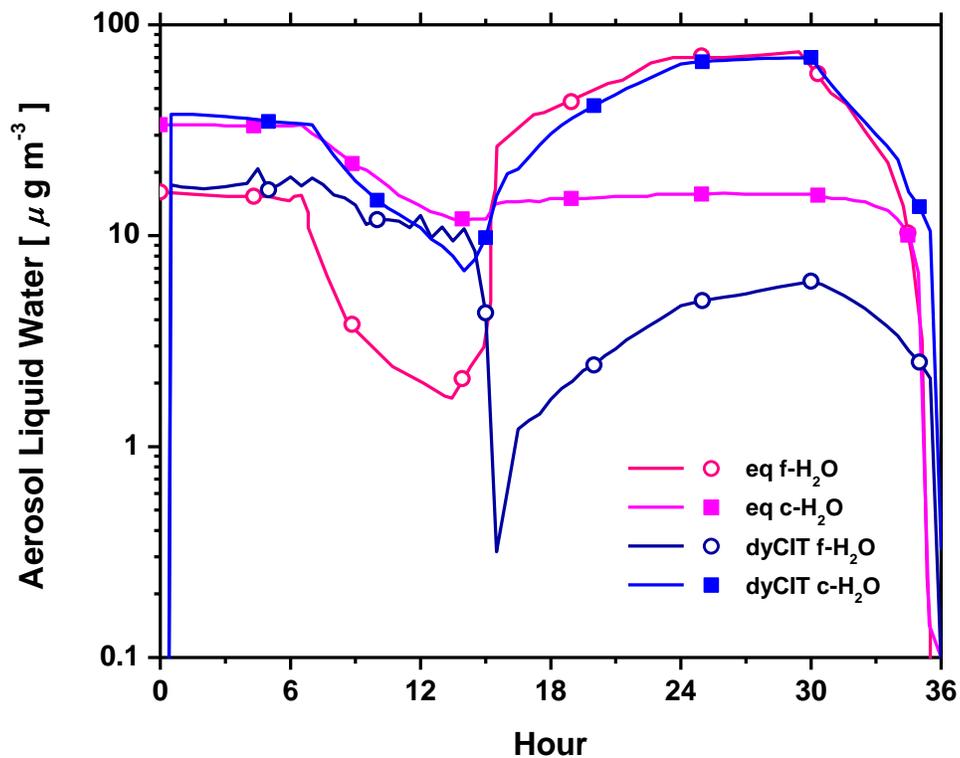
Figure 2.6 Predicted aerosol liquid water in fine and coarse modes by the two methods in the new aerosol module. The results predicted by the equilibrium approach are shown with red color; the dynamic CIT-PFISLM method with blue color.

CHAPTER 3

THE IMPACTS OF HETEROGENEOUS REACTIONS ON

ATMOSPHERIC CHEMISTRY

3.1 Introduction

It is well proven by modeling studies and field observations that heterogeneous chemistry can affect the photochemical oxidant cycle [*Zhang and Carmichael* 1999;*Dentener and Crutzen* 1993;*McNaughton et al.* 2009]. In a review *Jacob* [2000] recommended that standard O_3 models should include the heterogeneous uptakes of HO_2, NO_2, NO_3, and N_2O_5 by aqueous aerosols and clouds in their mechanisms. In most models heterogeneous reactions are treated in a relatively simplistic manner without considering the complexities of surface chemistry. They assume a heterogeneous reaction is modeled as a pseudo-first order kinetic reaction. The rate constant contains the number density of particles at a given radius, the uptake coefficient, and a gas-particle diffusion correction.

Results from laboratory studies show that surface chemistry of aerosols is complex. *Usher et al.* [2003a] recommended different mechanisms for heterogeneous chemistry of trace atmospheric gases on dust particles. These mechanisms provide molecular level insight into potentially important tropospheric reactions that can be incorporated into atmospheric chemistry models. However, most modeling studies treat heterogeneous reaction as simple pseudo-first order kinetic reaction with fixed uptake coefficient (or reaction probability) γ.

Krueger et al. [2004] investigated the heterogeneous uptake of HNO_3 on dust particles from different source regions. They found clear differences in the reactivity of mineral dusts from these different dust regions with nitric acid, which is mainly due to the particularly reactive carbonate components in these dust particles. They suggested that carbonate-containing minerals should be explicitly considered in the models because of their unique reactivity at least with respect to nitric acid in the atmosphere.

After atmospheric aging and processing, mineral dust particles are often coated with nitrates, sulfates, and organics. In laboratory experiments *Usher et al.* [2003b] found that the reactivity of mineral dust particles could be changed after being processed or aged in the atmosphere. In some cases, it was found that the reactivity of ozone with pretreated particles was significantly reduced whereas in other cases the reactivity was enhanced.

The reactions of acidic gases with mineral aerosol have been studied extensively in the laboratory [*Underwood et al.* 2001; *Usher et al.* 2002]. However, many results from laboratory studies are obtained from experiments on dry particles and often represent lower estimates for reaction rates. *Liu et al.* [2008] examined HNO_3 uptake on $CaCO_3$ particles over a wide range of relative humidity (from 10 to 80%) in laboratory experiments. The net reaction probability was found to increase with increasing relative humidity, from $\gamma_{net} \geq 0.003$ at RH = 10% to 0.21 at 80%. *Song et al.* [2007] investigated the dependence of the γ values on relative humidity (RH) and suggested that particular attention should be paid to the issue of the RH-dependent γ in future dust chemistry transport modeling studies along with the issue of aerosol mixing state.

The uptake of HNO_3 on dust is very important to atmospheric chemistry. Due to the formation of the deliquesced nitrate product in the aged dust particles, the uptake of nitric acid and other gas-phase pollutants (e.g. SO_2, NO_y, HO_x, O_3, organics, etc) may be enhanced by orders of magnitude. In turn, aqueous chemistry in the deliquescent coating will take place, e.g. uptake of SO_2 into particle droplets followed by its oxidation to sulfate. In addition, optical properties and the ability to serve as an effective CCN will be also greatly enhanced in the aged dust particles.

In this chapter the importance of different schemes for heterogeneous reactions on atmospheric chemistry is investigated in a box model. The findings about the complexity of surface chemistry are put in the context of the real atmosphere and assessed by modeling studies.

3.2 Model description

The effects of the complexity of heterogeneous reactions on tropospheric chemistry are studied by using a time-dependent, multiphase chemistry box model. Box model simulations were performed using the gas phase mechanism that is in the STEM-II model [*Carmichael et al.*, 1991]. The gas phase chemical mechanism is based on that of *Lurmann et al.* [1986] but has been modified to include low-NOx conditions and an explicit treatment of isoprene. It consists of 83 chemical species and 185 gas phase reactions.

Heterogeneous reactions are treated as pseudo-first order reactions in this model. This approach has been taken by several investigators for the purpose of modeling the interaction between the gas phase species and the dust/aerosol particles [*Zhang* 1994; *Dentener et al.* 1996; *Sander and Crutzen* 1996; *Saylor* 1997]. For the calculation of dC_j/dt, the following equations are used [*Fuchs and Sutugin*, 1970]:

$$\frac{\partial C_j}{\partial t} = \int_{r2}^{r1} 4\pi r^2 F(r) \frac{dn}{dr} \qquad (3.1)$$

$$F(r) = \frac{D_j(C_j - C_j^e)/r}{1 + f(\gamma, K_n)K_n} \qquad (3.2)$$

$$f(\gamma, K_n) = \frac{1.333 + 0.71 K_n^{-1}}{1 + K_n^{-1}} + \frac{4(1-\gamma)}{3\gamma} \qquad (3.3)$$

where C_j is the gas phase concentration of the absorbing species and C_j^e is the equilibrium gas phase concentration of species j that would be in equilibrium with the surface-adsorbed species (this term can be related to surface coverage and surface saturation effects), D_j is the gas phase diffusion coefficient in cm^2 s^{-1}, K_n is the dimensionless Knudsen number ($=\lambda/r$), λ is the effective free path of a gas molecule in air, r is the particle radius, $F(r)$ is the flux of the trace species to the surface of the aerosol particle with radius r in molecules cm^{-2} s^{-1}, dn/dr is the number-size distribution of

aerosol particles, and γ is the accommodation or uptake coefficient (sometimes denoted as α). In this case C^e_j is zero.

The uptake coefficient (or reaction probability) of a heterogeneous reaction is fixed as a constant during simulation in the base case. But for individual cases the scheme to calculate the uptake coefficient could be complex and the impacts of some factors (such as relative humidity, available active sites at surface and coating on surface) on heterogeneous reactions will be considered in the calculation of uptake coefficient.

3.3 Results and Discussions

3.3.1 The impacts of dust reactions in East Asia

Conditions representative of Cheju, Korea, were considered. Cheju is an island located in the East China Sea, which is impacted by anthropogenic pollution and mineral aerosol during the frequent continental outflow events in the spring. The case was used in *Underwood et al.* [2001] to quantify the role of heterogeneous reactions of gaseous nitrogen and nitric acid on mineral dust particles in tropospheric ozone formation. A lognormal distribution was utilized for the aerosol number-size distribution. The parameters for the Cheju simulation were taken from *Zhang* [1994]: $n = 7.98$ (numbers of particles per cm^3), $r = 0.88\mu$m, $\sigma = 0.23$. If dust density is assumed to 2.5 g/cm^3, the dust loading with this size distribution will be 192.07μg/m^3. More details about size distribution can be found in Table 3.1. The initial concentrations and conditions are listed in Table 3.2. This test case represents the impact of a dust storm on the background tracer concentrations of East Asia.

3.3.1.1 The effect of mineralogy

Usher et al. [2002] proposed that the uptake coefficient of a gaseous species on real mineral dust particles can be calculated by using the γ measured from pure mineral

oxides and carbonate. A dust sample would have a reactivity that can be calculated according to the equation below:

$$\gamma_{loess} = \sum f_i \gamma_i \tag{3.4}$$

where f_i is the fraction of the ith component in the dust sample and γ_i is the measured uptake of the ith component. For example, 10 atomic percent for Al and Fe will result in 5 percent Al_2O_3 and Fe_2O_3. The calculated γ of China Loess particles for SO_2 uptake was within the experimental error of measured value from real particles.

In this section equation 3.4 will be applied for all heterogeneous reactions. The effects of mineralogy on the heterogeneous uptakes of O_3, SO_2, N_2O_5 are individually evaluated in a box model. Each time only one reaction of one gas is tested with different mineralogical settings. Two types of dust are used to calculate the uptake coefficients in these model studies, Saharan dust and China Loess. The information of their chemical compositions is summarized in Table 3.3. The γ measured from different particles are listed in Table 3.4. For comparison we also show three results, the run with the γ measured from real China Loess, the run with the fixed γ used in STEM model, and the run without any heterogeneous reaction.

3.3.1.1.1 O_3

The results for O_3 reaction are shown in Figure 3.1a and 3.1b. The $\gamma(O_3)$ used in STEM model is 5×10^{-5} [*Dentener et al.*, 1996; *Jacob*, 2000; *Michel et al.*, 2003]. Plotted are O_3 and HNO_3 mixing ratios over a 120 hour period. Under model conditions, ozone quickly increases at first. However, the NOx in the system is rapidly converted to other forms (PAN, HNO_3, etc.) and the ozone production rate decreases quickly, and the system switches to a net ozone destructive environment after ~30 hours. After this time, ozone decreases due to chemical destruction and dry deposition. The effect of the O_3 heterogeneous reaction is to accelerate the O_3 loss rate. The heterogeneous uptake of O_3 can also slightly affect HNO_3 concentration in Figure 3.1b through the photochemical

cycles. In Figure 3.1a the run with γ measured from real China Loess has the lowest predicted O_3 value. The O_3 depletion due to heterogeneous reaction in this run is about two times the value in the run with γ calculated from the given chemical compositions of China Loess. The run with the fixed γ used in STEM model has the lowest O_3 depletion and is closed to the results with γ calculated from the given chemical compositions of dust. The results in this test case indicate that the ozone heterogeneous reaction is not sensitive to the mineralogy of dust particles.

3.3.1.1.2 N_2O_5 and SO_2

The results for N_2O_5 reaction are shown in Figure 3.1c. The $\gamma(N_2O_5)$ used in previous modeling study is 0.01 [*Song et al.*, 2007]. The effect of mineralogy on this reaction is shown not to be significant. Using a γ value of 0.01 could over-estimate the depletion of N_2O_5. Model results don't show a significant impact of N_2O_5 reaction on other species.

The results for SO_2 reaction are shown in Figure 3.1d. No impact can be seen in the figure due to lower uptake rate on dry particles.

3.3.1.2 Surface saturation

Underwood et al. [2001] studied the saturation effect on NO_2 heterogeneous reaction in a modeling study. When the surface saturation is accounted for in the model, the impact of NO_2 reaction was neglectable. The heterogeneous reactions of HNO_3 and SO_2 are currently included in the STEM model. Laboratory results show saturation effect exists on the surface of dry aerosol for these heterogeneous reactions. The importance of saturation effect is assessed in this study. Surface coverage is calculated and the uptake rate is a function of surface coverage:

$$\gamma = \gamma_0 (1 - \theta) \tag{3.5}$$

where γ_0 is the initial uptake coefficient and θ is the surface coverage. When saturation is reached, θ is equal to 1 and the uptake rate is equal to zero, then the reaction is shut down.

Dust in East Asia is often emitted from regions with low relative humidity. The results show that the uptake of HNO_3 and SO_2 on dry aerosols may be overestimated without consideration of saturation effect.

When $\gamma = 3.0 \times 10^{-5}$ is used for the uptake of SO_2, which is the lower limit, the surface is saturated after 2 hours in Figure 3.2a. When $\gamma = 1.14 \times 10^{-3}$ is used for the uptake of HNO_3, the surface is saturated after 16 hours (Figure 3.2b). But Figure 3.2c shows that the impact of HNO_3 reaction with this γ value is small.

3.3.1.3 Coating

In the troposphere, wind-blown particles can be transported over long distances, and during this transport these particles have ample opportunity to interact with other trace gases in addition to ozone, including inorganic gases such as the oxides of nitrogen and sulfur, as well as organics. Field studies show that atmospheric particulates are often coated in nitrate and sulfate species, and also with organic matter. *Usher et al.* [2003b] reports the effects of different coatings on aerosol for the O_3 reaction. In their papers, they discussed site-specific uptake of ozone on unprocessed and laboratory-processed α-Al_2O_3 and SiO_2. For coated aerosol, i.e. laboratory-processed α-Al_2O_3 aerosol by SO_2 or HNO_3, the reactive uptake of ozone is considered to have two contributions. One contribution is from ozone uptake on unreacted oxide active sites and the other is from ozone uptake on the adsorbate site. Thus for the laboratory-processed oxide one can write that

$$\gamma_{(processed)} = \sum f_i \gamma_i = f_1 \gamma_{(oxide\ active\ sites)} + f_2 \gamma_{(absorbate\ active\ sites)} \tag{3.6}$$

This can be generalized as follows:

$$\gamma_{(processed)} = \sum f_i \gamma_i \qquad\qquad (3.7)$$

where f_i is the fraction of sites either occupied by adsorbates or oxide active sites, and γ_i is the measured uptake value for each of these sites.

Equation 3.7 is applied in the box model to assess the impact of nitrate and sulfate coatings on the uptake of ozone. On the aerosols with coatings the reaction coefficient for O_3 reaction is changed. The nitrate coating reduces the reactivity of O_3; the sulfate coating increases the uptake of O_3. Figure 3.3 shows that both nitrate and sulfate coatings can affect O_3 reaction significantly.

3.3.1.4 RH-dependent heterogeneous uptake of HNO_3 and

mineralogy

Liu et al. [2008] reported HNO_3 uptake coefficients on $CaCO_3$ particles over a wide range of relative humidity (from 10 to 80%) in laboratory experiments. The RH-dependent uptake coefficients are listed in Table 3.5. The impact of this reaction on dust aging is assessed in a box model study.

Figure 3.4 shows the effect of relative humidity on the heterogeneous uptake of nitric acid gas on pure calcite particles. At dry condition (RH=0%), the concentration of gaseous HNO_3 decreases significantly due to the uptake of HNO_3 on dust. The present of water vapor in the atmosphere can promote the heterogeneous uptake of HNO_3 on pure calcite particles greatly. Even at low RH condition (RH=20%), the HNO_3 concentration after 120 hours drops ~50%. When RH is 40% or higher, the uptake of HNO_3 is limited by the available HNO_3. As the modeling results show, the heterogeneous uptake of HNO_3 on pure calcite particles is significantly affected by relative humidity.

The results from pure calcite were extended to real dust. The reactivity of dust particle can be calculated from the pure component oxides and carbonates by using the method from *Usher et al.* [2002]. The compositions of Saharan dust and China loess are taken from *Krueger et al.* [2004]. The γ values for each component are listed in Table 3.4.

The reaction probability of $CaCO_3$, not CaO, is used in the calculation. The effect of RH is considered for the $CaCO_3$ component in dust.

Figure 3.5 shows the effects of mineralogy and relative humidity on the heterogeneous uptake of HNO_3 on dust. The model results are summarized in Table 3.6. Five cases are shown on each figure. We chose three cases as background case. One is the case without heterogeneous reaction, which is used to demonstrate the impact of heterogeneous uptake by comparing with the cases with heterogeneous reaction. Since many models use fixed gamma with heterogeneous reaction, two cases with fixed gamma are shown here for comparison.   One case uses $\gamma = 0.1$ which is used in many models [*Dentener et al.* 1996; *Bauer et al.* 2004]. The other case used a gamma value of real china loess measured under dry condition. This gamma value may be a lower limit for real dust particle. Under dry condition all three cases using real or calculated gamma for dust got similar results. The effect of heterogeneous reaction in these cases is small. The case with $\gamma = 0.1$ predicted very big impact of heterogeneous reaction and resulted in very low concentrations of HNO_3. Under RH=40% condition China loess with its higher fraction of $CaCO_3$ caused more heterogeneous uptake of HNO_3, which is comparable with the case with $\gamma = 0.1$. Saharan dust with a lower fraction of $CaCO_3$ absorbed less HNO_3, but it was still much higher than the case with gamma from real china losses. So in real atmospheric conditions the effect of RH on the heterogeneous uptake of HNO_3 on dust is significant and the effect of mineralogy is also not neglectable. Under high relative humidity condition (RH=80%), both china loess and Saharan dust uptake a similar amount of HNO_3.

The case considering the effect of RH and mineralogy on the uptake of HNO_3 shows that the effect of mineralogy is significant and the impact of RH is much greater than mineralogy. Both of these two factors should be include in models. The case with $\gamma = 0.1$ tends to overestimate the heterogeneous uptake of HNO_3 on dust and nitrate concentration. The case with γ measured from real china loess represents a lower limit for

the effect of heterogeneous reaction of HNO_3 on dust. How to extrapolate laboratory data to real atmospheric condition needs to be considered carefully, when using this information in models.

3.3.2 The effect of RH-dependent heterogeneous uptake of HNO_3 on dust aging during transport

3.3.2.1 Model description

A case based on the back trajectory study from airborne observations during ACE-ASIA field campaign is used to test the hypothesis about the RH-dependent heterogeneous uptake of HNO_3 on dust. The case represents the dust chemical aging after passing through a polluted urban region. The initial concentrations of gaseous species are generated from the monthly average of 3-dimensional model results without considering dust effects. More details about the 3-D modeling results can be found in *Song et al.* [2007]. The heterogeneous uptake of HNO_3, NO_3, N_2O_5, SO_2, H_2SO_4 are included in the study. The aerosol size distribution is constrained by the observed aerosol geometric surface areas on the flight track. The surface areas for calculating the heterogeneous reaction rates are fixed as the value at the beginning of simulation. The average volume diameter for fine and coarse modes were 0.23 μm and 1.4 μm, respectively. The initial sulfate and nitrate concentrations were assumed to be zero. The initial concentrations and uptake coefficients are listed in Table 3.7.

We use results from two groups of runs to demonstrate the effects of RH on heterogeneous reactions and tropospheric chemistry. The first group will show the effect of different transport paths. There are different RH profiles along the different paths. Three paths from C130 Flight #8 are chosen for modeling study and are shown in Figure 3.6. These paths ended on the flight track at GMT time 03:59, 04:29 and 05:05. The RH values along these trajectories were extracted from 3-D model results for modeling study. In the second group the path ended at 05:05 is chosen for sensitive studies about the

RH-dependent uptake of HNO_3, which will be compared with the other two cases. In one case γ was calculated with a fixed RH (= 20%), the other uses fixed γ (=0.01), which is a common setting in previous studies, is shown here for comparison.

3.3.2.1.1 Effects on chemistry

Figure 3.7a shows the RH values used in each run. The calculated heterogeneous uptake coefficients in fine and coarse mode are show in Figure 3.7b and 3.7c. The γ calculated with the RH-dependent uptake coefficients show the same variability as the RH profiles. Uptake coefficient γ =0.01 is the lower limit for the γ values along these paths, and close to the γ at RH = 20%.

Figure 3.8a and b shows the variations of $[NO_3^-] + [SO_4^{2-}]$ (in meq/m^3) with time in fine and coarse mode dust particles. The saturation concentration (SC) for fine-mode dust particles was also introduced and these concentrations are marked in Figure 3.8a for the C130 flights. Here, the saturation concentration ($[NO_3^-] + [SO_4^{2-}]|_{SC}$) was defined as the $[NO_3^-] + [SO_4^{2-}]$ concentration by which (or when) carbonate in fine-mode dust particles is completely depleted. As shown in Figure 3.8a, the saturation concentrations for C130 Flight #8 is predicted to be reached within ~20 hrs, which is faster than the chemical aging times of 42–62 hrs estimated by trajectory analysis. Figure 3.6b shows the dust particles still don't reach the saturation concentration completely when they arrive at the flight track. Figure 3.8c shows the nitrate values in all runs arrived at the same constant in 10 hours due to fast uptake of HNO_3. After all calcite were consumed by HNO_3 the heterogeneous uptake of HNO_3 stopped and the nitrate on dust particle reached the same constant. The effect of RH-dependent heterogeneous uptake of HNO_3 can be seen clearly in Figure 3.8c. The nitrate value in the run of "Flight #8 0505" could be up to ~2 times of the nitrate calculated at low RH condition (the run "RH=20%").

Model results show that even when considering the RH-dependent HNO_3 uptake the simulations can't explain the observed slow dust aging. Compared with the case in

Section 3.3.1, the initial HNO_3 concentration in this section is very high. In the model setting of this section the uptake of dust is the major consumer of HNO_3, which is not true in many other scenarios. *Song et al.* [2007] suggested that including urban-derived pollution particles may bring a competitor for the uptake of HNO_3 and then can slow down the dust aging rate.

3.3.2.1.2 Impacts on aerosol optical properties

Particle extiction coefficients in the model are estimated as

$$b_{ext} = \sum_{i=1}^{N_B} n_i C_{ext,i} \, , C_{ext,i} = \pi D_{p,i}^2 Q_{ext,i}/4$$

In these equations, n_i is the particle number concentration in the size bin *i*, b_{ext} is aerosol extinction coefficients, $C_{ext,i}$ is the extinction cross-section of a particle, $D_{p,i}$ is the diameter of a particle, $Q_{ext,i}$ is the extinction efficiency of a particle. The extinction efficiency is determined from a Mie code for spherical particles.

The refraction index of a particle in a size bin can be calculated by using two methods. One is using the OPAC data set [*Hess et al.*, 1998]. This method is used in the currrent STEM model. OPAC calculates aerosol optical properties as an external mixture of different types of aerosols. Five types of aerosols can be used in our model.   They are dust, sea-salt, organic carbon, black carbon, and water-soluble inorganic aerosol. For our case, after aerosol size distribution and compositions are calculated, the internal mixture are seperated into two types of aerosols, dust and water-soluble aerosol. By inputing the mass concentrations of the two types of aerosols, OPAC calculates their optical properties according to assumed aerosol compositions and size distributions.

The other method considers particle as an internal mixture of all compositions. When detailed information about aerosols is available, the new aerosol model can calculate aerosol optical properties at 550 nm according to aerosol compositions and size distribution calculated by model. In this section we assume dust particle only have

scattering extinction. The method of partial molar refractions [*Stelson* 1990] was used to calculate the real portion of the refractive index. Values of the partial molar refractions of all chemical species were taken from Stelson's paper [*Stelson* 1990]. The complex refractive index at 550 nm was obtained by volume averaging the refractive index of the scattering and absorbing components.

The growth of dust particles are shown in Figure 3.9a and Figure 3.9b. Due to the fast uptake of HNO_3 on dust   and then the deliquescence of nitrate, a significant amount of water was absorbed onto dust particle, which causes the fast growth of particles in ~10 hr. For example, for "Flight #8 0505", the aerosol water content in fine mode increased ~6 ug/m3 (see Figure 3.9d, about 60% of initial aerosol mass. In order to see the effect of RH-dependent uptake more clearly, Figure 3.9c shows the growth of fine-mode particles in the first 10 hour. The radius in the run of "Flight #8 0505" could be up to 50% larger than the radius calculated at low RH condition (the run "RH=20%").

The difference in particle size will cause a difference in aerosol optical properties, which is shown in Figure 3.10. The fine-mode extinction coefficients b_{ext} calculated with the internal mixing method are presented in Figure 3.10a and Figure 3.10b. After 42~62 hr transport the final b_{ext} could be 4~7 times of the initial b_{ext}. The b_{ext} in the run of "Flight #8 0505" could be up to 50% larger than the b_{ext} calculated at low RH condition (the run "RH=20%").

The fine-mode extinction coefficients calculated by using OPAC are shown in Figure 3.10c. The final b_{ext} calculated with internal mixing method are 3~5 times of the b_{ext} calculated by OPAC after 42~62 hr transport. Since OPAC used assumed size distribution, the different growth rate in different aerosol modes can't be counted in OPAC, which tends to underestimate the fine-mode b_{ext}. The assumed chemical compositions in OPAC also possibly caused the underprediction of absorbed water when compared with the hygroscopic growth of $Ca(NO_3)_2$.

3.4 Conclusions

The studies in laboratory and field observation show surface chemistry is complex. However, heterogeneous reactions are usually treated in a relatively simplistic manner and modeled as a pseudo-first order kinetic reaction with fix uptake coefficient. A box model is used to assess the importance of different complex schemes for heterogeneous reactions on tropospheric chemistry.

Model results show that considering surface saturation in heterogeneous reactions usually reduces the impact of heterogeneous reactions greatly. The effect of mineralogy is significant on the ozone heterogeneous reaction. Though the impact of mineralogy is not significant for the uptake of HNO_3 on dry dust particles, it becomes significant after considering RH-dependent uptake of HNO_3 on $CaCO_3$.

A box model study is used to assess the effect of the RH-dependent uptake of HNO_3 on dust aging during transport. Before $CaCO_3$ is consumed completely, the importance of RH-dependent uptake is confirmed by modeling study. But the predicted fast dust aging rate in modeling study is not consisted with observations. It is suggested that including urban pollution particles may be very important to the accurate prediction of dust aging.

Table 3.1 Aerosol size distributions in Section 3.3.1. D_p is the diameter of particle.

	Fine-mode (D_p <1 μm)	Coarse-mode (D_p >1 μm)
Mass concentration (μg/m³)	191.27	0.79
Surface areas (μm/cm³)	2.28	132.01
Number mean diameter (μm)	0.78	2.23

Table 3.2 Summary of initial physical and chemical simulation conditions used in Section 3.3.1.

Species	Concentration (ppb)
Initial Conditions	
NO	1.5
NO_2	0.5
HNO_3	0.0005
NH_3	1.0
SO_2	8.0
H2SO$_4$	0.8
O_3	50.0
C_2H_6	2.843
C_3H_8	1.379
Alkane (higher alkane than propane)	1.233
C_2H_4	3.461
Alkene (higher alkene than ethene)	0.692
Aromatic	6.290
C_2H_2	0.895
H_2O_2	2.0
Isoprene	5.0
Dimethylsulfide	0.005
H_2S	0.001
CO	150.0
Meteorological and Other Factors	
Temperature(K)	300K
RH	80%
with and without surface emissions or NO Dry deposition included	5×10^4 molecules$\cdot$cm^{-3}s^{-1}

Table 3.3 Average chemical compositions of mineral dust particles from different source regions. (adapted from *Krueger et al.* 2004)

Atomic percent	Saharan	China Loess
%Si	46	31
%Al	17	7
%Mg	6	13
%Ca	17	39
%Na	2	4
%Fe	7	3
%K	3	1

Table 3.4 Measured γ values from mineral oxides, calcite, and real dust particles, which used in the calculation of reactivity of dust in Section 3.3.1.

Gas phase reactant	Mineral	Reaction probability on dry particle	Note and source
HNO$_3$	CaCO$_3$	2.00×10^{-3}	Liu et al., 2008
	SiO$_2$	2.90×10^{-5}	Underwood et al. 2001a
	Fe$_2$O$_3$	5.30×10^{-5}	Underwood et al. 2001a
	MgO	3.70×10^{-4}	Underwood et al. 2001a
	Al$_2$O$_3$	9.70×10^{-5}	Underwood et al. 2001a
	Gobi dust	5.20×10^{-5}	Underwood et al. 2001a
O$_3$	CaCO$_3$	2.00×10^{-4}	Michel et al. 2003
	SiO$_2$	9.00×10^{-5}	Usher et al. 2003b
	Al$_2$O$_3$	1.20×10^{-4}	Usher et al. 2003b
	Saharan dust	6.00×10^{-5}	Michel et al. 2003
SO$_2$	CaCO$_3$	1.40×10^{-4}	Usher et al. 2002
	SiO$_2$	No significant uptake	Usher et al. 2002
	Al$_2$O$_3$	1.50×10^{-4}	Usher et al. 2002
	Fe$_2$O$_3$	7.00×10^{-5}	Usher et al. 2002
	TiO$_2$	1.00×10^{-4}	Usher et al. 2002
	MgO	5.10×10^{-4}	Usher et al. 2002
	Saharan dust	6.40×10^{-3}	Usher et al. 2002
NO$_2$	CaO	2.20×10^{-5}	Underwood et al. 2001
	SiO$_2$	1.00×10^{-9}	Underwood et al. 2001
	Al$_2$O$_3$	9.10×10^{-6}	Underwood et al. 2001
	Fe$_2$O$_3$	7.70×10^{-6}	Underwood et al. 2001
	TiO$_2$	1.30×10^{-7}	Underwood et al. 2001
	MgO	1.20×10^{-5}	Underwood et al. 2001
	China loess	2.10×10^{-6}	Underwood et al. 2001
N$_2$O$_5$	CaCO$_3$	1.90×10^{-4}	Mogili et al. 2006
	SiO2	4.40×10^{-5}	Mogili et al. 2006
	CaCO$_3$	9.80×10^{-4}	Adapted from Karagulian et al. 2006; accounting for BET SA

Table 3.5 RH-dependent uptake coefficients γ used in modeling study [*Liu et al.*, 2008].

RH	$\gamma = f(RH)$	$\gamma_{wet} / \gamma_{dry}$
0	2.0×10^{-3}	1
20%	0.014	7.0
40%	0.060	30.0
60%	0.100	50.0
80%	0.210	105.0

Table 3.6 Effects of mineralogy and RH on heterogeneous uptake of HNO_3

Case	γ	$(\Delta HNO_3)_{max}$ (ppbv)	$(\Delta HNO_3)_{average}$ (ppbv)	$(\Delta HNO_3\%)_{max}$ (%)	$(\Delta HNO_3\%)_{average}$ (%)
model, γ =0.1	0.1	-0.705	-0.324	-99.0	-94.6
Saharan dust					
RH=0	3.87×10^{-4}	-0.0440	-0.0251	-11.8	-7.79
RH=40%	1.02×10^{-2}	-0.478	-0.230	-85.6	-68.2
RH=80%	3.57×10^{-2}	-0.648	-0.299	-96.8	-87.4
China loess					
RH=0	8.65×10^{-4}	-0.0920	-0.0513	-23.2	-15.9
RH=40%	2.34×10^{-2}	-0.602	-0.281	-94.6	-82.4
RH=80%	8.20×10^{-2}	-0.698	-0.321	-98.8	-93.6
real China loess	1.10×10^{-3}	-0.113	-0.0626	-28.5	-19.4

Table 3.7 The initial conditions for the case in Section 3.32. (adapted from *Song et al.* 2007)

	AREA II
Initial conditions	
NO (ppb)	0.18
NO_2 (ppb)	1.41
HNO_3 (ppb)	2.02
SO_2 (ppb)	9.06
O_3 (ppb)	48.42
C_2H_6 (ppb)	7.44
C_3H_8 (ppb)	2.82
ALKA (ppb)	1.86
ETHE (ppb)	0.04
ALKE (ppb)	0.01
AROM (ppb)	0.04
HCHO (ppb)	3.18
ALD2 (ppb)	0.29
H_2O_2 (ppb)	1.33
PAN (ppb)	0.44
ISOP (ppb)	0.03
Temperature (^{o}C)	8.5
Reaction probability (γ_i)	
SO_2	10^{-5}
H_2SO_4	1.0
NO_3	3×10^{-3}
N_2O_5	0.01
HNO_3	0.01
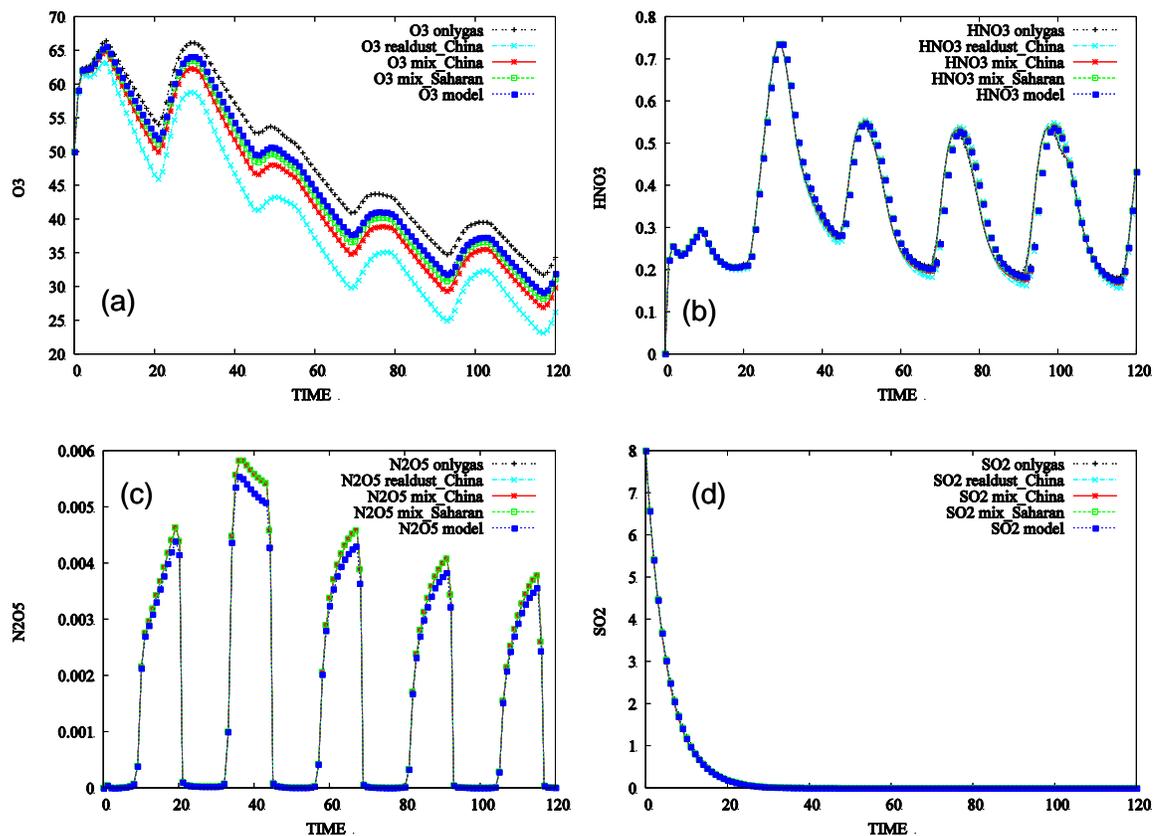
Figure 3.1 The effect of mineralogy on O$_3$ heterogeneous reaction for (a) O$_3$ and (b) HNO$_3$;
The effect of mineralogy on the uptake of (c) N$_2$O$_5$ and (d) SO$_2$.
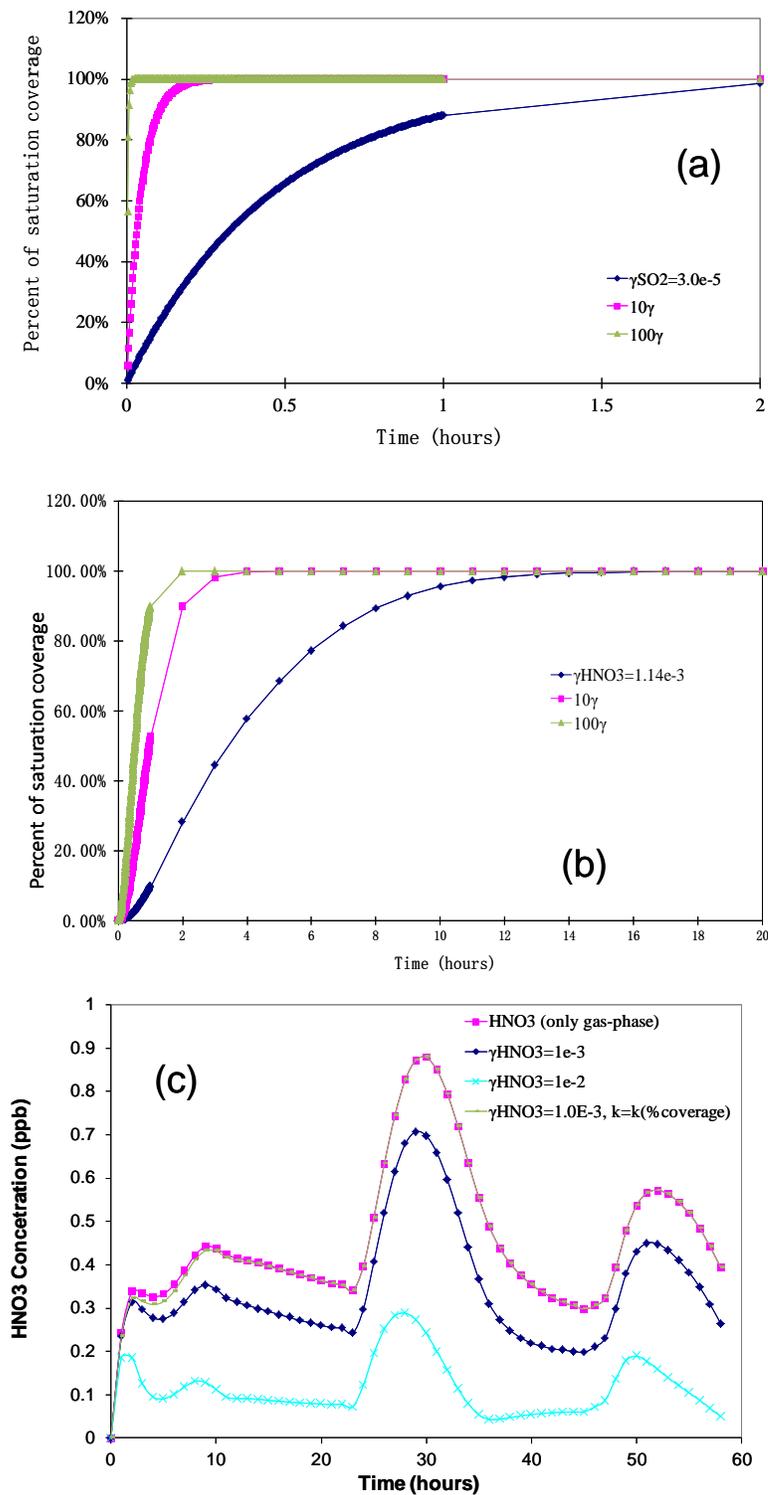
Figure 3.2 Surface saturation for the heterogeneous uptakes of (a)SO$_2$ and (b)HNO$_3$; (c)saturation effect on HNO$_3$ heterogeneous reaction.
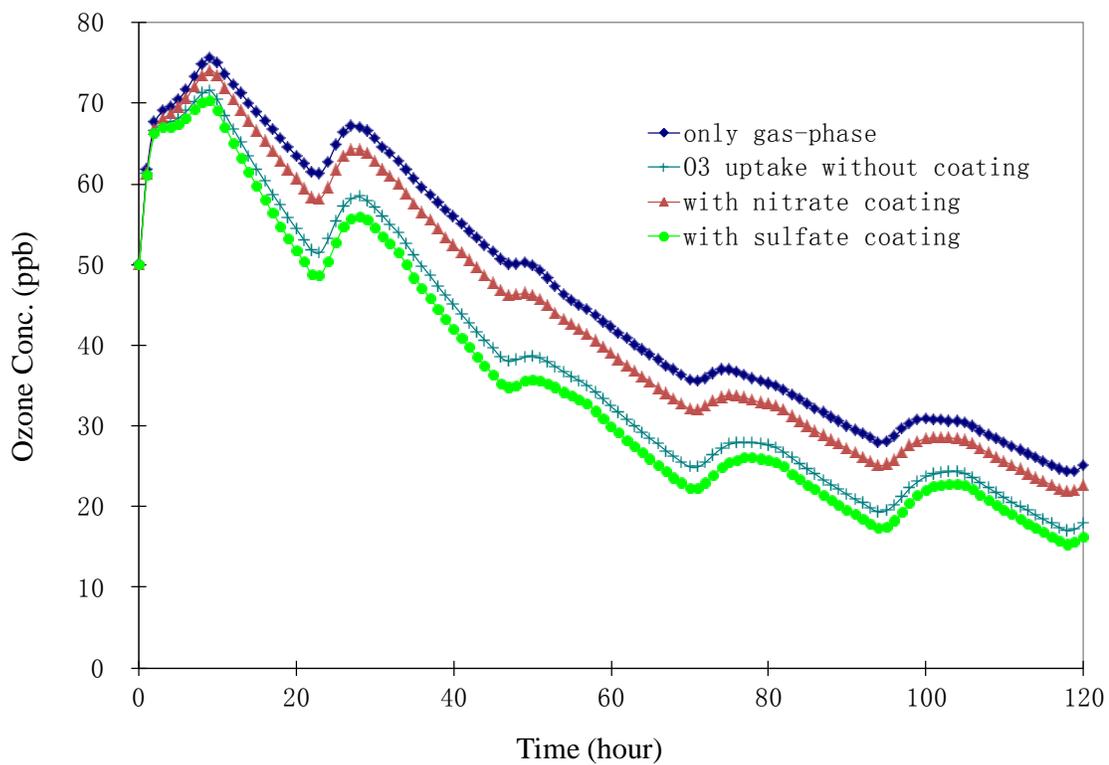
Figure 3.3 The effects of sulfate or nitrate coating on the heterogeneous uptake of O_3.
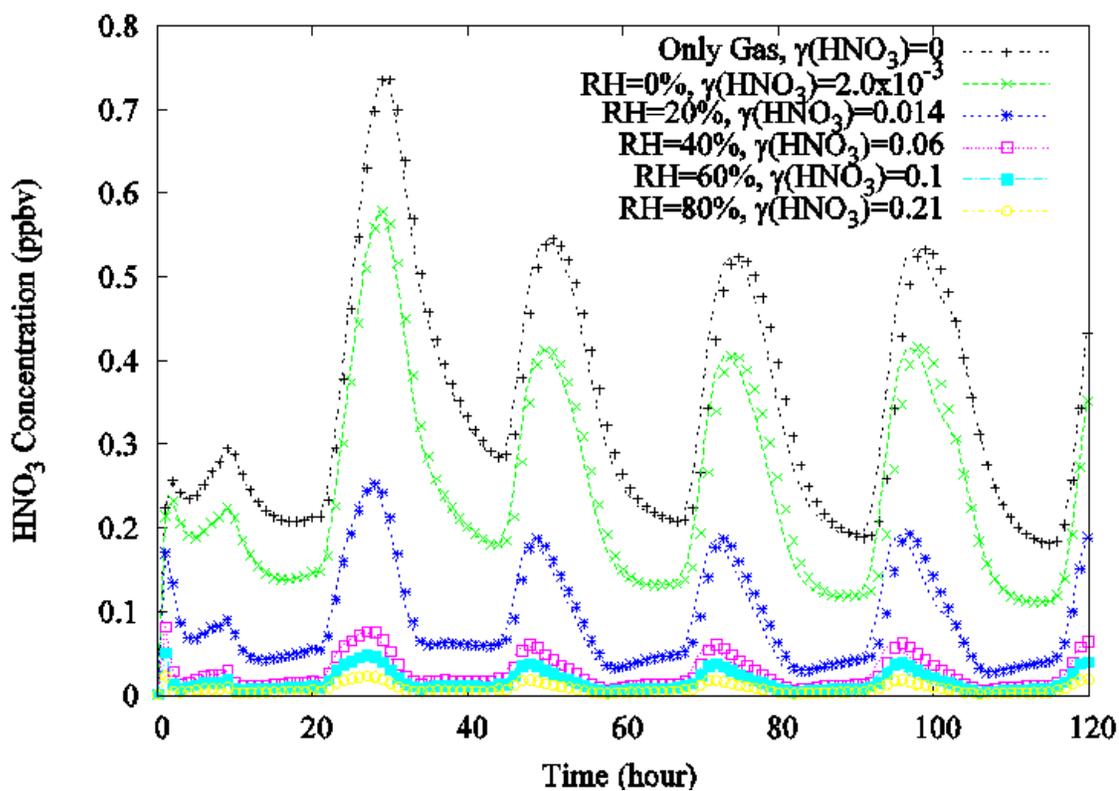
Figure 3.4 The effect of relative humidity on the heterogeneous uptake of nitric acid gas on pure calcite particles.
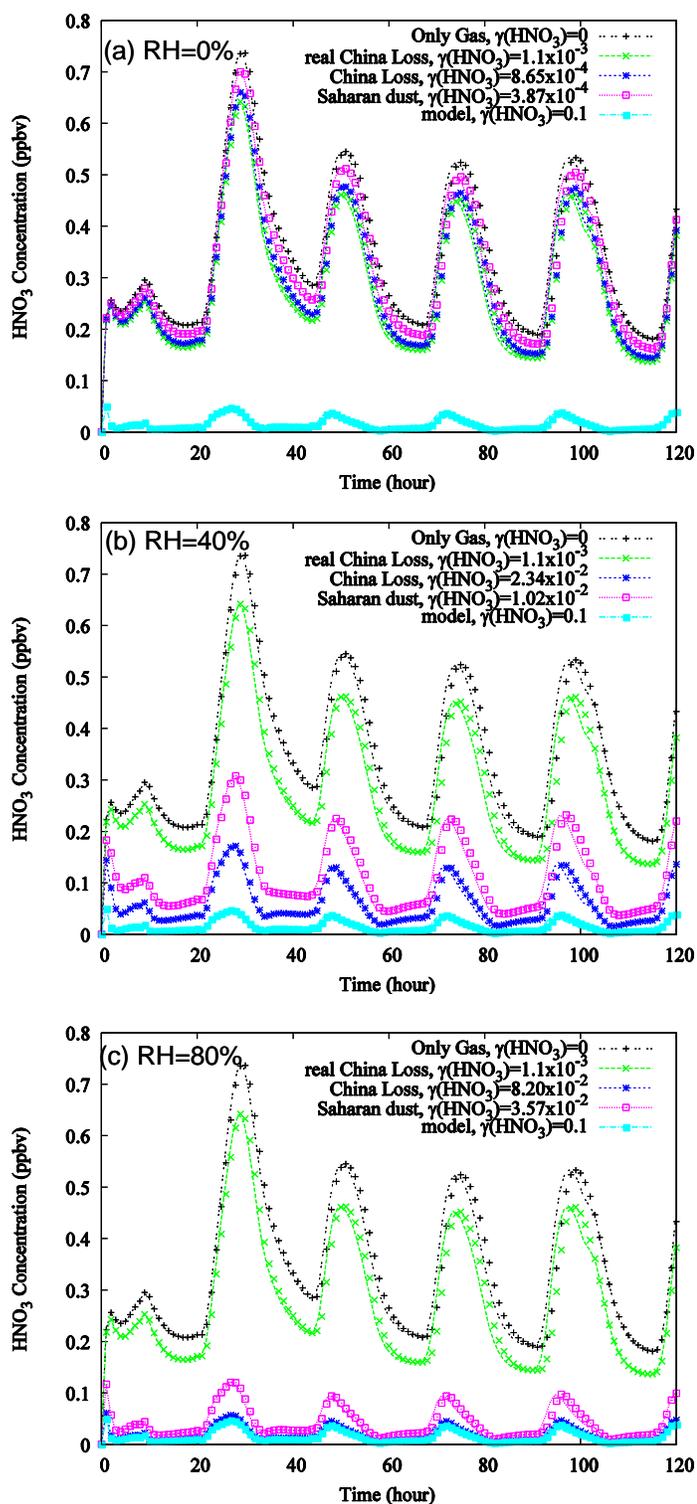
Figure 3.5 The effects of relative humidity and mineralogy on the heterogeneous uptake of nitric acid gas on different dust particles.
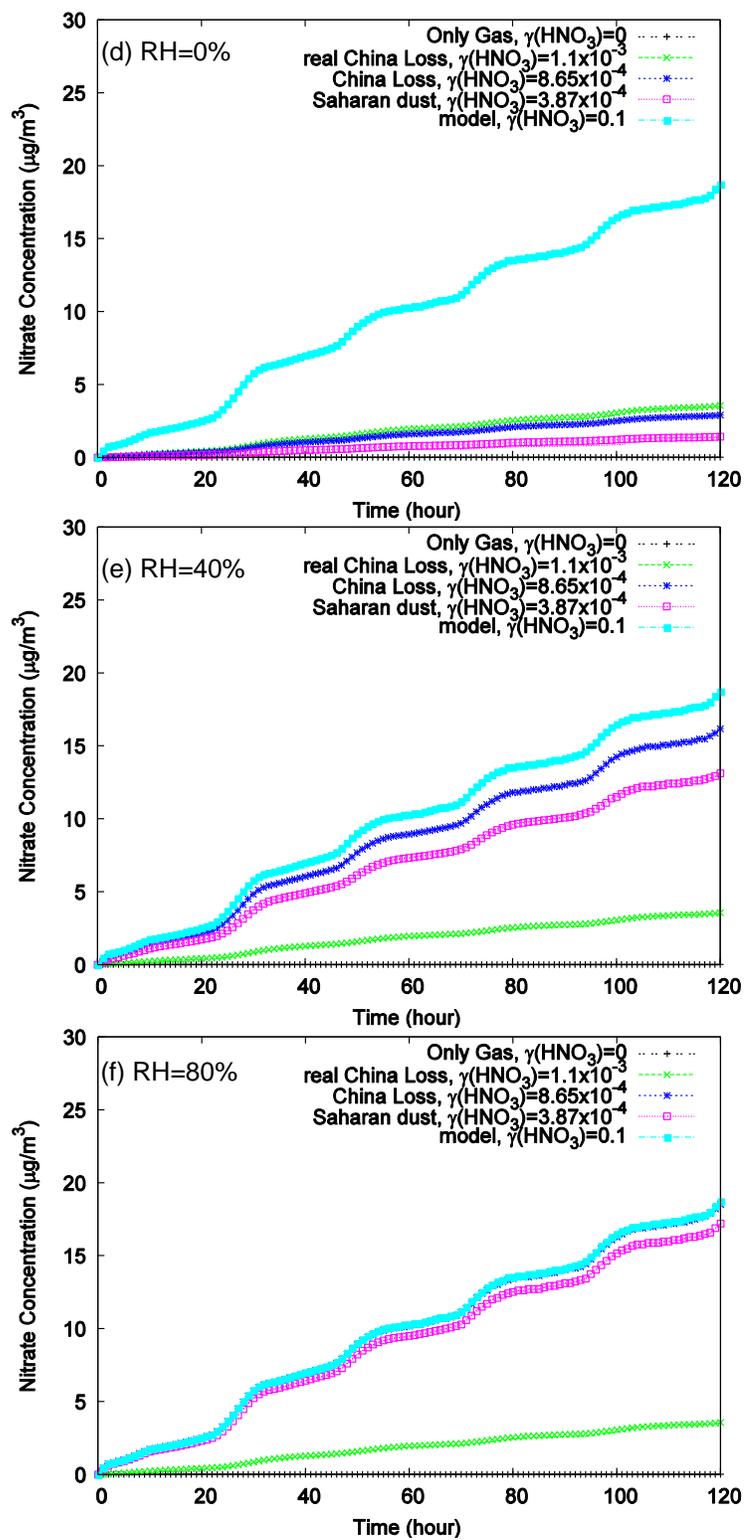
Figure 3.5 continued.
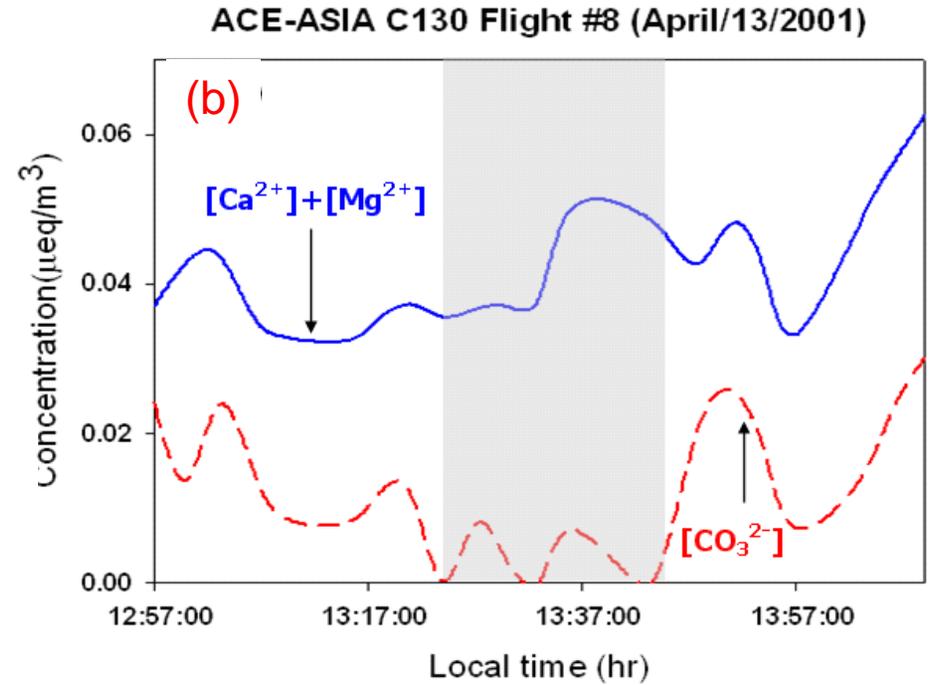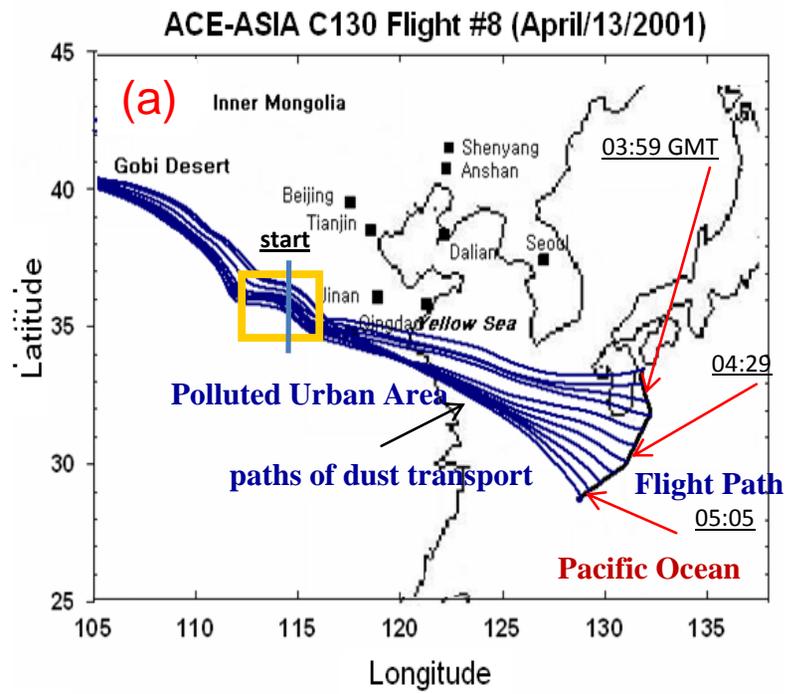
Figure 3.6 Five-day backward trajectories and variations of $[Ca^{2+}]$ + $[Mg^{2+}]$ and $[CO_3^{2-}]$ equivalences with time. (The data for $[Ca^{2+}]$ + $[Mg^{2+}]$ and $[CO_3^{2-}]$ are smoothed.) (adapted from *Song et al.* 2007)
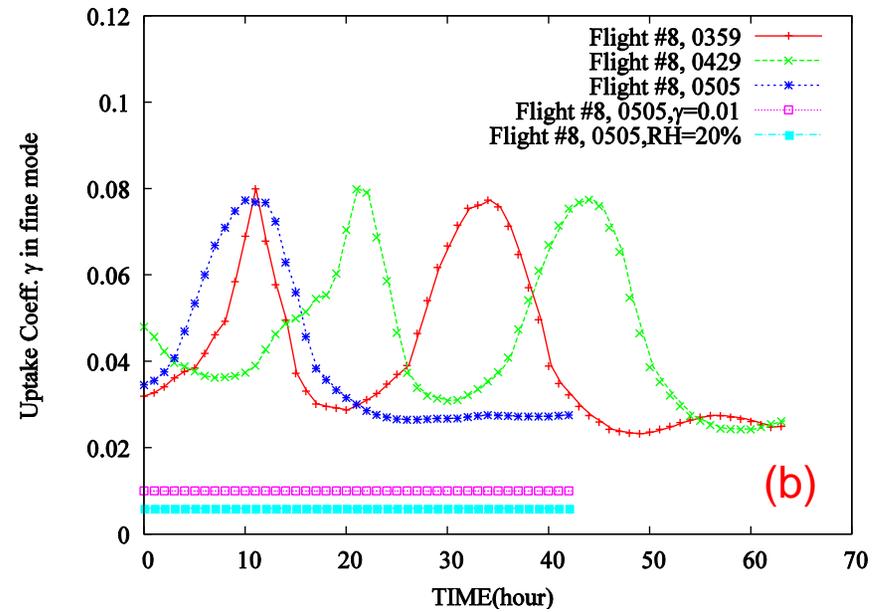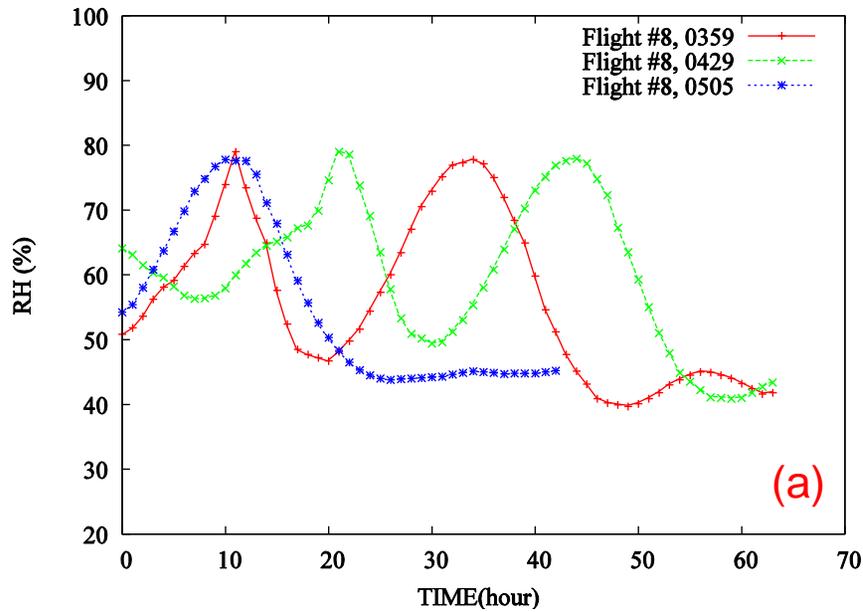
Figure 3.7 Results from model simulations. Shown are the time-series of (a) relative humidity; and (b) uptake coefficient in fine mode.
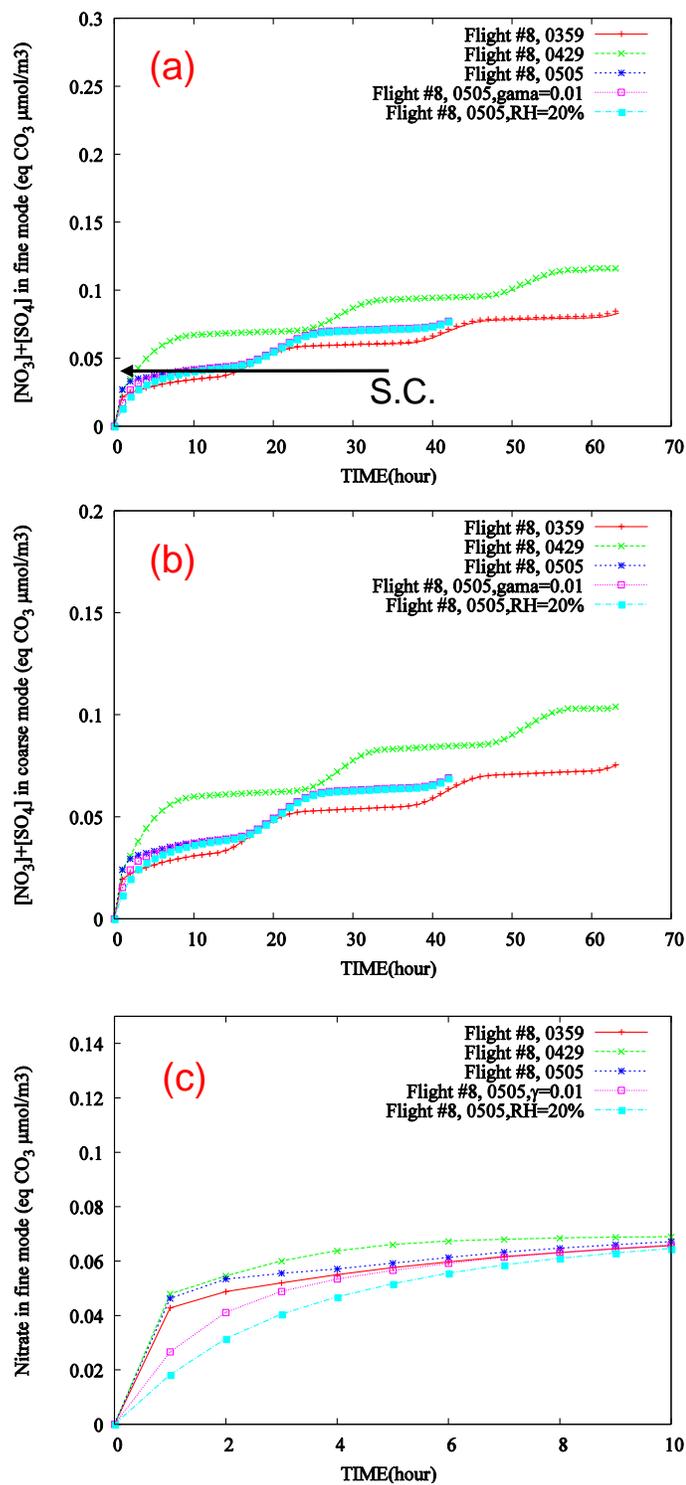
Figure 3.8 Results from model simulations. Shown are the time-series of $[NO_3^+]+[SO_4^{2-}]$ in (a) fine mode; (b) in coarse mode; and (c) nitrate in fine mode during the first 10 hours.
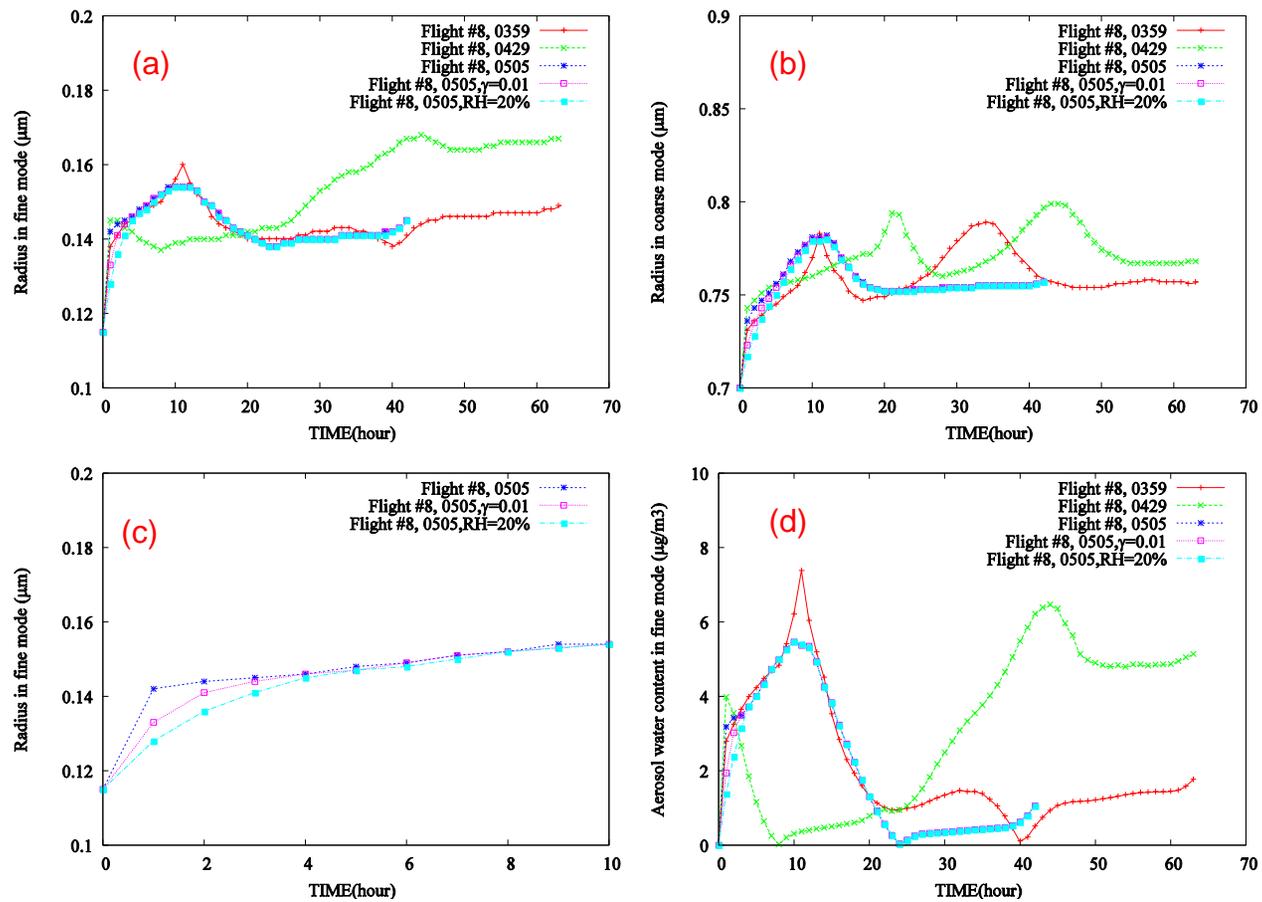
Figure 3.9 Results from model simulations. Shown are the time-series of radius in (a) fine mode; (b) in coarse mode; (c) radius in fine mode during the first 10 hours; and (d) aerosol water content in fine mode.
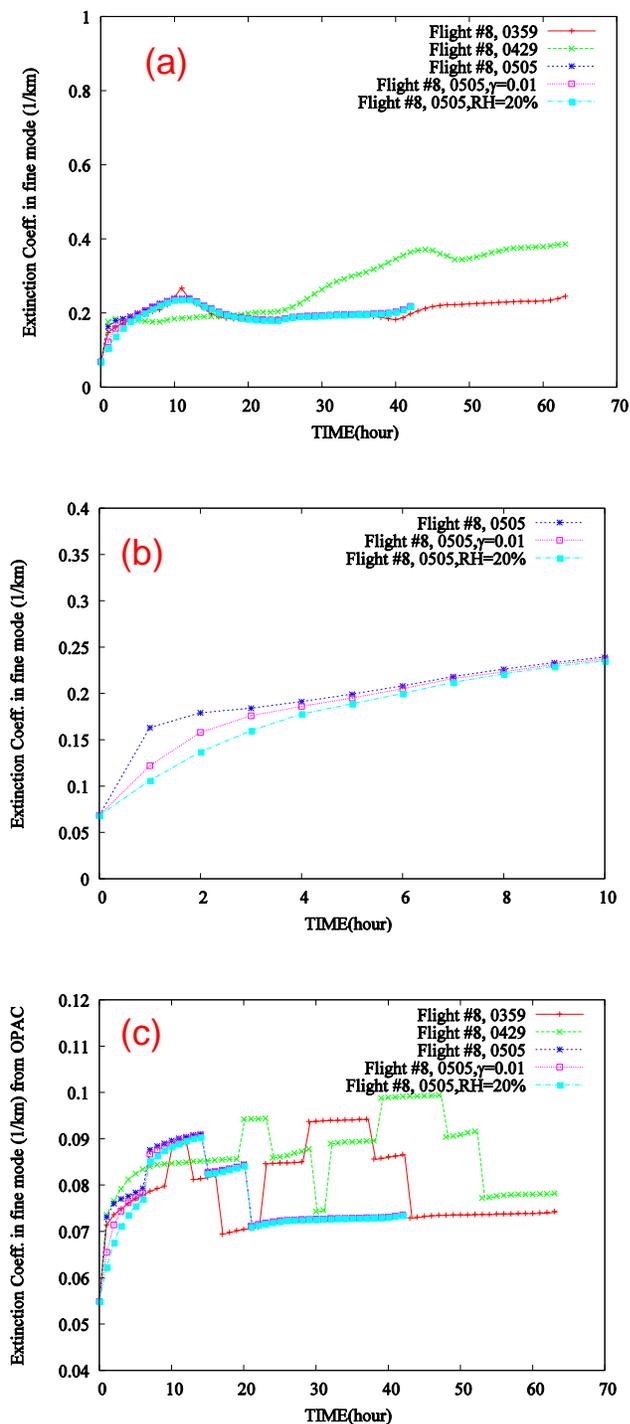
Figure 3.10 Results from model simulations. Shown are the time-series of (a) extinction coefficient in fine mode; (b) extinction coefficient in fine mode during the first 10 hours; and (c) extinction coefficient in fine mode calculated by OPAC.

CHAPTER 4

A 3-D MODELING ANALYSIS OF THE GAS-AEROSOL

PARTITIONING OF HNO_3 AND THE IMAPCT OF

HETEROGENEOUS REACTION

4.1 Introduction

During each spring in East Asia, dust storms frequently erupt and inject alkaline

dust particles into the atmosphere, which are then transported with a long distance. During

this transport the alkaline dust takes up acidic gases such as SO_2, H_2SO_4, and HNO_3 [*Bauer*

et al., 2004; *Dentener et al.*, 1996; *Ro et al.*, 2005; *Song and Carmichael*, 2001a, 2001b;

Tang et al., 2004; *Xiao et al.*, 1997; *Zhang and Iwasaka*, 1999; *Zhang et al.*, 2003].

Because of the uptake of acidic gases in the atmosphere, the dust particles undergo

chemical evolution (also referred to as chemical aging). The degree of chemical aging of

East Asian dust particles has been estimated in various modeling and theoretical studies

[*Dentener et al.*, 1996; *Meskhidze et al.*, 2003; *Song and Carmichael*, 2001a, 2001b; *Zhang*

et al., 1999]. Critical elements of these studies include assumptions related to the reaction

rates and the mixing state of the aerosol. The reactions of acidic gases with mineral aerosol

have been studied extensively in the laboratory [*Goodman et al.*, 2001; *Hanisch and*

Crowley, 2001; *Underwood, et al.*, 2001a, 2001b; *Usher et al.*, 2002] and these reaction

probabilities (hereafter, γ) of sulfate and nitrate precursors (SO_2, H_2SO_4, NO_3, N_2O_5, and

HNO_3) onto mineral dust are being used to inform the modeling studies. However, the

laboratory studies often represent a lower estimate for the reaction rates (e.g., because of

low humidity conditions, etc.), while models often have to use a higher estimation of these

reaction rates to account for the ambient conditions. Therefore, there remains large

uncertainty in the estimates of the rates of chemical aging for mineral aerosols.

Several observation-based studies have reported that although East Asian dust

particles have long contact times with sulfate and nitrate precursors, they contain only

small amounts (typically, less than 10–50%) of sulfate and nitrate [e.g., *Maxwell-Meier et al.*, 2004; *Ro et al.*, 2005; *Song et al.*, 2007; *Zhang and Iwasaka*, 1999; *Zhang et al.*, 2003 etc.]. These observations provide a means to help constrain and evaluate the reaction rates used in aerosol models.

The main purpose of this study is to evaluate how the different treatments on gas-aerosol conversion affect the distributions of aerosols and trace gases and assess the impact of the RH-dependent heterogeneous uptake of HNO_3 on tropospheric chemistry. A modified 3-dimentional regional chemical transfer STEM model, with a new size and chemical resolved dynamic aerosol module, is employed in this study. Observations from INTEX-B field campaign are utilized for helping to analyze the model results.

4.2 Model description and emission inventory

4.2.1 Modified 3-D STEM Model and Settings

The STEM model was developed at the University of Iowa in the early 1980s [*Carmichael et al.*, 1986] and has continuously undergone development since then to its current version which is the STEM-2K3 version [*Tang et al.*, 2004]. The STEM model is a regional chemical transport model which features the SAPRC-99 chemical mechanism [*Carter*, 2000]. Online photolysis rate calculations in the STEM model are performed using the TUV (Tropospheric Ultra-Violet Radiation) model [*Madronich*, 2002]. The TUV model needs total ozone column to calculate the absorption of UV radiation by ozone molecules. Since the STEM model is a regional model simulating the troposphere, column ozone data from satellite is used. For this study, we have used the column ozone data from the Ozone Mapping Spectrometer (OMI) (including STEM calculation for the troposphere) instrument on board the NASA Aura spacecraft. Thirty different photolysis rates are calculated using the STEM-TUV model.

The STEM model uses the SCAPE II aerosol module to simulate inorganic gas to particle conversion and aerosol particle growth [*Kim et al.*, 1993a; 1993b; *Kim and*

Seinfeld, 1995; *Meng et al.*, 1995]. The inorganic aerosols in the STEM-SCAPE II model are binned into four size bins of 0.1-0.3μm, 0.3-1.0μm, 1.0-2.5μm and 2.5 – 10.0μm. For serving the purpose of current study, the full-dynamics AeroSolver (see Chapter 2) is exclusively embedded into the SCAPE II aerosol module for comparison with the traditional Equilibrium approach (CIT hybrid method). To evaluate the impact of relative humidity on the HNO_3 uptaken on dust particle, laboratory derived RH-dependent uptake coefficients (see Chapter 3) are applied in the 3-D model instead of assuming constant values. The modified 3-D STEM model run for the selected cases during the INTEX-B field campaign with one week for model spinning-up.

STEM does not require a uniform horizontal grid and can be mapped to any map projection based on the meteorological model. STEM preprocessor extracts all of the topography and other land use variables that were used in the meteorological model along with the meteorological parameters necessary for simulating chemical transport and removal processes. Thus, STEM has the same map projection and grid resolution as the meteorological model. For this study, the WRF-ARW (Weather Research & Forecasting Model with ARW dynamic solver) Version 2.1.2 meteorological model developed at NCAR was used [*Skamarock et al.*, 2005]. The WRF model horizontal resolution was 50x50 kilometer with 314x200 grid cells. The model has 21 vertical levels with the model top at 50 hPa. Vertical spacing was defined to have the highest density in the first kilometer. The STEM model is parameterized to simulate the pollutant transport and chemistry in the troposphere. Therefore the chemistry model was simulated with only the first 18 layers reaching up to 10.5 kilometer above ground layer (AGL) height. Significant stratospheric air-mass intrusion within the model domain at higher latitudes (without any stratospheric chemistry/parameterization in the STEM model) limited the chemistry model's ability to simulate higher altitudes. GFS 1 °x1 ° model forecast at 18 UTC from the National Center for Environmental Prediction (NCEP) was used to initialize the WRF model and as a boundary condition at a 6 hour interval. The physics options used in the WRF model are as

follows: WSM-3 class simple ice scheme for microphysics, RRTM scheme for longwave/shortwave radiation, Monin-Obukhov scheme for surface layer, Noah land-surface model, YSU scheme for the boundary layer option and Grell-Devenyi ensemble scheme for the cumulus parameterization. The WRF model prediction skills are evaluated with INTEX-B observations later in the Section 4.2.

4.2.2 Dust Emissions and Consideration of Asian Dust

Dust is a major aerosol component in the East Asia outflow during the spring. The dust emission and gaseous sorption processes (with saturation effects) and heterogenic reaction on dust surface have been treated in the STEM model.

Dust emissions are calculated online using a parameterization based on previous studies using the STEM model [*Tang et al.*, 2004a; *Uno et al.*, 2004]. It is estimated using a modified form of the method by Liu and Westphal (2001). Total dust emissions were calculated using

$$E_{dust} = A(U^* - U_{th})U^{*3}, \text{ when } U^* > U_{th}, \tag{1}$$

where E_{dust} is the dust emission flux in g/m^2/s, A is dimensional emission factor ($A = 4.5$E-4 in current study), U^* is surface friction speed in m/s, and U_{th} is the threshold U^*, values above which dusts can be emitted. In this study, a U_{th} value of 0.4 m/s is applied to the Asian dust, according to *Tang et al.* [2004a]. A is determined by the upper limit of the dust particle diameter. Here we only consider the dust particles whose diameters are smaller than 10 μm, since these dust particles can be transported over sufficiently long distances to over the Pacific reaching the INETX-B observation locations. The USGS 24-category land use data are used as the basis to locate the desert and semiarid areas. During springtime in this region, additional land cover (i.e., when they are not snow covered and before the grass emerges). These aspects were included in this study. In this study, dust is modeled in 4 bins as other aerosol chemical compositions. In the dust source regions, dust is assumed to be uniformly distributed within the boundary layer.

The composition of dust plays a critical role in determining the importance of the interactions of dust with ambient air, including gaseous sorption processes and subsequent surface heterogeneous reactions. We used the same setting of dust composition from *Tang et al.* [2004b], which is determined according the specific observation about the East Asian dust on board the DC-8 flights during ACE-Asia field campaign. The method they used to determine dust compositions is described in brief here. As also found in previous studies (e.g. *Andronova et al.*, 1993; *Cao*, 2005; *Gomes and Gillette*, 1993; *Liu*, 1985; *Song and Carmichael*, 2001a, 2001b; *Song et al.*, 2007) that the reactive constituents of dust particles in East Asia are $CaCO_3$ (the most predominate form of carbonates in mineral dust accounting for >90% in carbonates), $MgCO_3$ and $CaMg(CO_3)_2$, CO_3^{2-} has been also found be to main anion in the emitted dust. They derive the dust CO_3^{2-} from the observed soluble calcium amount.   It was assumed that the original dust emitted into the atmosphere did not contain gypsum [*Mori et al.*, 2003]. It is important to emphasize that the absolute value of the total dust mass was unconstrained by direct measurement.   The Ca^{2+} is determined to account for 1.14% of the total dust weight, which is consistent with the studies about dust originated from the Inner Mongolia Autonomous Region [*Mori et al.*, 2003].

Aerosol particles in each bin are treated as internal mixed. In the currently study, we defining the portion of the calcium in the dust that was active for chemical reaction to be 30, 30, 20 and 10% for the four aerosol bins, accounted for the previous experimental studies, e.g., *Song et al.* [2007] and [*Maxwell-Meier et al.*, 2004]. The detailed explain about the dust surface fresh ratio can be found in *Tang et al.* [2004b].

The reactions of O_3, SO_2, NO_2, and HNO_3 with dust particles have been taken into account. Unlike in *Tang et al.* [2004b], not only constant uptaken coefficient (γ) but also the laboratory derived RH-dependent γ are alternatively treated in different sensitivity runs.   Details about the laboratory derived RH-dependent γ can be found in Chapter 3. The more descriptions about different sensitivity cases will be provide in Section 4.3.

4.2.3 Anthropogenic and Other Emissions

Gridded anthropogenic emissions for Asia were obtained from the emissions inventory developed for the INTEX-B mission [*Zhang et al.*, 2009]. The horizontal resolution of the gridded emissions inventory was 0.5 °x0.5 °ranging from 8-50 °N and 80-150 °E. Emissions of Volatile Organic Compounds (VOCs) were available based on the SAPRC-99 speciation. The National Emissions Estimate (NEI-2001v3) obtained from Jeff Vukovich, who updated the NEI 1999 emissions, at the US Environmental Protection Agency (EPA) were used an input for the region of North America. This emissions inventory has been previously used as input in STEM model, to study the regional air quality over North America during the ICARTT mission [*Mena-Carrasco et al.*, 2007; *Tang et al.*, 2007]. The global emissions inventory from the EDGAR database was used for regions outside the INTEX-B Asia and North America domains [*Olivier and Berdowsky*, 2001].

Daily emissions forecasts from biomass burning were available from the Regional Air Quality Modeling System (RAQMS) modeling group during the INTEX-B field campaign [*Al-Saadi et al.*, 2008]. The same biomass burning emissions was utilized in this post field mission study. Biogenic emissions of terpene and isoprene were taken from a 12 year averaged data from the ORCHIDEE model [*Lathiere et al.*, 2006]. It has been shown that using the top and lateral boundary conditions from a global model enhances STEM model prediction skill [*Tang et al.*, 2007]. In this study, the Model for Ozone and Related Chemical Tracers (MOZART-4) global model was used to provide top and lateral boundary conditions [*Pfister et al.*, 2008]. Emissions of sea salt within the STEM model are based on the work by S. L. Gong [*Gong*, 2003]. The tracer version of the STEM model has been utilized for emissions sensitivity runs. The tracer model employs simple decaying rates for most primary species without chemical reactions but includes wet scavenging and dry deposition to produce tracer model predictions.

4.3 Simulation conditions

Figure 4.1a illustrates the horizontal modeling domain of the WRF-STEM model (Chemical Transfer Model STEM driven by Weather Research & Forecasting Model WRF). Figures 4.1a and 4.1b also present the flight tracks of the DC-8 and the C-130 during the INTEX-B field campaign. As shown in figure 4.1, there is substantial amount of geographic space covered by the DC-8 flights over the central Pacific while the C-130 airborne observations cover a good portion of the eastern Pacific during the 2006 spring season. Since the object of the current study is to investigate how the Asian dust plume encountered anthropogenic pollution and evolved during the long range transport, back trajectory analyses along the flight tracks are applied helping to pick up the appropriate cases for the model scenario simulations.

Figure 4.2 presents the back trajectories along the flight tracks of the DC-8 and C-130 during INTEX-B. Three flights each from Hawaii (RF 11, 12, 13) and Alaska portions (RF 15, 16, 17) of the DC-8 mission were selected and 5-day back trajectories were calculated using the WRF simulated meteorology fields for way points (latitude, longitude) along the flight tracks. Similarly, five C-130 (RF 15, 17, 18 21, 24) flights that had substantial sampling over the eastern Pacific were chosen to calculate back trajectories. The trajectories were initiated at the actual latitude, longitude, altitude and time of the airplane research flights. They were calculated along every minute of the flight path. However, to reduce the clutter in Figure 4.2a, trajectories are plotted only every thirty minutes and colored by the altitude along the trajectory.   In Figure 4.2b, the tagged CO tracers illustrate the source regions of air masses sampled by the selected DC-8 and C-130 flights.

The back trajectory analyses reveal different transport patterns for the three portions of the mission. The Hawaii portion is dominated by air masses passing over east central China reaching as far back as South Asia. The air masses sampled by the C-130 mission have spent a substantial time over the Gulf of Alaska with a mixture of two

patterns. Therefore, in the following part we will only focus the model scenario simulations on the Hawaii portion and chose the time period from April 16 to 30, 2006.

Four cases of model run were used in this study and summarized in Table 4.1. Case "r2c2" is the base case. Any result without specific mention about case in this chapter refers to this case. As aforementioned, four heterogeneous reactions (O_3, NO_2, HNO_3, SO_2) on dust are considered in this base case. The heterogeneous uptake coefficients are assumed to be constant, with values for $\gamma(O_3)$, $\gamma(SO_2)$, $\gamma(NO_2)$ and $\gamma(HNO_3)$ of 5×10^{-5} [*Dentener et al.*, 1996; *Jacob*, 2000; *Michel et al.*, 2002], 1×10^{-4} [*Goodman et al.*, 2001; *Phadnis and Carmichael*, 2000; *Usher et al.*, 2002; *Zhang and Carmichael*, 1999], 1×10^{-4} [*Underwood et al.*, 2001b] and 0.01 [*Goodman et al.*, 2000; *Hanisch and Crowley*, 2001; *Prince et al.*, 2002], respectively. CIT hybrid approach is used to treat the partitioning between the bulk gas phase and particles. Case "r6c2" is similar to Case "r2c2", while all the heterogeneous reactions have been turned off. The results from Case "r2c2" and "r2c6" are used and discussed in *Adhikary et al.* [2010]. But the results in this paper are shown for mission wide average, and the discussion about aerosols is only very small part. Compared with Case "r2c2", the CIT hybrid approach is replaced by the newly developed aerosol module, full-dynamics AeroSolver, in Case "2k9case2". Case "2k9case3" is similar to Case "r2c2", but the laboratory derived RH-dependent heterogeneous uptake coefficients for the uptake of HNO_3 on dust are specifically considered instead of the constant value. Due to the consuming of long computational time, the case with the combination of dynamic AeroSolver and RH-dependent γ has not been conducted in the current study, which is planned be done in the future studies. Here we could only determine the sole effect on the heterogeneous reactions on dust either by dynamic aerosol core versus equilibrium method, or by the constant γ versus RH-dependent γ.

4.4 Results and discussions

4.4.1 Spatial distribution of aerosols and gases

4.4.1.1 General transport pattern of major aerosols and gases
over Pacific

The modeled mean distributions of CO, O_3, dust, sulfate, nitrate and RH at 3 km a.g.l. for the study period (16 April–30 April 2006) during the INTEX-B are shown in Figure 4.3. These figures provide a general feature under which the aircraft experiments were conducted. The CO distribution (Figure 4.3a) reveals emission hotspots associated with anthropogenic sources (such as those over India and eastern China), and those associated with open biomass burning (e.g., northern Thailand and Vietnam and western Russia). These sources are stronger than the anthropogenic and open burning emission sources in North American for this domain and time period. These result in a significant west to east gradient of decreasing CO. Due to these major CO inputs and the transport patterns over the Pacific during this period, the region of enhanced CO (>120 ppb) shifts northward during transport over the Pacific, with peak values at latitudes greater than 30N over the eastern Pacific.

The modeled mean ozone distribution at 3 km a.g.l. (Fig. 4.3c) shows strong enhancements (>70 ppb) between 25N and 40N over the Asian continent, due to a combination of stratospheric influence (e.g., over the Tibetan Plateau) and anthropogenic activities (e.g., eastern China and Japan). The influence of anthropogenic emissions from and around major cities (e.g., Delhi, Kolkata, Los Angeles) and around the major open biomass burning areas in Siberia and Alaska are also identified. The ozone distribution shows a stronger zonal pattern than CO.

The modeled mean horizontal distributions of aerosol sulfate, nitrate and dust are presented in Fig. 4.3b, d, and f, respectively. These aerosol distributions show a stronger zonal pattern than the gas species discussed previously, reflecting the fact that the aerosol

particles typically have a shorter lifetime and thus are less influenced by continental transport and more dominated by emission source regions. For example, sulfate shows a strong west to east gradient, with the peak values in the west reflecting the heavy populated and industrial regions of India and China, and is transported across the Pacific at latitudes between 20N–50N. Particulate nitrate has a different pattern, with elevated levels on both sides of the Pacific reflecting regions with high NOx and NH_3 emissions. The relative importance of sulfate with respect to nitrate decreases from west to east across the Pacific, with nitrate dominating over California. Both sulfate and nitrate show enhancements due to Hawaii emissions from anthropogenic and volcanic sources (in the case of sulfate).

Further insights into the distribution of CO over the Pacific are shown in the cross section plots in Figure 4.4. The CO emissions from East Asia are transported with an outflow over the Pacific via frontal systems resulting in lifting of the CO above the boundary layer into the free troposphere. The bulk of the transported CO is at altitudes of 3–5 km as shown in the zonal cross section along 145E longitude (see Figure 4.4c). As the polluted air-masses reach the eastern Pacific, the frontal systems tend to move poleward. The subsiding aged air-masses mix with CO emitted from North America leading to enhanced CO levels within the boundary layer (see Figure 4.4d).

4.4.1.2 Spatial distribution of RH and its potential impacts
on and interaction with dust particles

The spatial distributions of dust and RH over the Pacific are shown by the horizontal plots in Figure 4.3e and f and by the cross section plots in Figure 4.5. Horizontally, the dust distribution shows maximum values in the western part of the domain corresponding to the strong source regions during this time period (i.e., Central Asia and China). The region of elevated levels of dust extends across the Pacific (see Figure 4.3f). This transport feature of dust will have significant impacts on the atmospheric heterogenic chemistry, which will be investigated in the following sections. Dust particles

were transported across the Pacific between 20N to 50N latitude (see Figure 4.3f and Figure 4.5b, c and d). The modeled mean RH distribution at 3 km a.g.l. (see Fig. 4.3e) shows the correlation between low RH (about 40%) and dust transport pathway (20N-50N), except some narrow regions in the central Pacific Ocean. It indicates the dust particles may contain less water on the surface during the long range transport. Low RH and less water uptaken may result in a lower pH value in the liquid phase on the surface of particles (see Chapter 3) and the calculated heterogeneous uptake coefficient of HNO_3 on dust based on the RH in Case "2k9case3" may be therefore lower and closer to the constant assumed in Case "r2c2".

In Figure 4.5a, vertical profile of dust over dust source regions along 30N latitude shows that the dust emitted from North China is lifted by frontal system and transported at altitudes of 3-6 km (see Figure 4.5b, c and d). When we look at the RH profile along the dust transport pathway, over continental China, dust particles experienced always relatively low RH (about or less than 40-50%) from ground to high altitude (see 80E-130E longitude in Figure 4.5a and e, as well as 20N-40N latitude in Figure 4.5b and f), while the high RH layer in marine boundary layer favors the removal processes of dust particles below 2km (see 130E-120W in Figure 4.5e, and 10N-50N in Figure 4.5c, g, d, and h). This feature can be also seen in the observed dust vertical profile by the DC-8 flight 11 to 13 in the later discussions.   However, dust particles nearly always encountered air mass with relatively low RH (about or less than 40-50%) above 2 km, no matter over continent or over Pacific Ocean.

Another interesting feature of Figure 4.5 is that along the dust pathway (20N-40N latitude), the RH over marine surface below 2 km seems anti-correlated with the dust loading. This might imply some radiative forcing effects of dust particles.   Dust particles may shadow the marine surface along its pathway or serve as cloud condensation nuclei and thus change the cloud albedo. This may change the surface radiative flux and temperature, and thus weaken the water evaporation on the marine surface along its

pathway.   However, this suspect requires further studies with meteorology and chemical feedback model to confirm.

4.4.2 Comparison of model predictions with aircraft observations

4.4.2.1 Validation of modeled meteorology field

The chemical transport model STEM is driven by the simulated meteorology field driven by WRF-ARW. In this section, the WRF model skill is evaluated against the in-situ observation onboard the DC-8 for four key meteorological parameters including temperature, Relative Humidity (RH), wind speed and wind direction in Figure 4.6. These four meteorological parameters are essential for chemical transport with observations. The model predicted values and DC-8 observations are binned into 10 levels in altitude from ground to about 10 km and then plotted as an average over Flight #11-13 in blue and red, respectively. The horizontal error bars are the standard deviations of both model predictions and observations. Figure 4.6a shows that the model captures the vertical profile of both temperature and pressure (not shown) quite well. The standard deviation of the model and observed variables are also similar.

The comparison of RH is strictly not a robust evaluation of WRF model skill since it is based on the governing RH parameterized equation. However, since RH is an important parameter for chemical transport models, we present the comparison here in Figure 4.6b. Model does fairly well in capturing the vertical distribution of the RH. It shows a small positive bias in the lower and upper troposphere and a larger bias in the middle troposphere. This means, even though we have seen a relative low RH (<40%) along the dust path way above 2km till about 6km(see Figure 4.5 in Section 4.1.2), the actually observed the RH values at these locations is even about 30 to 50% lower than the model prediction.

As shown in Figure 4.6c, the WRF model captures the observed wind speed measured by the DC-8 flights up to 6 kilometer after which the model has a negative bias. For wind direction, the model shows low negative bias around 3 km and larger positive around 4km (Figure 4.6d).

4.4.2.2 Comparison of modeled and observed aerosol
compositions

The comparison of observations to modeled aerosol compositions along the flight tracks is challenging. It is mainly due to the fact that aerosol particles have relative short life time comparing to gaseous species and they are thus transported in relatively discrete plumes across the Pacific, as already shown stronger zonal distributions of aerosols in model domain in Figure 4.3b, d and f. This makes it difficult for models to capture the aerosol chemical concentrations at some specific locations where the flight sampling the air. *Dunlea et al.* [2009] also reported that for some of the flights during INTEX-B, even though the models slightly dislocated their transport pathway, these large polluted air masses are so intense that missing these concentrations could easily modify the average vertical profiles of aerosol chemical compositions.

Figure 4.7a shows the comparison of predicted and observed calcium. In general model well captured the shape of the profile. This indicates that our dust emission scheme in STEM model is good and also the treatment of parameterized calcium percentage in total dust is reasonable. However, model has slight positive bias from about 2km to 4km, and it significantly over-predicts the calcium concentration above 7km. As shown in Figure 4.1a, DC-8 flights #11-13 cover the region between 175W-150W and 20N to 45N, especially 20N~30N. If we take a look at this region in Figure 4.5d and h, the modeled RH above 3km till about 6km are very low, less than 10%. This may indicate that the wet removal of dust in this altitude is not enough due to the very low relative humidity. For the largely over-prediction above 7 km, it can be seen that in Figure 4.7a, the observation

deviation is very small. When we exam the statistic, it is found that there are only about 10 data points included into the statistic in these levels (Other layers the data points included into the statistic are generally over 50 and maximum is 180.), which means that the statistic for these high altitude is rather poor.   On the other hand, even though when the dust particles reaches the locations where DC-8 flight 11-13 sampled, they have already been transported over several hundred kilometer, the dust air mass is still quite concentrated between 25N to 35 N according to the model results in Figure 4.5d.   Inside the dust air mass, dust concentration can be about 10 to 20 ug/m^3; while just outside of the dust air mass, the dust concentration may be as low as less than 1 ug/m^3.   At the mean time, the WRF model obviously underpredicts the wind speed at high altitude above about 7 km than at the low altitude (see Figure 4.6c). These again make the model difficult to capture the observed dust concentration at high altitude above 7 km.

Ammonium is systematically underpredicted in all cases even when we compare total NH4 (gas+particle) with observed particle NH_4^+, which may imply the lower NH_3 emissions in model. Figure 4.7c implied there is less predicted NH_3 gas in Case "2k9case2" than other cases, which may be due to the longer time to reach gas-particles thermodynamic equilibrium for ammonia when using the dynamic method for gas-to-particles conversion.

Figure 4.8 presents the comparison of model predicted and observed nitrate and HNO_3 from the DC-8. Figure 4.9 shows the partitioning of nitrate from model and observation. Figure 4.8a shows that nitrate concentrations in case "2k9case2" are lower than the values from the other three cases at all altitudes and closer to observation only around 2km. This difference is due to the different treatment for gas-to-particular conversion in Case "2k9case2". The predicted nitrates in the other cases are similar. They are all underpredicted above 4km and overpredicted below 4km. Figure 4.8b shows the modeled HNO_3 gas phase values are underpredicted in all cases. Even with the comparison of total nitrate (gas + particulate nitrate), we still see the underpredictions at lower altitudes

in Figure 4. This suggests that the treatment for gas-to-particular conversion may play more important role on dust aging than the heterogeneous uptake of HNO_3. The HNO_3 partitioning between gas phase and particulate phase will be discussed in details later. The underpredicted HNO_3 and overpredicted nitrate at altitudes below 2km may be contributed to the high RH value in the layer. The predicted condensation rate and heterogeneous uptake rate could be very high under high RH condition. Stratospheric concentrations of HNO_3 are typically higher than those observed in the free troposphere, which could explain the model underpredictions of HNO_3 and nitrate at high altitudes.

Figure 4.10 presents the comparison of model predicted and observed sulfate and SO_2 from the DC-8. Figure 4.11 shows the partitioning of sulfate from model and observation. The model SO_2 profiles from all cases are very similar. The predicted SO_2 values are generally well captured for the DC-8 flights in terms of both mean values and variability above 5km. However, the model fails to capture the elevated SO_2 levels below 5 km, especially in boundary layer. In addition the predicted variability is also much lower than the observations. It is possible that the current emission inventory might be low on SO_2 emissions or miss some local sources. All cases have similar sulfate values with small under-prediction above 4km and large under-prediction at 1-4 km. The underprediction in boundary layer may be due to emission and also MBL sulfate production from DMS oxidation. In Figure 4.11 total sulfate (gas + particulate sulfate) is well captured in the lower troposphere. This suggests that the calculated partitioning into the particulate phase on dust and sea salt is too strong.

4.4.3 The impact of heterogeneous reactions on tropospheric chemistry over the Pacific Ocean

We examined the importance of heterogeneous chemistry on the trace species distributions during INTEX-B. An additional simulation (Case "r6c2") was performed where the reactions of ozone, SO_2 and NO_2 and HNO_3 on dust were turned off. The change

in trace species distributions are presented in Figure 4.13. In the East Asia outflow the impact of heterogeneous reactions on dust is significant, increasing the average aerosol sulfate and nitrate by up to 10% and 20%, respectively, while reducing ozone levels by 5 to 10%. Over the central and eastern Pacific, where the INTEX-B flights were conducted, the mean impacts of the heterogeneous reactions on dust for sulfate and nitrate were 1–5%.

We also investigated the impact of RH-dependent heterogeneous uptake of HNO_3 (Case "2k9case3") on the trace species distributions during INTEX-B. The change in trace species distributions are presented in Figure 4.14. In the East Asia outflow the impact of heterogeneous reactions on dust is decreased, while the impact on sulfate is slightly increased. The impact on ozone is similar. Over the central and eastern Pacific the mean impacts of the heterogeneous reactions on dust for sulfate and nitrate are enhanced significantly. The impact on OH is increased in central Pacific and decreased on the both sides of Pacific. By considering a RH-dependent heterogeneous uptake of HNO_3, the size distributions are significantly changed for sulfate in lower and mid troposphere (see Figure 4.9 and 4.11, and later discussion). There are more fine-mode sulfate and nitrate in Case "2k9case3". This change is very important for radiation balance calculation.

However the impacts of the heterogeneous reactions at specific times during dust transport episodes can be much larger than the mean impacts discussed above. *McNaughton et al.* [2009] analyzed the aerosol and gas phase measurements on the DC-8 aircraft to show that in the presence of dust both sulfate and nitrate aerosol production is increased, and that as a result of the dust reactions, gas phase nitric acid levels are reduced appreciably. In Figure 4.12a we show plots of observed sulfate to total potential sulfate (sum of sulfate and SO_2) as a function of aerosol Ca for all three DC-8 flights, for altitudes above 1.5 km, CO and O_3 greater than 90 and 40 ppb, respectively, and [7]Be less than 800 fCi s/m^3 to exclude data influenced by clean air-masses and stratosphere. The data points show an envelope, with the ratio increasing with increases in Ca. Also shown are the predicted values for the same ratio plotted as a function of predicted dust concentration.

The model shows a similar behavior (Figure 4.12c, e, g, i) as that based on the observations. In Figure 4.12b, d, f, h and j, we plot the observed and modeled ratio of particulate nitrate to total nitrate (sum of particulate nitrate and gaseous nitric acid). Observations show that for Ca concentrations above 0.5 μg/m^3, the nitric acid partitions into the dust, reducing the gas phase concentrations by 50% (as discussed further in *McNaughton et al.* [2009]). The model shows different behaviors for the partitioning of nitrate in different cases. Case "2k9case3" shows qualitatively a similar behavior. Case "r2c2" and "r6c2" predict similar partitioning for dust concentrations above 10 μg/m^3, but more nitric acid partitioned into the dust with Ca concentrations below 10 μg/m^3. Case "2k9case3" shows slightly less nitric acid partitioned into the dust, but similar distribution of partitioning to observations.

4.4.4 Equilibrium vs. Dynamics approach for gas-aerosol partitioning

We investigated the impact of different treatment for gas-to-particular conversion on the trace species distributions by comparing Case "r2c2" and "2k9case2". The change in trace species distributions are presented in Figure 4.15. There is no significant change on ozone. The OH concentrations in Case "r2c2" is lower in central Pacific and higher on the both sides of Pacific. Compared with the full dynamics method used in Case "2k9case2", the CIT hybrid approach in Case "r2c2" increases the nitrate and sulfate production greatly. The equilibrium approach for gas-to-particle conversion usually underestimates the time to reach gas-aerosol thermodynamic equilibrium, especially the equilibrium between gas and coarse-mode particles. So it often overpredicts particle concentrations.

The discussions in Chapter 2 also show the equilibrium approach cannot deal with the mass transfer between different aerosol size bins due to the non-equilibrium status between different size bins. The aerosol compositions in different size bins are quite different, which usually results in the different pattern of gas-particle equilibrium in

different size bin. So compared with full dynamic method, equilibrium approach tends to predict a different aerosol size distribution. The sulfate fine ratio (fine-mode sulfate/total aerosol sulfate) and nitrate fine ratio (fine-mode nitrate /total aerosol nitrate) in all cases are plotted in Figure 4.16 and Figure 4.17. Case "2k9case2" predicated higher sulfate fine ratio than Case "r2c2" and "r6c2". The less acidic coarse mode dust particles tend to attract more acid than the more acidic fine mode urban-derived aerosols. More fine-mode sulfate could be predicted with dynamic method in this condition. In Figure 4.16d sulfate production in fine mode is suppressed by higher value of fine-mode nitrate in this case. So lower sulfate fine ratio is seen in this case. HNO_3 partitioning is more affected by heterogeneous reaction than sulfate partitioning. Higher nitrate in fine mode could cause more water absorption, and then larger surface areas and faster mass transfer rate with equilibrium approach. So we can clearly see the impact of heterogeneous chemistry in Figure 4.14a, b, and d. Dynamic method usually predicted faster gas-to-particle conversion rate in fine-mode particle than equilibrium method. So higher nitrate fine ratio also can be seen in Figure 4.17c.

4.5 Conclusions

STEM, a regional chemical transport model, was used to simulate the outflow of aerosols and trace gases from Asia to North America during the spring of 2006. The model performance was evaluated with observations from the NASA INTEX-B field campaign. The STEM model chemical transport was driven by the recently developed WRF meteorological model. The results from the WRF model showed that the model was able to capture the meteorological variables adequately to simulate chemical transport.

Model results captured the vertical profile of Ca well, which indicate successful prediction on dust emission. Big difference between modeled ammonium and observation imply the current NH_3 emission is too low. Model underpredicted both HNO_3 gas and nitrate in the upper troposphere, which may be due to the impact of stratosphere.

Overpredicitons of nitrate and underprediction of HNO_3 in the lower troposphere in model results indicate the overestimated gas-to-particle conversion rate in current version of STEM model. Comparisons of modeled sulfate to airborne observations show that the model overestimates the magnitude of sulfate concentration, except at surface. Modeled SO2 is seen to be completely depleted and underpredicts the observations. Therefore, it seems that the current sulfate emissions developed for the INTEX-B campaign is low and MBL sulfate production is underestimated.

Modeling experiments were carried out to study the impact of heterogeneous chemistry on dust surfaces to evaluate if they were significant in altering the composition of atmospheric trace gases and aerosols over the Pacific. The results show while these mechanisms are important over the source region, they are not significant over Central. The effects of heterogeneous chemistry over Eastern Pacific show large difference when considering a RH-dependent heterogeneous uptake of HNO_3 in model. Stronger effects of heterogeneous chemistry are shown over this region in Case "2k9case3" due to low RH values here and the RH-dependent uptake coefficients of HNO_3 reaction on dust. Considering a RH-dependent heterogeneous uptake of HNO_3 in model may not change nitrate and sulfate concentration too much, but affect the size distributions significantly.

A new dynamic method to treat the gas-to-particle conversion is compared with the equilibrium approach (CIT hybrid approach) used in current STEM model. The CIT hybrid approach for gas-to-particular conversion usually causes overpredictions on nitrate and sulfate during long range transport of dust. Using a full dynamics approach may solve this problem sometimes.

Table 4.1 The list of cases in the study

Case name	Descriptions
r2c2	Base case. heterogeneous reactions and equilibrium approach
r6c2	Similar to r2c2, but without heterogeneous reactions
2k9case2	Similar to r2c2, but using dynamical approach
2k9case3	Similar to r2c2, but considering the RH-dependent heterogeneous uptake of HNO_3 on dust
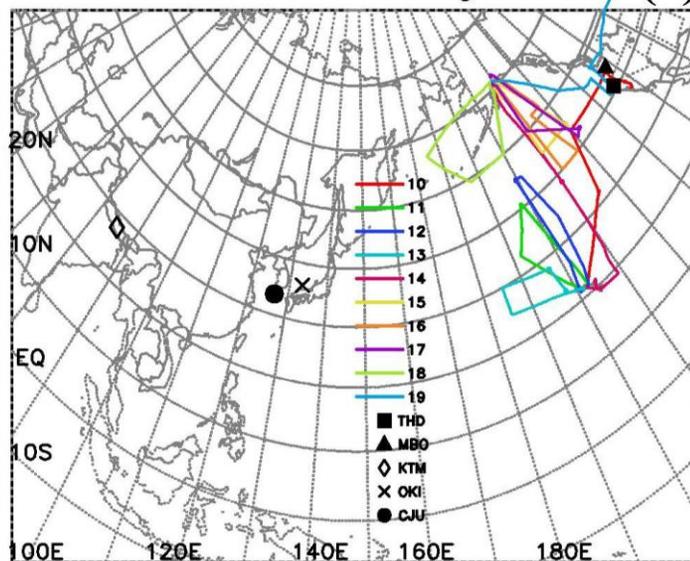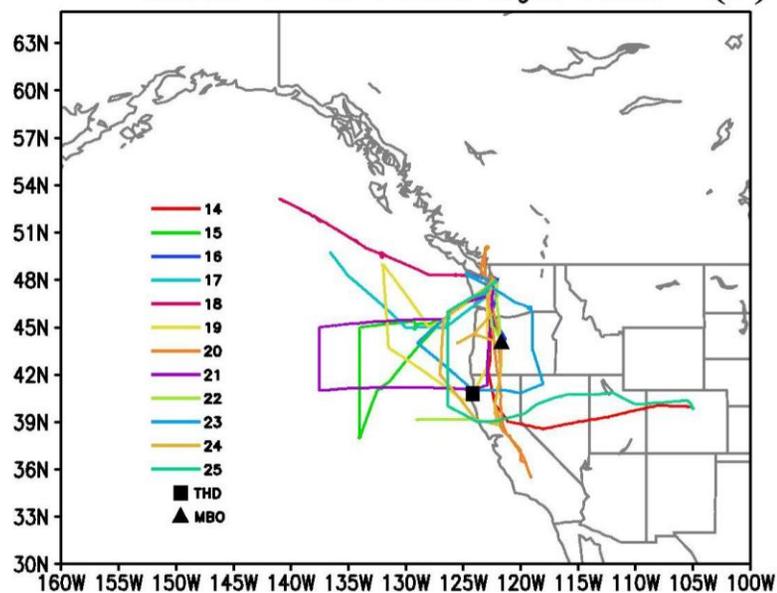
Figure 4.1 NASA DC-8 and NCAR/NSF C-130 flight tracks along with the location of ground based observation sites including Kathmandu (KTM), Trinidad Head (THD) and Mt. Bachelor (MBO) during the INTEX-B (Phase 2) experiment. The numbers denote the research flight numbers for the DC-8 and C-130 aircraft.
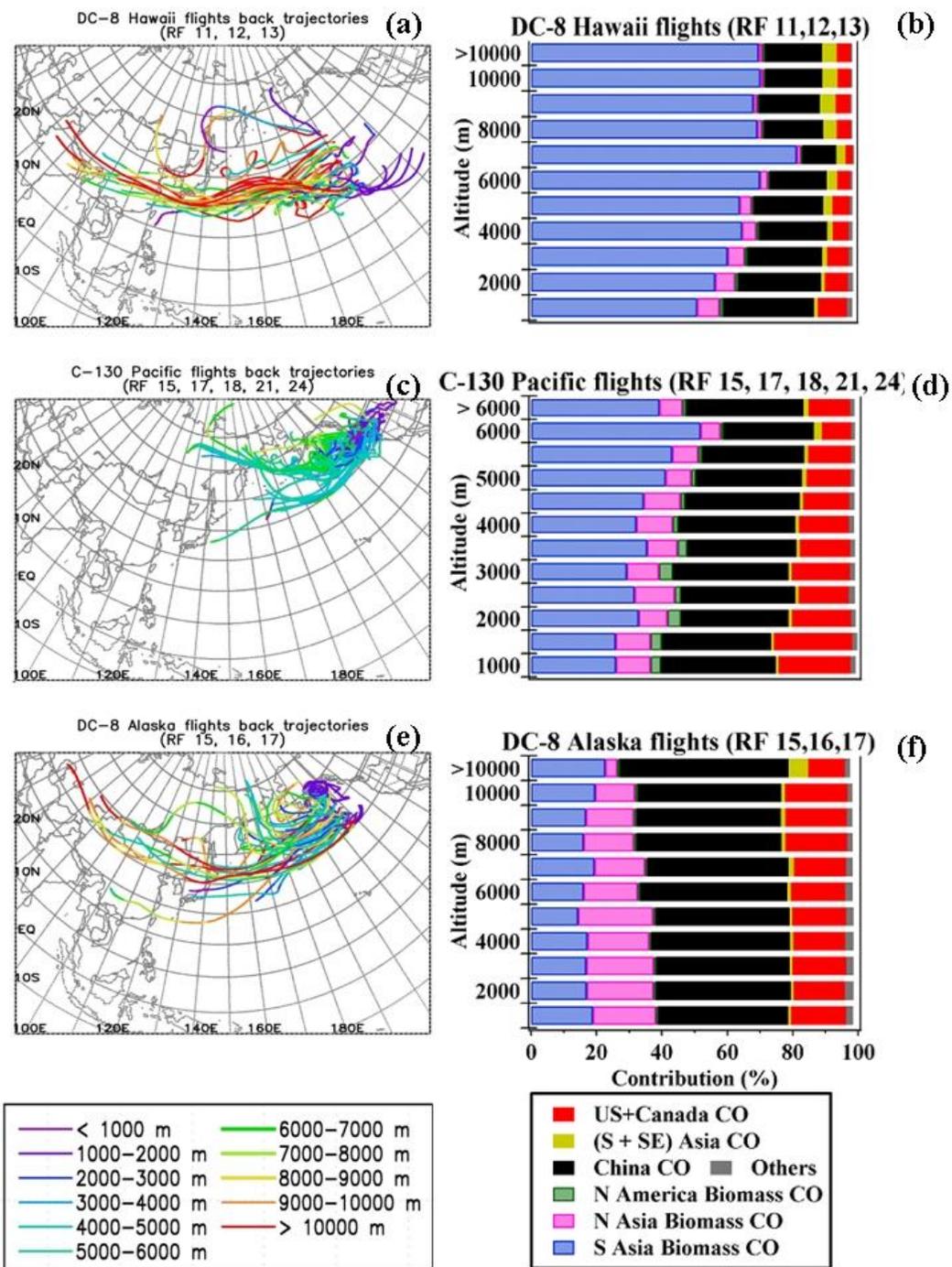
Figure 4.2 Back trajectories of wind vectors and tagged CO tracers illustrating the source region of air masses sampled by the selected DC-8 and C-130 flights.
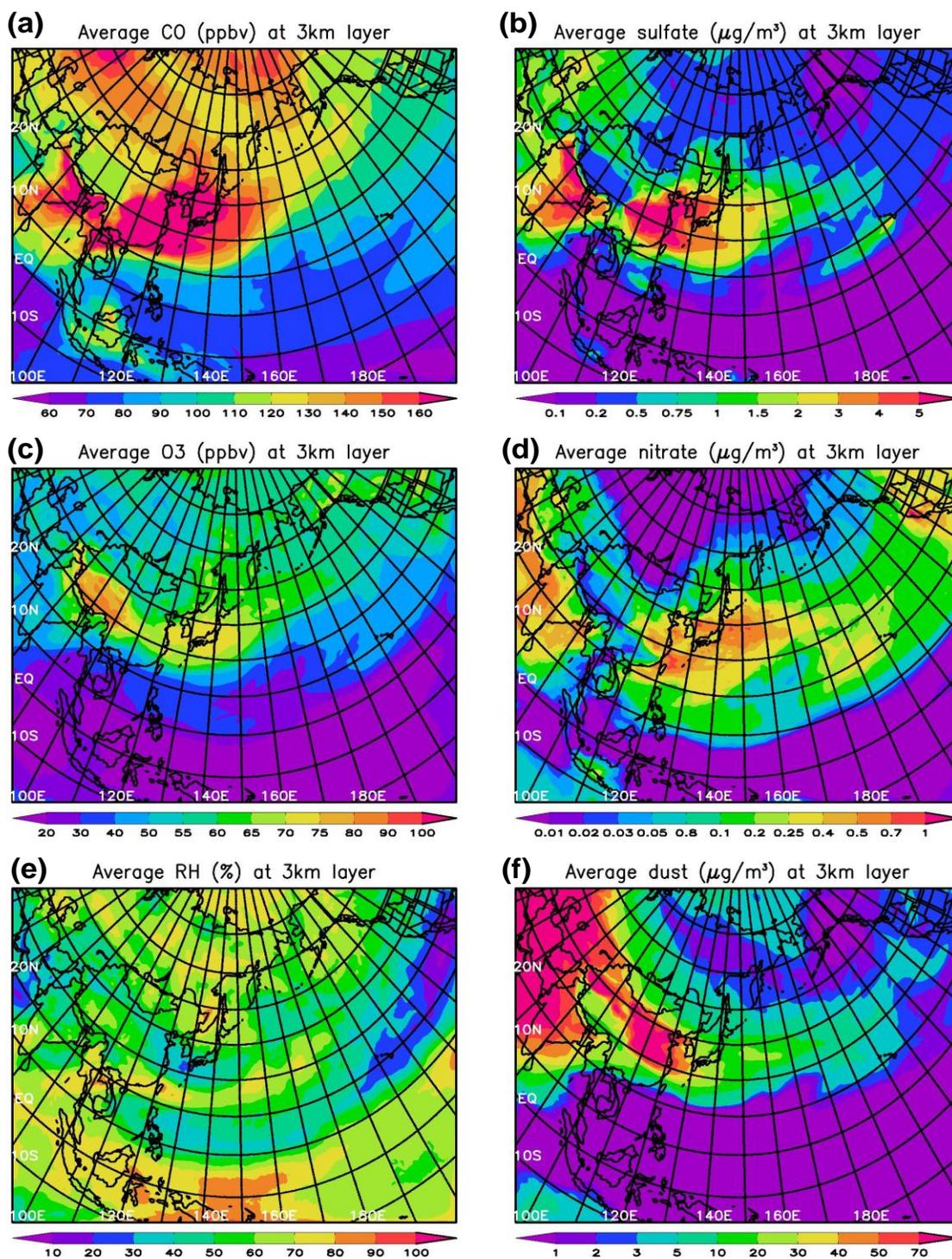
Figure 4.3 Average distributions of trace gases and aerosols at 3 km a.g.l. for the study period (April 16-30) during INTEX-B **(a)** CO (ppb) **(b)** Sulfate (μg/m3) **(c)**Ozone (ppb) **(d)** Nitrate (μg/m3) **(e)** RH (%) and **(f)** Dust (μg/m3).
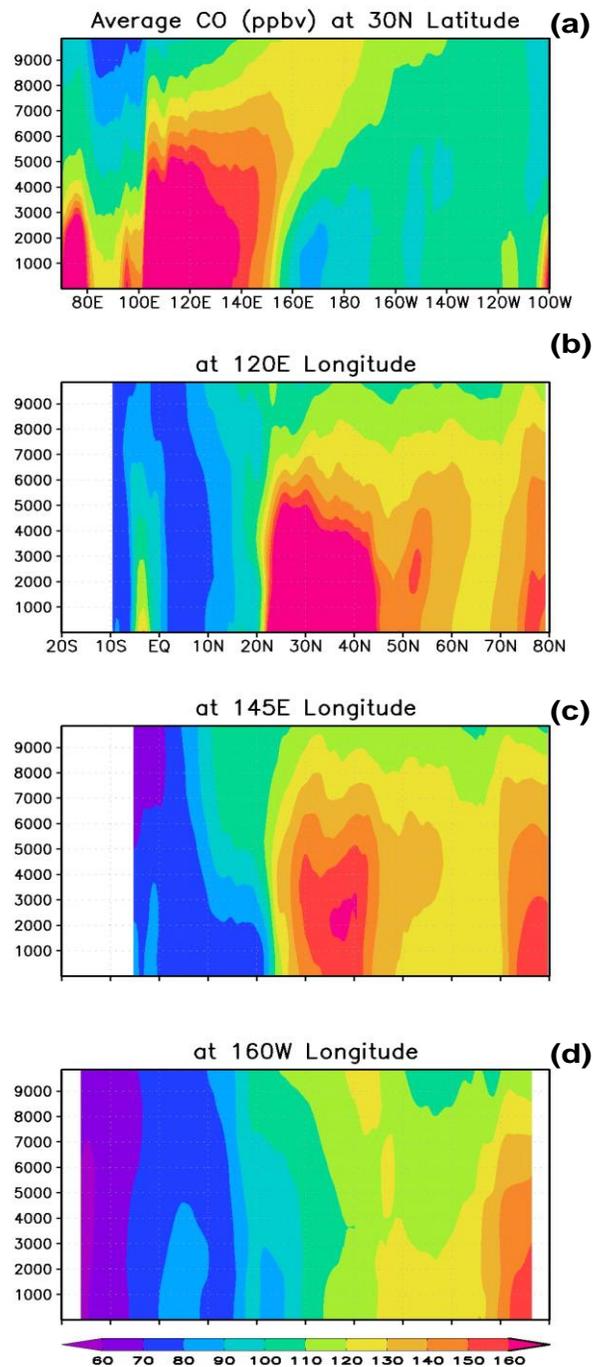
Figure 4.4 Average latitudinal and longitudinal distributions for the study period (April 16-30) during INTEX-B **(a)** Meridonial cross section of CO at 30 N; Zonal cross section of CO **(b)** at 120 E **(c)** at 145 E **(d)** at 160 W.
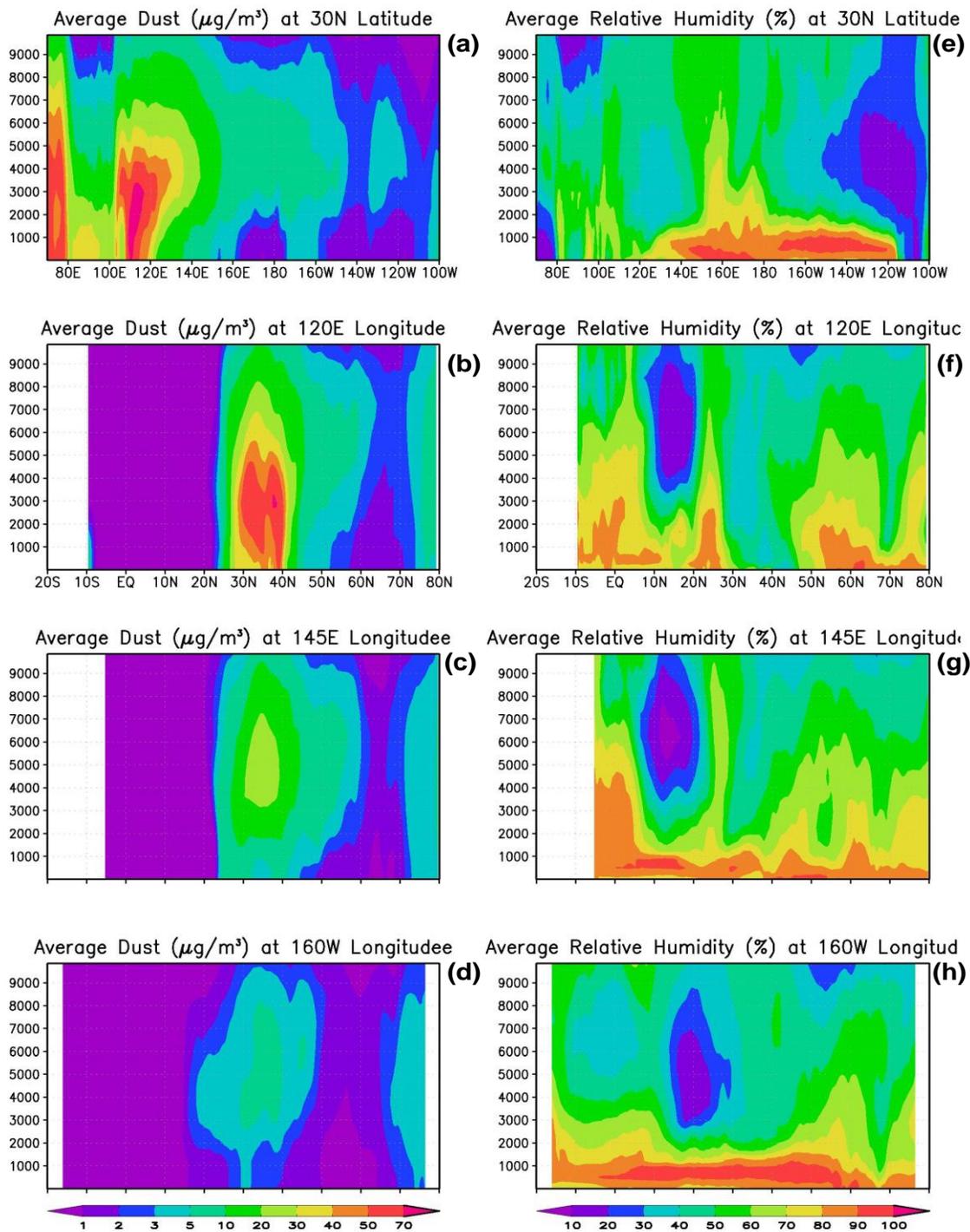
Figure 4.5 Average latitudinal and longitudinal distributions for the study period (April 16-30) during INTEX-B **(a)** Meridional cross section of dust at 30 N; Zonal cross section of dust **(b)** at 120 E **(c)** at 145 E **(d)** at 160 W **(e)** Meridional cross section of RH at 30 N; Zonal cross section of RH **(f)** at 120 E **(g)** at 145 E **(h)** at 160 W.
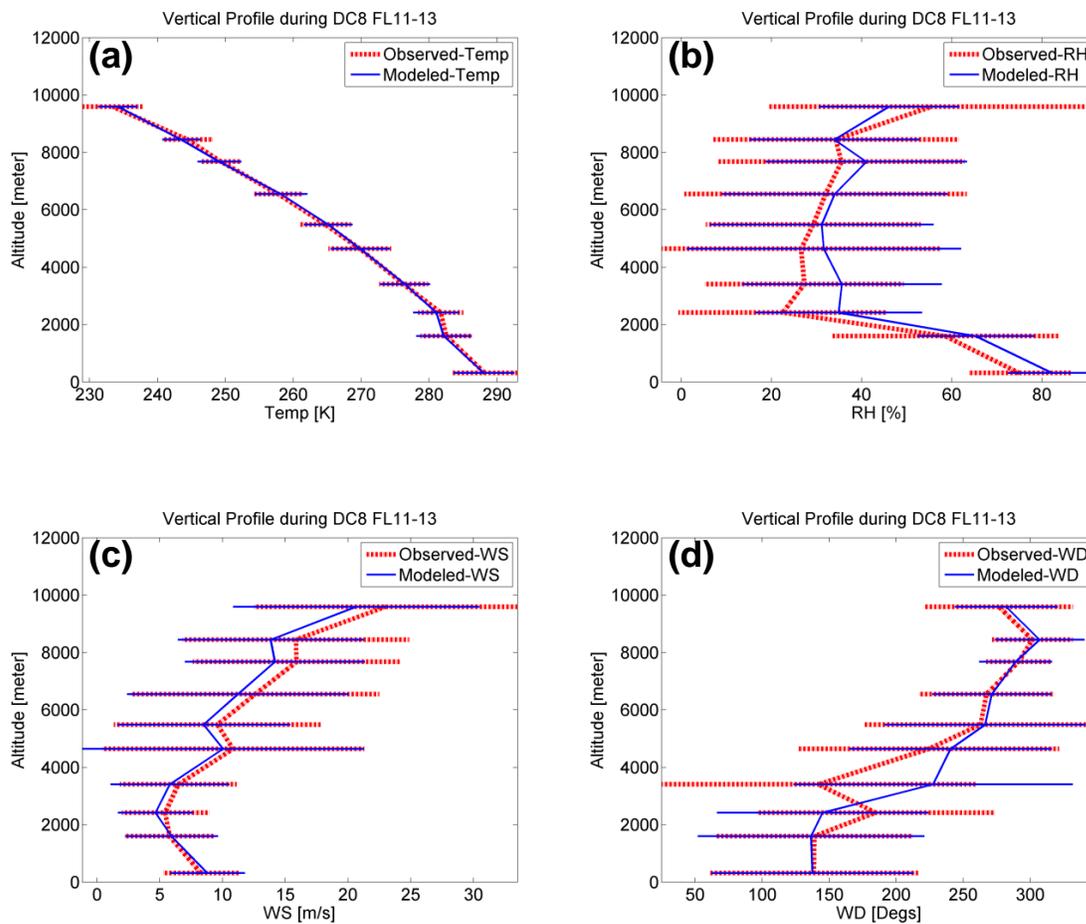
Figure 4.6 Comparison of meteorological variables from the WRF model with DC-8 observations. (a) Temperature, (b) RH, (c) Wind Speed, (d) Wind Direction
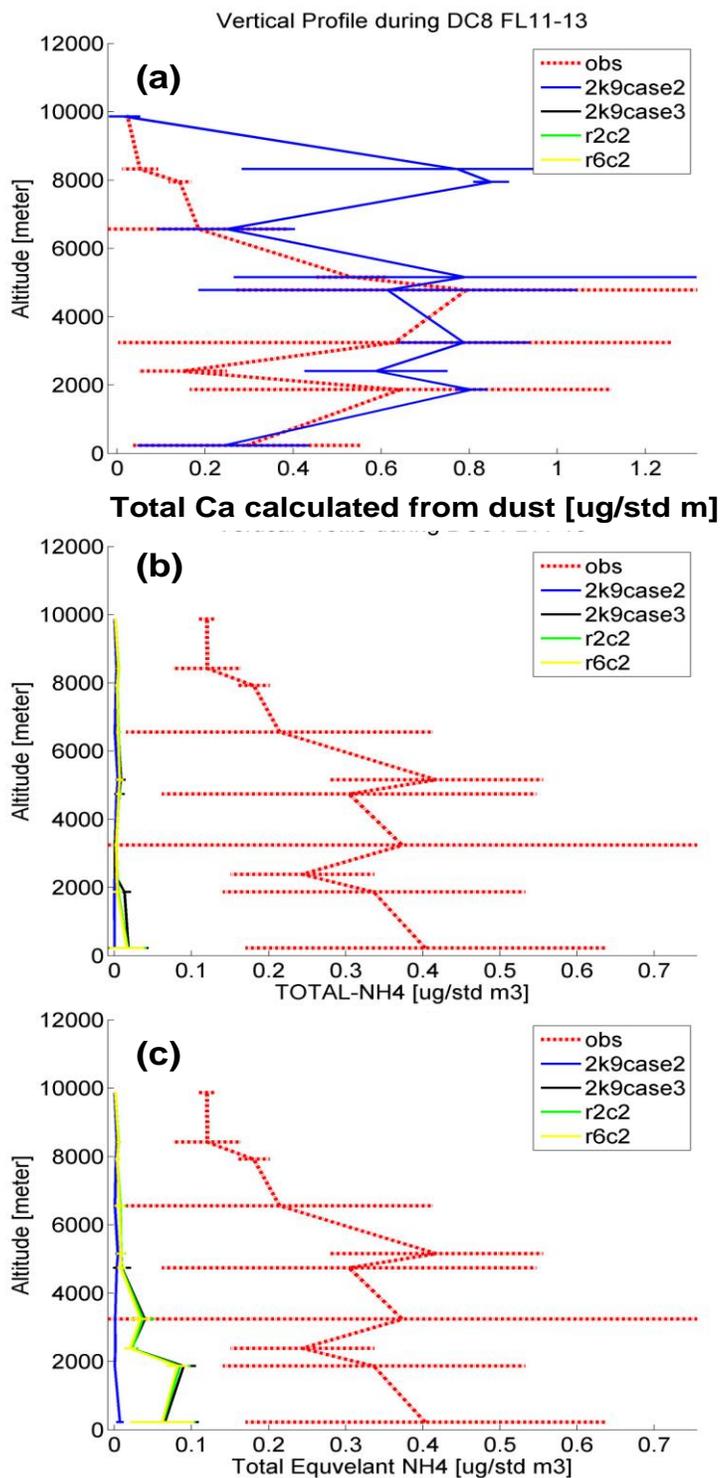
Figure 4.7 Comparison of STEM model predictions versus observations from the DC-8 for (**a**) Calcium (**b**) NH_4^+ (**c**) total NH_4 (gas + particle)
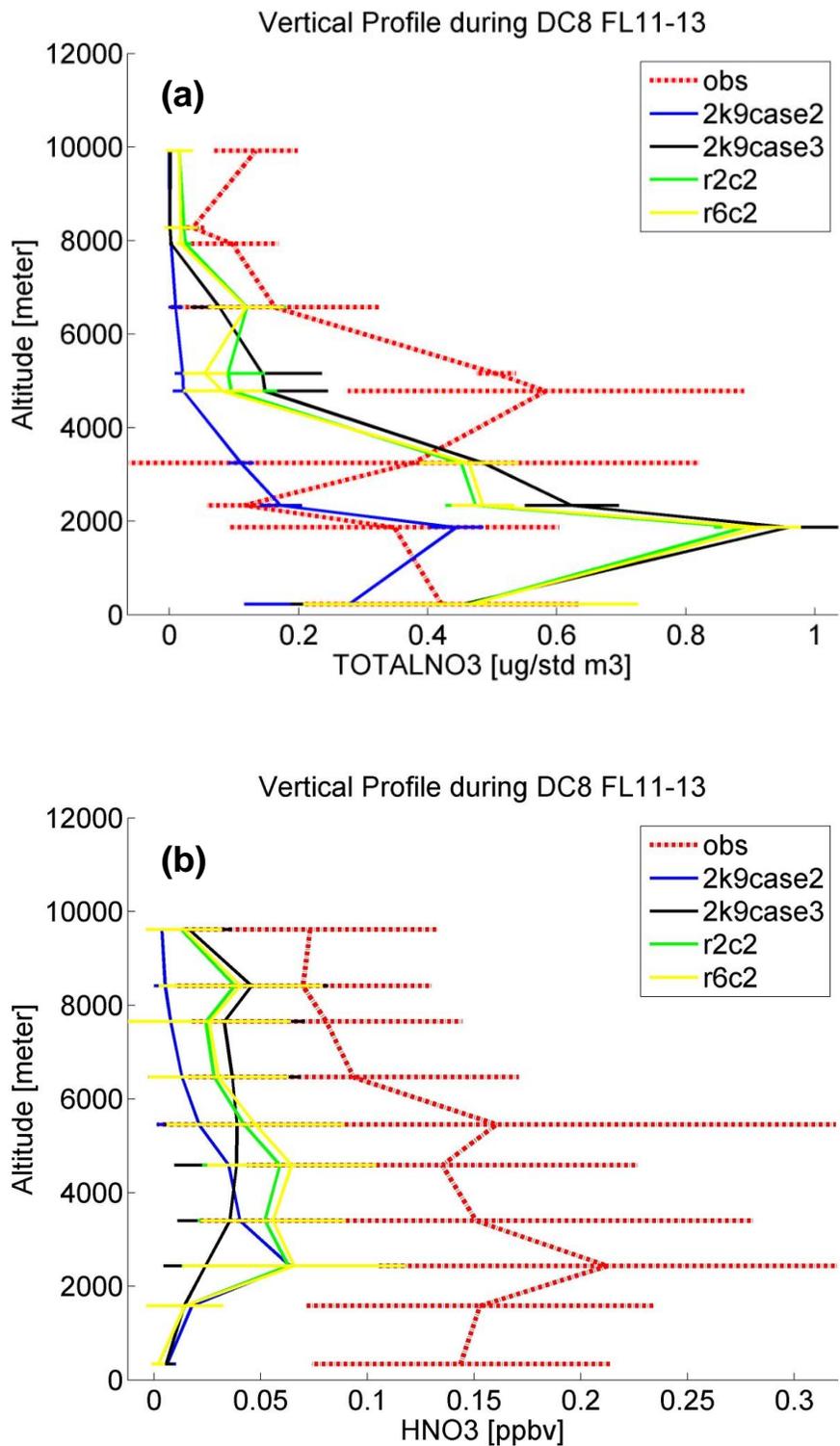
Figure 4.8 Comparison of STEM model predictions versus observations from the DC-8 for
(a) nitrate and **(b)** HNO$_3$
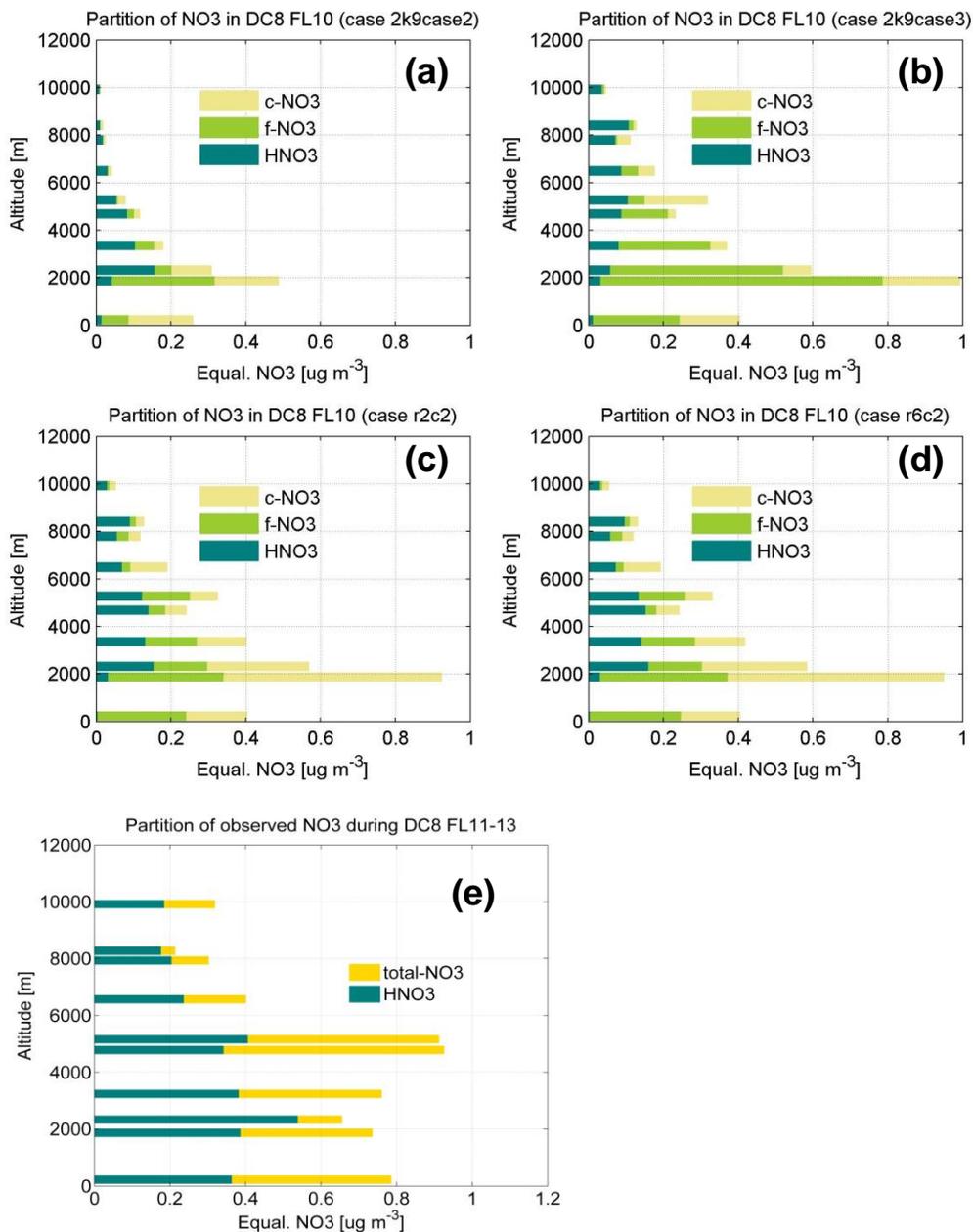
Figure 4.9 Comparison of model predicted and observed NO$_3$ components **(a)** Case "2k9case2" **(b)** Case "2k9case3" **(c)** Case "r2c2" **(d)** Case "r6c2" **(e)** Observation
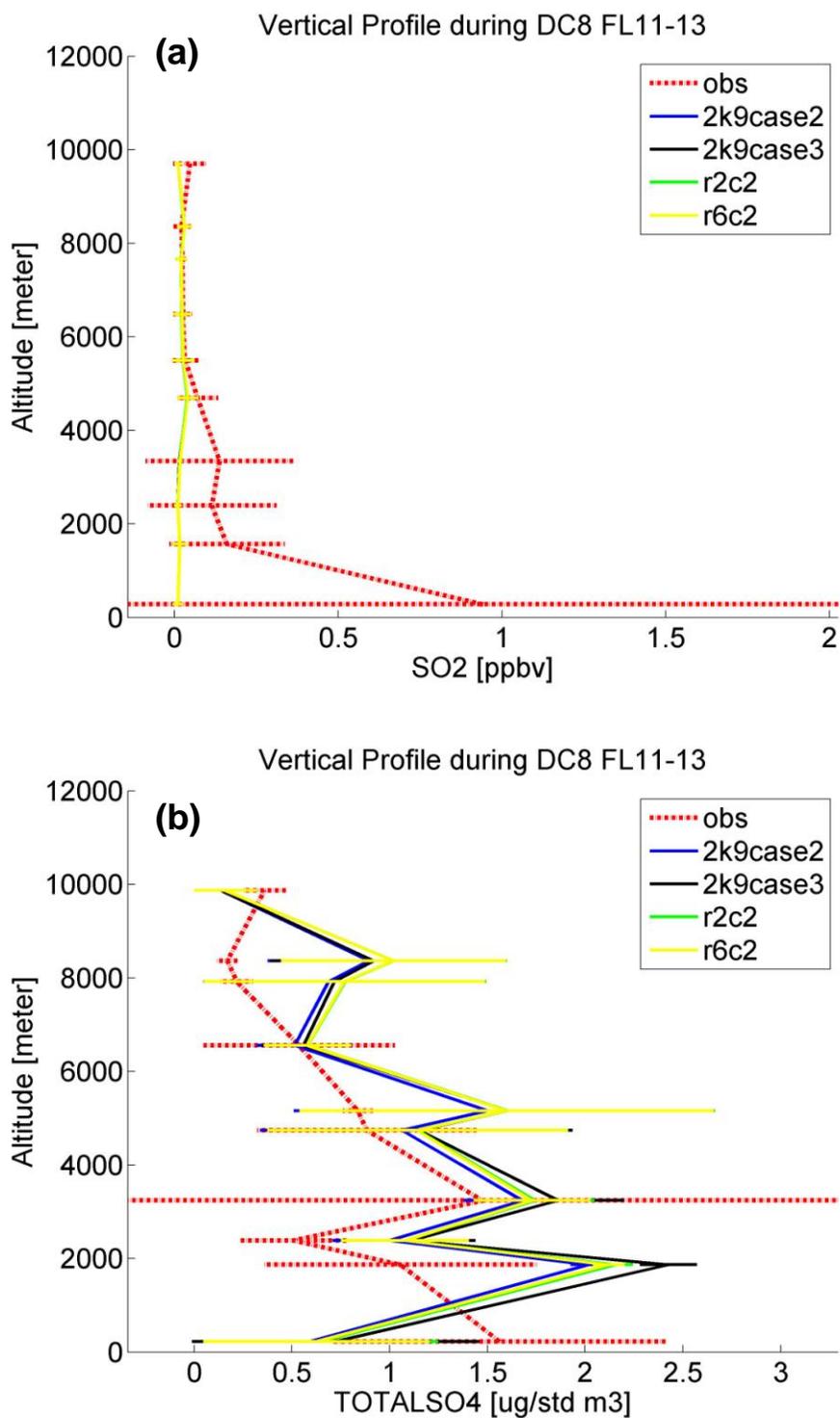
Figure 4.10 Comparison of STEM model predictions versus observations from the DC-8 for **(a)** sulfate and **(b)** SO$_2$
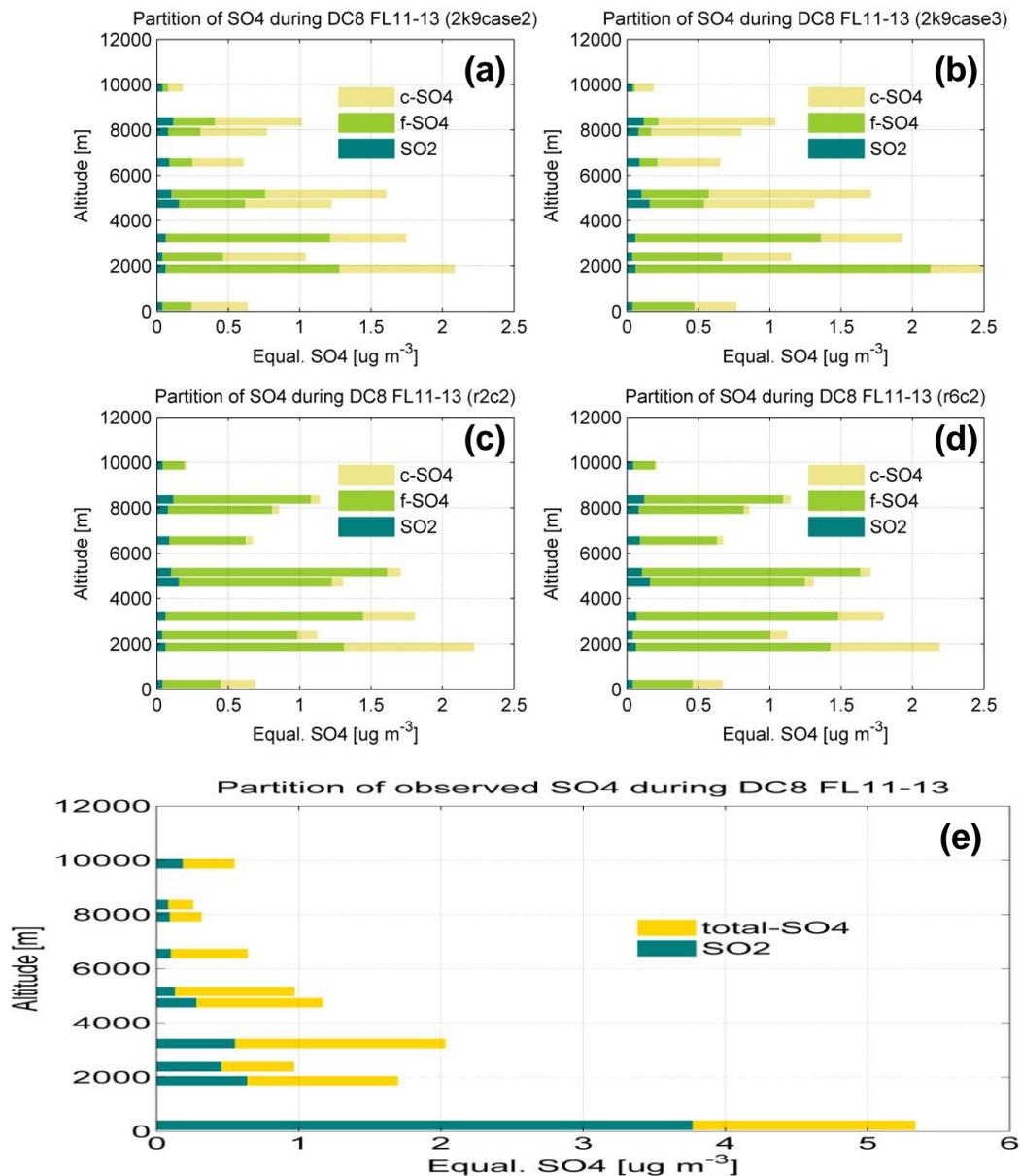
Figure 4.11 Comparison of model predicted and observed SO₄ components **(a)** Case "2k9case2" **(b)** Case "2k9case3" **(c)** Case "r2c2" **(d)** Case "r6c2" **(e)** Observation
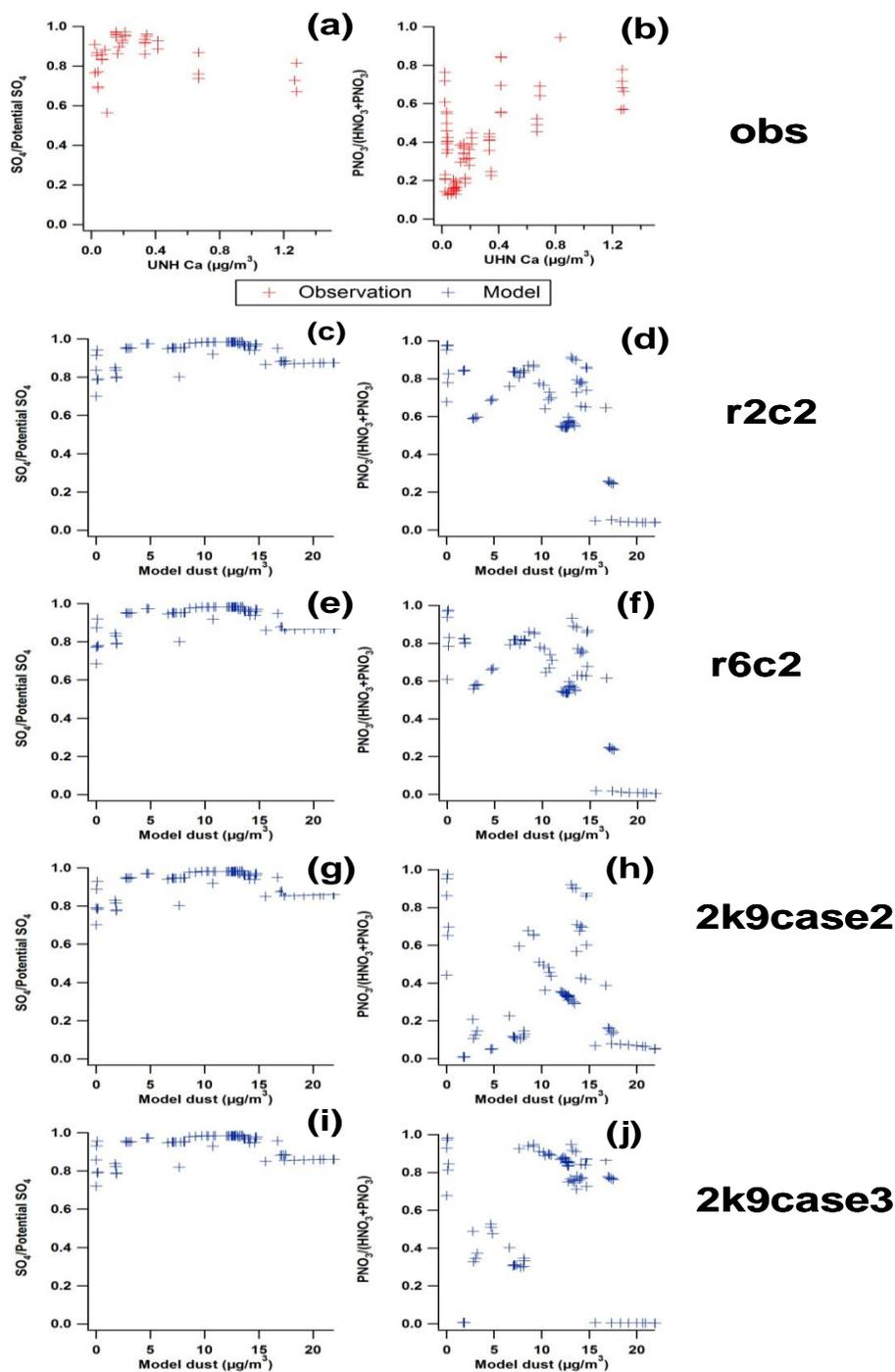
Figure 4.12 Comparison of model predicted ratios with DC-8 observations **(a)** observed SO₄/Potential SO₄ ratio **(b)** observed aerosol NO₃/(aerosol NO₃+HNO₃); Model results **(c)(d)** for Case "r2c2" **(e)(f)** for Case "r6c2" **(g)(h)** for Case "2k9case2" **(i)(j)** Case "2k9case3"

Figure 4.13 Average percent change in the concentration of trace gases and aerosols without heterogeneous chemistry during the Hawaii portion ofINTEX-B **(a)** OH **(b)** Ozone **(c)** Nitrate and **(d)** Sulfate. Shown are ((heterogeneous − without heterogeneous)/without heterogeneous) 100 (or (r2c2-r6c2)/r6c2 100).The values on the maps denote the contour labels at sharp gradients.
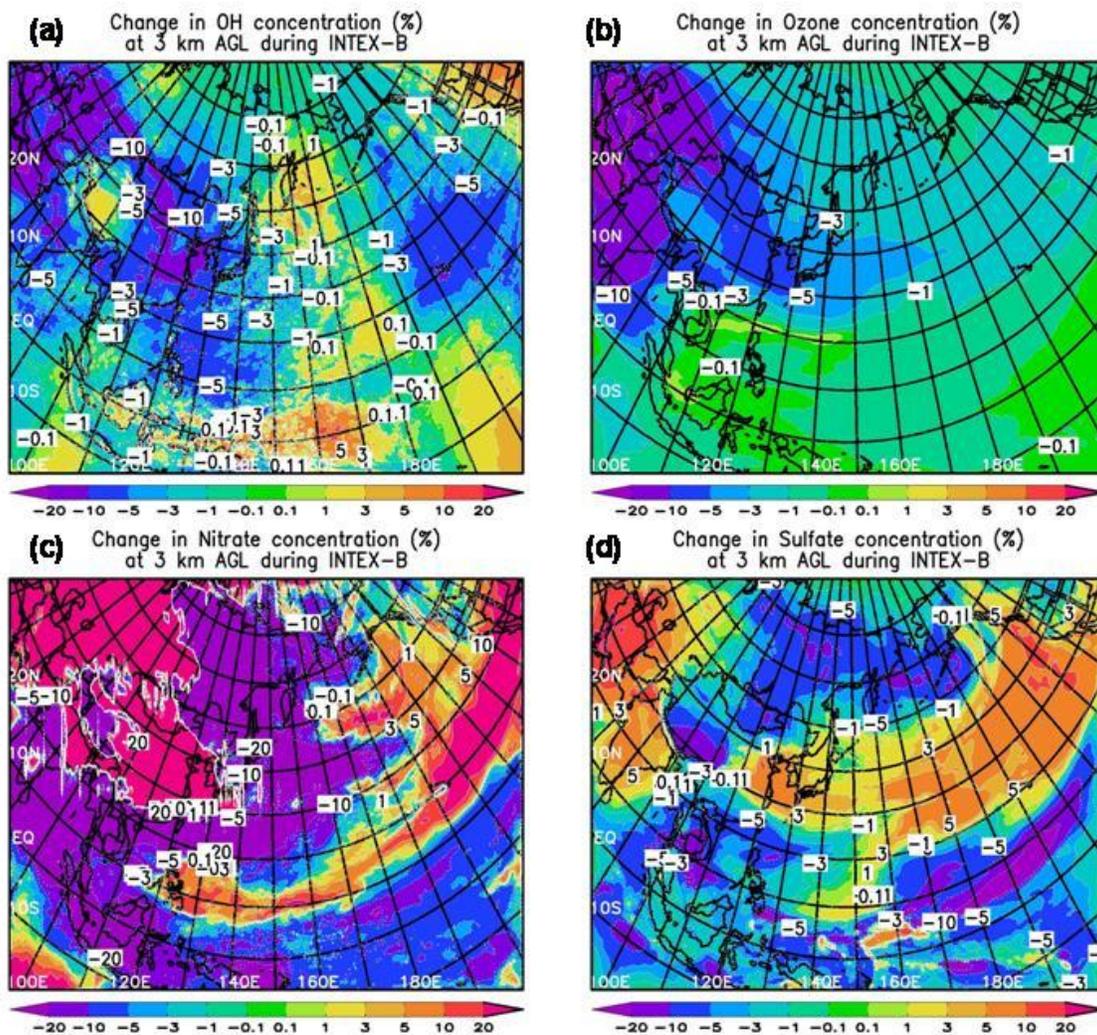
Figure 4.14 Average percent change in the concentration of trace gases and aerosols without heterogeneous chemistry during the Hawaii portion of INTEX-B **(a)** OH **(b)** Ozone **(c)** Nitrate and **(d)** Sulfate. Shown are (2k9case3-r6c2)/r6c2 100. The values on the maps denote the contour labels at sharp gradients.
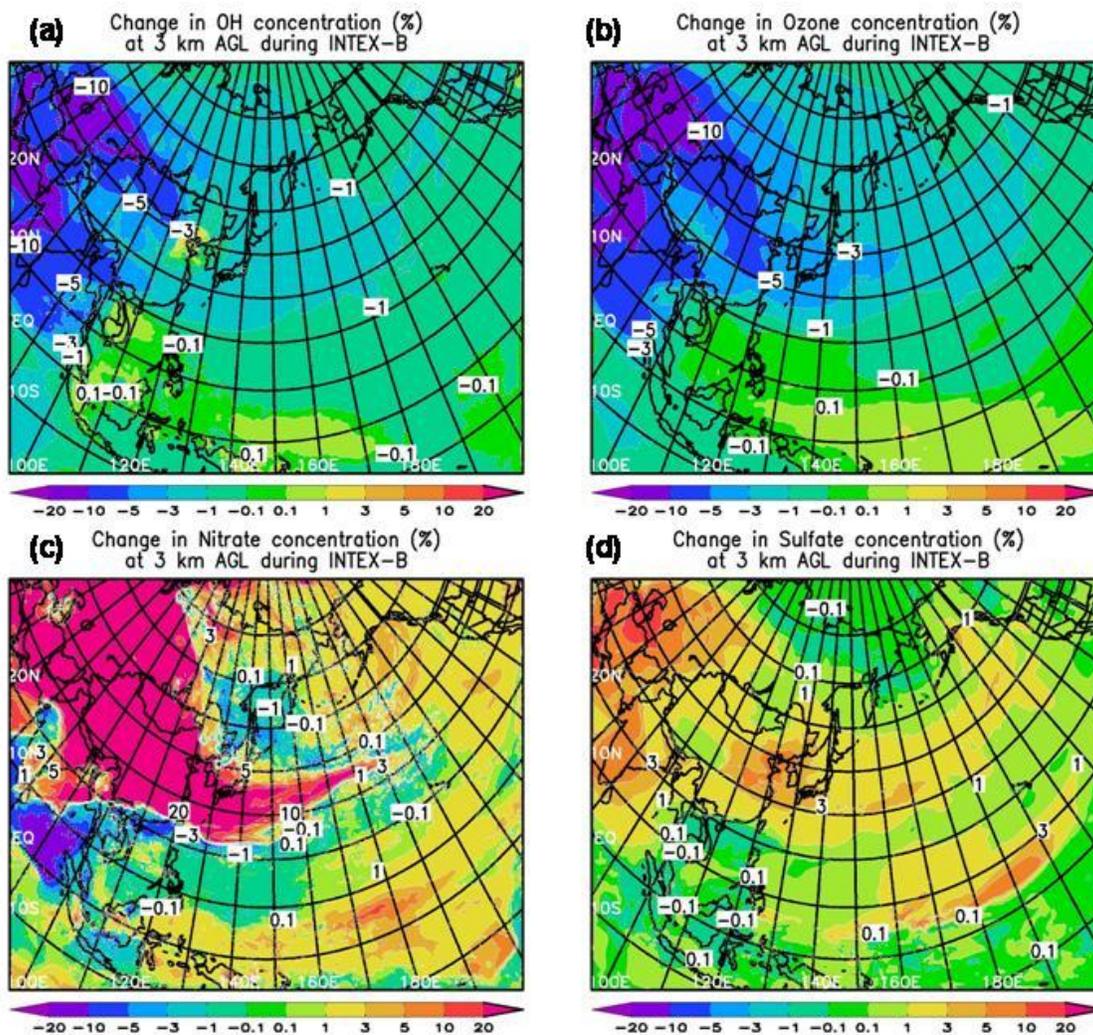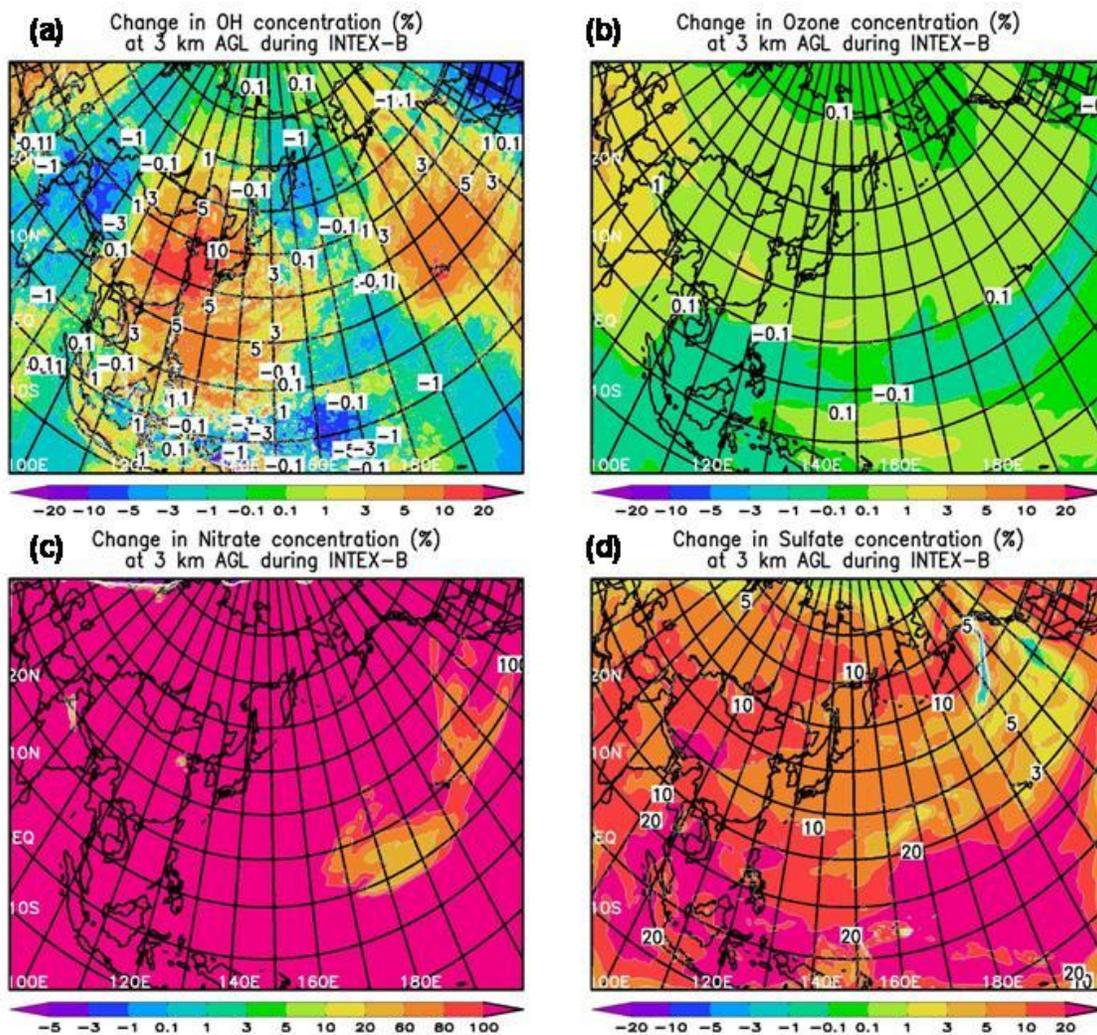
Figure 4.15 Average percent change in the concentration of trace gases and aerosols during the Hawaii portion of INTEX-B **(a)** OH **(b)** Ozone **(c)** Nitrate and **(d)** Sulfate. Shown are (r2c2-2k9case2)/2k9case2 100. The values on the maps denote the contour labels at sharp gradients.
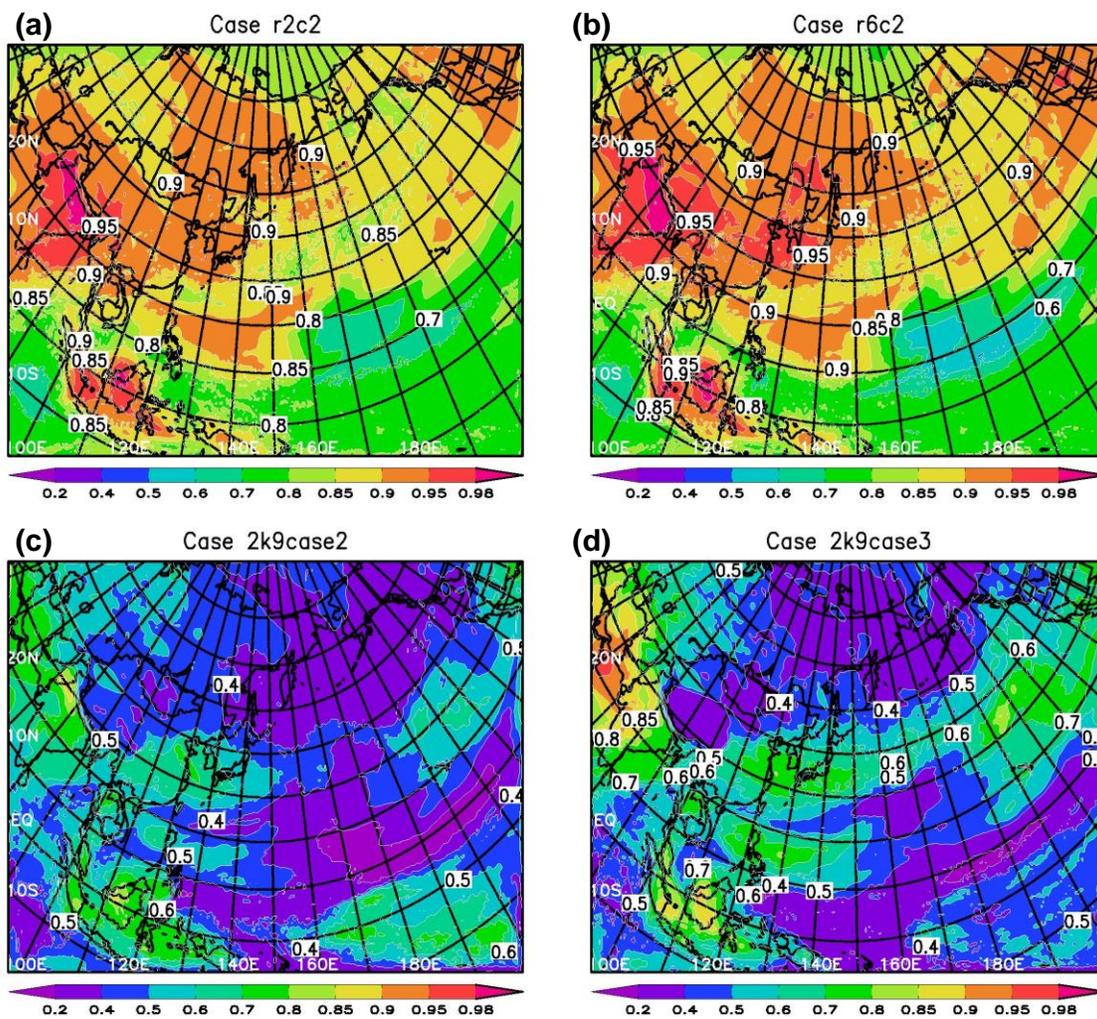
Figure 4.16 Simulated average sulfate fine ratio, fine-mode sulfate/total aerosol sulfate, during the Hawaii portion of INTEX-B for **(a)** Case "r2c2" **(b)** Case "r6c2" **(c)** Case "2k9case2" **(d)** Case "2k9case3"
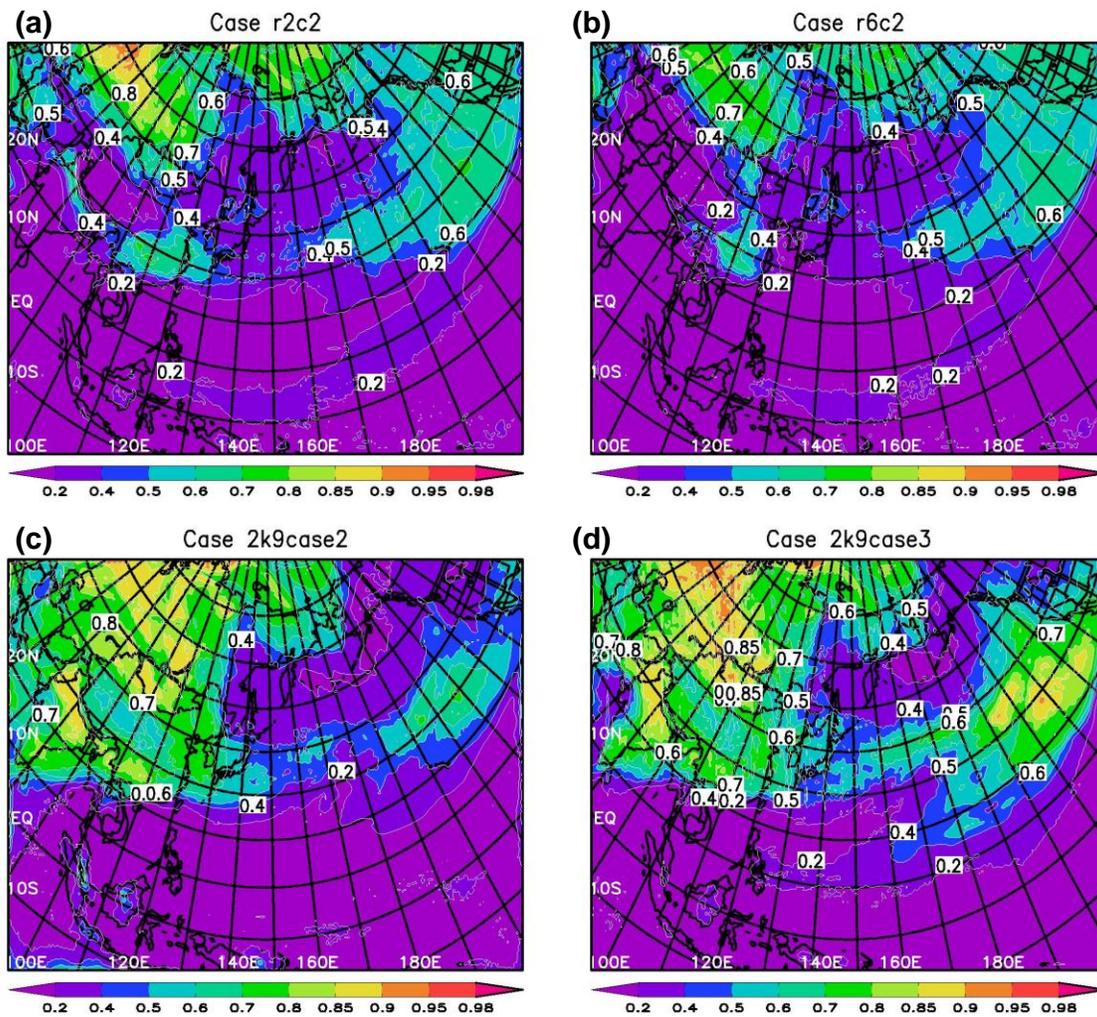
Figure 4.17 Simulated average nitrate fine ratio, fine-mode nitrate/total aerosol nitrate, during the Hawaii portion of INTEX-B for **(a)** Case "r2c2" **(b)** Case "r6c2" **(c)** Case "2k9case2" **(d)** Case "2k9case3"

CHAPTER 5

SUMMARY

In this thesis, a new aerosol module is developed for STEM in order to understand the chemical aging of dust during long range transport better and assess the impact of heterogeneous reactions on tropospheric chemistry.

The new aerosol module is verified and tested in box model studies before coupling with STEM model. The dynamic approach to treat gas-to-particular conversion is included into the new aerosol module to replace the equilibrium method (CIT hybrid method) in STEM model (Chapter 2). A new numerical method (AeroSolver) solving the aerosol dynamics equation is introduced into model. This new aerosol module significantly improved the simulating accuracy and computational efficiency during a test case. The results by using AeroSolver with 4 bins and piecewise quadratic are even more accurate than the results by using CIT- PFISLM method with 20 bins in the test case. Compared with the equilibrium method in STEM model, new dynamic approaches have more reasonable results on predicating the different hygroscopicity and different chemical aging pattern in different aerosol size bin. Compared with the MADE model, the two dynamic methods in the new aerosol model show significant discrepancies. Comparing model results from the two methods with observations will be needed to assess their performance and analysis the discrepancies between different methods.

New findings from laboratory experiments about heterogeneous reactions on mineral oxides and dust particles are included and assessed in box model studies (Chapter 3) in order to consider the complexity of surface chemistry (such as surface saturation, coating and relative humidity). Model results show the impacts of surface saturation and coating on heterogeneous reaction. But many of these data used in these studies come from the measurements on dry particle, which could limit their applications in real atmosphere. Modeling results recommend that the impacts of mineralogy and relative humidity on

heterogeneous reactions are significant and should be considered in atmospheric chemistry modeling with first priority.

Later, this new aerosol model is coupled into STEM model, to explore the data from INTEX-B field experiment (Chapter 4). New dynamic approach for gas-to-particular conversion and RH-dependent heterogeneous uptake of HNO_3 in model could improve model predictions on aerosols under different conditions. The case with new dynamic method predicted slower chemical aging and less aerosol mass in general. Including RH-dependent heterogeneous uptake of HNO_3 in model may not change nitrate and sulfate concentration too much, but influence the size distributions of them significantly. We still need at least two cases for better understanding the chemical aging of dust and the impacts of heterogeneous reactions. One is the case with the combination of new dynamic method and RH-dependent heterogeneous uptake of HNO_3. The other is the case with new dynamic method, but without any heterogeneous reactions.

REFERENCES

Adhikary, B. et al. (2010), A regional scale modeling analysis of aerosol and trace gas distributions over the eastern Pacific during the INTEX-B field campaign, *Atmospheric Chemistry and Physics*, *10*(5), 2091–2115.

Al-Abadleh, H., H. Al-Hosney, and V. Grassian (2005), Oxide and carbonate surfaces as environmental interfaces: the importance of water in surface composition and surface reactivity, *JOURNAL OF MOLECULAR CATALYSIS A-CHEMICAL*, *228*(1-2), 47-54.

Al-Saadi, J. et al. (2008), Intercomparison of near-real-time biomass burning emissions estimates constrained by satellite fire data, *JOURNAL OF APPLIED REMOTE SENSING*, *2*, doi:10.1117/1.2948785.

Andronova, A., L. GOMES, V. SMIRNOV, A. IVANOV, and L. SHUKUROVA (1993), Physicochemical Characteristics of Dust Aerosols Deposited During the Soviet-American Experiment (tajikistan, 1989), *ATMOSPHERIC ENVIRONMENT PART A-GENERAL TOPICS*, *27*(16), 2487-2493.

Bauer, S., Y. Balkanski, M. Schulz, D. Hauglustaine, and F. Dentener (2004), Global modeling of heterogeneous chemistry on mineral aerosol surfaces: Influence on tropospheric ozone chemistry and comparison to observations, *JOURNAL OF GEOPHYSICAL RESEARCH-ATMOSPHERES*, *109*(D2).

Binkowski, F., and U. Shankar (1995), The Regional Particulate Matter Model .1. Model description and preliminary results, *JOURNAL OF GEOPHYSICAL RESEARCH-ATMOSPHERES*, *100*(D12), 26191-26209.

Cao, J. J. (2005), Characterization of airborne carbonate over a site near Asian dust source regions during spring 2002 and its climatic and environmental significance, *J. Geophys. Res.*, *110*(D3), doi:10.1029/2004JD005244.

Capaldo, K., C. Pilinis, and S. Pandis (2000), A computationally efficient hybrid approach for dynamic gas/aerosol transfer in air quality models, *ATMOSPHERIC ENVIRONMENT*, *34*(21), 3617-3627.

Carmichael, G., L. Peters, and T. Kitada (1986), A 2nd Generation Model for Regional-Scale Transport Chemistry Deposition, *ATMOSPHERIC ENVIRONMENT*, *20*(1), 173-188.

Carmichael, G., L. Peters, and R. Saylor (1991), The Stem-II Regional Scale Acid Deposition and Photochemical Oxidant Model .1. and Overview of Model Development and Applications, *ATMOSPHERIC ENVIRONMENT PART A-GENERAL TOPICS*, *25*(10), 2077-2090.

Carmichael, G. et al. (2003), Regional-scale chemical transport modeling in support of the analysis of observations obtained during the TRACE-P experiment, *JOURNAL OF GEOPHYSICAL RESEARCH-ATMOSPHERES*, *108*(D21).

Carter, W. P. (2000), *Development and Evaluation of the Saprc-99 Chemical Mechanism, final report to California Air Resources Board, Contract No. 92-329.*, Air Pollution Research Center and College of Engineering Center for Environmental Research and Technology, University of California, Riverside,CA,USA.

Charlson, R., S. Schwartz, J. Hales, R. Cess, J. Coakley, J. Hansen, and D. Hofmann (1992), Climate Forcing by Anthropogenic Aerosols, *SCIENCE*, *255*(5043), 423-430.

Conant, W., J. Seinfeld, J. Wang, G. Carmichael, Y. Tang, I. Uno, P. Flatau, K. Markowicz, and P. Quinn (2003), A model for the radiative forcing during ACE-Asia derived from CIRPAS Twin Otter and R/V Ronald H. Brown data and comparison with observations, *JOURNAL OF GEOPHYSICAL RESEARCH-ATMOSPHERES*, *108*(D23).

Dentener, F., G. Carmichael, Yang Zhang, J. Lelieveld, and P. Crutzen (1996), Role of mineral aerosol as a reactive surface in the global troposphere, *JOURNAL OF GEOPHYSICAL RESEARCH-ATMOSPHERES*, *101*(D17), 22869-22889.

Dentener, F., and P. Crutzen (1993), Reaction of N2O5 on Tropospheric Aerosols - Impact on the Global Distributions of NOx, O3, and OH, *JOURNAL OF GEOPHYSICAL RESEARCH-ATMOSPHERES*, *98*(D4), 7149-7163.

Dunlea, E. J. et al. (2009), Evolution of Asian aerosols during transpacific transport in INTEX-B, *Atmos. Chem. Phys.*, *9*(19), 7257-7287.

Fuchs, N. A., and A. G. Sutugin (1970), *Highly dispersed aerosols*, Halsted Press, New York.

Gelbard, F., and J. Seinfeld (1978), Coagulation and Growth of a Multicomponent Aerosol, *JOURNAL OF COLLOID AND INTERFACE SCIENCE*, *63*(3), 472-479.

Gomes, L., and D. Gillette (1993), A Comparison of Characteristics of Aerosol from Dust Storms in Central-Asia with Soil-Derived Dust from Other Regions, *ATMOSPHERIC ENVIRONMENT PART A-GENERAL TOPICS*, *27*(16), 2539-2544.

Gong, S. (2003), A parameterization of sea-salt aerosol source function for sub- and super-micron particles, *GLOBAL BIOGEOCHEMICAL CYCLES*, *17*(4), doi:10.1029/2003GB002079.

Goodman, A., E. Bernard, and V. Grassian (2001), Spectroscopic study of nitric acid and water adsorption on oxide particles: Enhanced nitric acid uptake kinetics in the presence of adsorbed water, *JOURNAL OF PHYSICAL CHEMISTRY A*, *105*(26), 6443-6457.

Goodman, A., P. Li, C. Usher, and V. Grassian (2001), Heterogeneous uptake of sulfur dioxide on aluminum and magnesium oxide particles, *JOURNAL OF PHYSICAL CHEMISTRY A*, *105*(25), 6109-6120.

Goodman, A., G. Underwood, and V. Grassian (2000), A laboratory study of the heterogeneous reaction of nitric acid on calcium carbonate particles, *JOURNAL OF GEOPHYSICAL RESEARCH-ATMOSPHERES*, *105*(D23), 29053-29064.

Grassian, V. (2002), Chemical reactions of nitrogen oxides on the surface of oxide, carbonate, soot, and mineral dust particles: Implications for the chemical balance of the troposphere, *JOURNAL OF PHYSICAL CHEMISTRY A*, *106*(6), 860-877.

Hanisch, F., and J. Crowley (2001), The heterogeneous reactivity of gaseous nitric acid on authentic mineral dust samples, and on individual mineral and clay mineral components, *PHYSICAL CHEMISTRY CHEMICAL PHYSICS*, *3*(12), 2474-2482.

Hess, M., P. Koepke, and I. Schult (1998), Optical properties of aerosols and clouds: The software package OPAC, *BULLETIN OF THE AMERICAN METEOROLOGICAL SOCIETY*, *79*(5), 831-844.

Jacob, D. (2000), Heterogeneous chemistry and tropospheric ozone, *ATMOSPHERIC ENVIRONMENT*, *34*(12-14), 2131-2159.

Karagulian, F., C. Santschi, and M. Rossi (2006), The heterogeneous chemical kinetics of N2O5 on CaCO3 and other atmospheric mineral dust surrogates, *ATMOSPHERIC CHEMISTRY AND PHYSICS*, *6*, 1373-1388.

Kim, Y., and J. Seinfeld (1995), Atmospheric Gas-Aerosol Equilibrium .3. Thermodynamics of Crustal Elements Ca2+, K+, and Mg2+, *AEROSOL SCIENCE AND TECHNOLOGY*, *22*(1), 93-110.

Kim, Y., J. Seinfeld, and P. Saxena (1993a), Atmospheric Gas Aerosol Equilibrium .1. Thermodynamic Model, *AEROSOL SCIENCE AND TECHNOLOGY*, *19*(2), 157-181.

Kim, Y., J. Seinfeld, and P. Saxena (1993b), Atmospheric Gas-Aerosol Equilibrium .2. Analysis of Common Approximations and Activity-Coefficient Calculation Methods, *AEROSOL SCIENCE AND TECHNOLOGY*, *19*(2), 182-198.

Krueger, B., V. Grassian, J. Cowin, and A. Laskin (2004), Heterogeneous Chemistry of Individual Mineral Dust Particles from Different Dust Source Regions: The Importance of Particle Mineralogy, *ATMOSPHERIC ENVIRONMENT*, *38*(36), 6253-6261.

Lathiere, J., D. Hauglustaine, A. Friend, N. De Noblet-Ducoudre, N. Viovy, and G. Folberth (2006), Impact of climate variability and land use changes on global biogenic volatile organic compound emissions, *ATMOSPHERIC CHEMISTRY AND PHYSICS*, *6*, 2129-2146.

Liu, T. S., and others (1985), *Loess and the Environment*, China Ocean Press, Beijing.

Liu, Y., E. Gibson, J. Cain, H. Wang, V. Grassian, and A. Laskin (2008), Kinetics of heterogeneous reaction of CaCO3 particles with gaseous HNO3 over a wide range of humidity, *JOURNAL OF PHYSICAL CHEMISTRY A*, *112*(7), 1561-1571.

Lurmann, F., A. Lloyd, and R. Atkinson (1986), A Chemical Mechanism for Use in Long-Range Transport Acid Deposition Computer Modeling, *JOURNAL OF GEOPHYSICAL RESEARCH-ATMOSPHERES*, *91*(D10), 905-936.

Madronich, S. (2002), The Tropospheric visible Ultra-violet (TUV) model web page, *National Center for Atmospheric Research, Boulder, CO*. [online] Available from: http://www. acd. ucar. edu/TUV

Madronich, S., and S. Flocke (1999), The Role of Solar Radiation in Atmospheric Chemistry, in *Environmental photochemistry*, vol. 2, p. 1.

Maxwell-Meier, K., R. Weber, C. Song, D. Orsini, Y. Ma, G. Carmichael, and D. Streets (2004), Inorganic composition of fine particles in mixed mineral dust-pollution plumes observed from airborne measurements during ACE-Asia, *JOURNAL OF GEOPHYSICAL RESEARCH-ATMOSPHERES*, *109*(D19).

103

McNaughton, C. S. et al. (2009), Observations of heterogeneous reactions between Asian pollution and mineral dust over the Eastern North Pacific during INTEX-B, *Atmos. Chem. Phys.*, *9*(21), 8283-8308.

Mena-Carrasco, M. et al. (2007), Improving regional ozone modeling through systematic evaluation of errors using the aircraft observations during the International Consortium for Atmospheric Research on Transport and Transformation, *JOURNAL OF GEOPHYSICAL RESEARCH-ATMOSPHERES*, *112*(D12).

Meng, Z., D. Dabdub, and J. Seinfeld (1998), Size-resolved and chemically resolved model of atmospheric aerosol dynamics, *JOURNAL OF GEOPHYSICAL RESEARCH-ATMOSPHERES*, *103*(D3), 3419-3435.

Meng, Z., and J. Seinfeld (1996), Time scales to achieve atmospheric gas-aerosol equilibrium for volatile species, *ATMOSPHERIC ENVIRONMENT*, *30*(16), 2889-2900.

Meng, Z., J. Seinfeld, P. Saxena, and Y. Kim (1995), Atmospheric Gas-Aerosol Equilibrium .4. Thermodynamics of Carbonates, *AEROSOL SCIENCE AND TECHNOLOGY*, *23*(2), 131-154.

Meskhidze, N., W. Chameides, A. Nenes, and G. Chen (2003), Iron mobilization in mineral dust: Can anthropogenic SO2 emissions affect ocean productivity?, *GEOPHYSICAL RESEARCH LETTERS*, *30*(21).

Michel, A., C. Usher, and V. Grassian (2002), Heterogeneous and catalytic uptake of ozone on mineral oxides and dusts: A Knudsen cell investigation, *GEOPHYSICAL RESEARCH LETTERS*, *29*(14), doi:10.1029/2002GL014896.

Michel, A., C. Usher, and V. Grassian (2003), Reactive uptake of ozone on mineral oxides and mineral dusts, *ATMOSPHERIC ENVIRONMENT*, *37*(23), 3201-3211, doi:10.1016/S1352-2310(03)00319-4.

Mogili, P., P. Kleiber, M. Young, and V. Grassian (2006), N2O5 hydrolysis on the components of mineral dust and sea salt aerosol: Comparison study in an environmental aerosol reaction chamber, *ATMOSPHERIC ENVIRONMENT*, *40*(38), 7401-7408.

Mori, I., M. Nishikawa, T. Tanimura, and H. Quan (2003), Change in size distribution and chemical composition of kosa (Asian dust) aerosol during long-range transport, *Atmospheric Environment*, *37*(30), 4253-4263, doi:10.1016/S1352-2310(03)00535-1.

Nguyen, K., and D. Dabdub (2002), Semi-lagrangian flux scheme for the solution of the aerosol condensation/evaporation equation, *AEROSOL SCIENCE AND TECHNOLOGY*, *36*(4), 407-418.

Olivier, J. G. J., and J. J. M. Berdowsky (2001), Global emission sources and sinks, in *The climate system*, pp. 33–77, A.A. Balkema Publishers.

Pandis, S., A. Wexler, and J. Seinfeld (1993), Secondary Organic Aerosol Formation and Transport .2. Predicting the Ambient Secondary Organic Aerosol-Size Distribution, *ATMOSPHERIC ENVIRONMENT PART A-GENERAL TOPICS*, *27*(15), 2403-2416.

Pfister, G., L. Emmons, P. Hess, J. Lamarque, J. Orlando, S. Walters, A. Guenther, P. Palmer, and P. Lawrence (2008), Contribution of isoprene to chemical budgets: A model tracer study with the NCAR CTM MOZART-4, *JOURNAL OF GEOPHYSICAL RESEARCH-ATMOSPHERES*, *113*(D5), doi:10.1029/2007JD008948.

Phadnis, M., and G. Carmichael (2000), Forest fire in the Boreal Region of China and its impact on the photochemical oxidant cycle of East Asia, *ATMOSPHERIC ENVIRONMENT*, *34*(3), 483-498.

Pielke, R. et al. (1992), A Comprehensive Meteorological Modeling System - RAMS, *METEOROLOGY AND ATMOSPHERIC PHYSICS*, *49*(1-4), 69-91.

Pilinis, C. (1990), Derivation and Numerical-Solution of the Species Mass-Distribution Equations for Multicomponent Particulate Systems, *ATMOSPHERIC ENVIRONMENT PART A-GENERAL TOPICS*, *24*(7), 1923-1928.

Pilinis, C., K. Capaldo, A. Nenes, and S. Pandis (2000), MADM - A new multicomponent aerosol dynamics model, *AEROSOL SCIENCE AND TECHNOLOGY*, *32*(5), 482-502.

Pilinis, C., and J. Seinfeld (1988), Development and Evaluation of an Eulerian Photochemical Gas Aerosol Model, *ATMOSPHERIC ENVIRONMENT*, *22*(9), 1985-2001.

Prince, A., J. Wade, V. Grassian, P. Kleiber, and M. Young (2002), Heterogeneous reactions of soot aerosols with nitrogen dioxide and nitric acid: atmospheric chamber and Knudsen cell studies, *ATMOSPHERIC ENVIRONMENT*, *36*(36-37), 5729-5740.

Ro, C., H. Hwang, Y. Chun, and R. Van Grieken (2005), Single-particle characterization of four "Asian Dust" samples collected in Korea, using low-Z particle electron probe X-ray microanalysis, *ENVIRONMENTAL SCIENCE & TECHNOLOGY*, *39*(6), 1409-1419.

Sander, R., and P. Crutzen (1996), Model study indicating halogen activation and ozone destruction in polluted air masses transported to the sea, *JOURNAL OF GEOPHYSICAL RESEARCH-ATMOSPHERES*, *101*(D4), 9121-9138.

Sandu, A. (2006), Piecewise polynomial solutions of aerosol dynamic equation, *AEROSOL SCIENCE AND TECHNOLOGY*, *40*(4), 261-273, doi:10.1080/02786820500543274.

Sandu, A., and C. Borden (2003), A framework for the numerical treatment of aerosol dynamics, *APPLIED NUMERICAL MATHEMATICS*, *45*(4), 475-497, doi:10.1016/S0168-9274(02)00251-9.

Saylor, R. (1997), An estimate of the potential significance of heterogeneous loss to aerosols as an additional sink for hydroperoxy radicals in the troposphere, *ATMOSPHERIC ENVIRONMENT*, *31*(21), 3653-3658.

Skamarock, W. C., J. B. Klemp, J. Dudhia, D. O. Gill, D. M. Barker, W. Wang, and J. G. Powers (2005), *A description of the Advanced Research WRF Version 2*, Mesoscale and Microscale Meteorology Division, National Center for Atmospheric Research, Boulder, CO.

Song, C., and G. Carmichael (2001a), A three-dimensional modeling investigation of the evolution processes of dust and sea-salt particles in east Asia, *JOURNAL OF GEOPHYSICAL RESEARCH-ATMOSPHERES*, *106*(D16), 18131-18154.

Song, C., and G. Carmichael (2001b), Gas-particle partitioning of nitric acid modulated by alkaline aerosol, *JOURNAL OF ATMOSPHERIC CHEMISTRY*, *40*(1), 1-22.

Song, C., C. Kim, Y. Lee, G. Carmichael, B. Lee, and D. Lee (2007), An evaluation of reaction probabilities of sulfate and nitrate precursors onto East Asian dust particles, *JOURNAL OF GEOPHYSICAL RESEARCH-ATMOSPHERES*, *112*(D18).

Stelson, A. (1990), Urban Aerosol Refractive-Index Prediction by Partial Molar Refraction Approach, *ENVIRONMENTAL SCIENCE & TECHNOLOGY*, *24*(11), 1676-1679.

Tang, Y., G. Carmichael, G. Kurata, et al. (2004), Impacts of dust on regional tropospheric chemistry during the ACE-Asia experiment: A model study with observations, *JOURNAL OF GEOPHYSICAL RESEARCH-ATMOSPHERES*, *109*(D19).

Tang, Y., G. Carmichael, J. Seinfeld, et al. (2004), Three-dimensional simulations of inorganic aerosol distributions in east Asia during spring 2001, *JOURNAL OF GEOPHYSICAL RESEARCH-ATMOSPHERES*, *109*(D19).

Tang, Y. et al. (2007), Influence of lateral and top boundary conditions on regional air quality prediction: A multiscale study coupling regional and global chemical transport models, *JOURNAL OF GEOPHYSICAL RESEARCH-ATMOSPHERES*, *112*(D10).

Tang, Y. et al. (2003), Impacts of aerosols and clouds on photolysis frequencies and photochemistry during TRACE-P: 2. Three-dimensional study using a regional chemical transport model, *JOURNAL OF GEOPHYSICAL RESEARCH-ATMOSPHERES*, *108*(D21).

Underwood, G., P. Li, H. Al-Abadleh, and V. Grassian (2001), A Knudsen cell study of the heterogeneous reactivity of nitric acid on oxide and mineral dust particles, *JOURNAL OF PHYSICAL CHEMISTRY A*, *105*(27), 6609-6620.

Underwood, G., C. Song, M. Phadnis, G. Carmichael, and V. Grassian (2001), Heterogeneous reactions of NO2 and HNO3 on oxides and mineral dust: A combined laboratory and modeling study, *JOURNAL OF GEOPHYSICAL RESEARCH-ATMOSPHERES*, *106*(D16), 18055-18066.

Uno, I. et al. (2004), Numerical study of Asian dust transport during the springtime of 2001 simulated with the Chemical Weather Forecasting System (CFORS) model, *JOURNAL OF GEOPHYSICAL RESEARCH-ATMOSPHERES*, *109*(D19).

Usher, C., H. Al-Hosney, S. Carlos-Cuellar, and V. Grassian (2002), A laboratory study of the heterogeneous uptake and oxidation of sulfur dioxide on mineral dust particles, *JOURNAL OF GEOPHYSICAL RESEARCH-ATMOSPHERES*, *107*(D23), doi:10.1029/2002JD002051.

Usher, C., A. Michel, and V. Grassian (2003), Reactions on mineral dust, *CHEMICAL REVIEWS*, *103*(12), 4883-4939.

Usher, C., A. Michel, D. Stec, and V. Grassian (2003), Laboratory studies of ozone uptake on processed mineral dust, *ATMOSPHERIC ENVIRONMENT*, *37*(38), 5337-5347.

Wexler, A., and J. Seinfeld (1990), The Distribution of Ammonium-Salts Among a Size and Composition Dispersed Aerosol, *ATMOSPHERIC ENVIRONMENT PART A-GENERAL TOPICS*, *24*(5), 1231-1246.

Xiao, H., G. Carmichael, J. Durchenwald, D. Thornton, and A. Bandy (1997), Long-range transport of SOx and dust in East Asia during the PEM B Experiment, *JOURNAL OF GEOPHYSICAL RESEARCH-ATMOSPHERES*, *102*(D23), 28589-28612.

Zhang, D., and Y. Iwasaka (1999), Nitrate and sulfate in individual Asian dust-storm particles in Beijing, China in spring of 1995 and 1996, *ATMOSPHERIC ENVIRONMENT*, *33*(19), 3213-3223.

Zhang, D., J. Zang, G. Shi, Y. Iwasaka, A. Matsuki, and D. Trochkine (2003), Mixture state of individual Asian dust particles at a coastal site of Qingdao, China, *ATMOSPHERIC ENVIRONMENT*, *37*(28), 3895-3901, doi:10.1016/S1352-2310(03)00506-5.

Zhang, Q. et al. (2009), Asian emissions in 2006 for the NASA INTEX-B mission, *ATMOSPHERIC CHEMISTRY AND PHYSICS*, *9*(14), 5131-5153.

Zhang, Y. (1994), The chemical role of mineral aerosols in the troposphere in East Asia, The University of Iowa, United States.

Zhang, Y., and G. Carmichael (1999), The role of mineral aerosol in tropospheric chemistry in East Asia - A model study, *JOURNAL OF APPLIED METEOROLOGY*, *38*(3), 353-366.

Zhang, Y., B. Pun, K. Vijayaraghavan, S. Wu, C. Seigneur, S. Pandis, M. Jacobson, A. Nenes, and J. Seinfeld (2004), Development and application of the model of aerosol dynamics, reaction, ionization, and dissolution (MADRID), *JOURNAL OF GEOPHYSICAL RESEARCH-ATMOSPHERES*, *109*(D1), doi:10.1029/2003JD003501.

Zhang, Y., C. Seigneur, J. Seinfeld, M. Jacobson, and F. Binkowski (1999), Simulation of aerosol dynamics: A comparative review of algorithms used in air quality models, *AEROSOL SCIENCE AND TECHNOLOGY*, *31*(6), 487-514.